ENHANCED GROWTH RATE AND SILANE UTILIZATION IN AMORPHOUS SILICON AND NANOCRYSTALLINE-SILICON SOLAR CELL DEPOSITION VIA GAS PHASE ADDITIVES

Final Technical Report

For the period

1 August 2009 – 1 April 2012

August 31, 2012

Award Number DE-EE0000580

Air Products and Chemicals, Inc.

Principal Investigator: Dr. Robert G. Ridgeway
Contract Administrator: Gregory H. Daub

DOE Project Team:
Field Award Administrator: Diana Martinez
Field Project Officer: Daniel Stricker

DISCLAIMER

FULL PROJECT TEAM

Air Products and Chemicals, Inc.

Dr. Patrick T. Hurley	*Original Principal Investigator*
Dr. Robert G. Ridgeway	*Current Principal Investigator*
Gregory H. Daub	*Contract Administrator*

University of Delaware

Dr. Steven S. Hegedus	*Scientist, Institute of Energy Conversion*
Dr. Ujjwal K. Das	*Associate Scientist, Institute of Energy Conversion*
Lala Zhu	*Graduate Student, Dept. of Physics and Astronomy*
Dr. Chandin Das	*Post-Doctoral Researcher*

University of Toledo

Dr. Nikolas J. Podraza	*Assistant Professor of Physics, Dept. of Physics and Astronomy*

TABLE OF CONTENTS

PART 1: INTRODUCTION & BACKGROUND

Thin-film Si photovoltaic modules that have been commercialized use the tandem "micromorph" structure with an α-Si high- bandgap top cell and a microcrystalline (μCSi) low-bandgap bottom cell showing improved, stabilized performance over previous α-Si-based modules. Several groups have reported devices with over 12% stabilized efficiency, and modules or large-area cells have been produced with stabilized efficiencies of 10%. Original equipment manufacturers Applied Materials and Oerlikon have each sold several α-Si/μCSi tandem module fabrication lines in the past. Many other manufactures have also invested in tandem module production lines.

A critical issue for the low-cost commercial production of tandem cells is the thickness of the nc-Si layer coupled with a low growth rate, which limits the process throughput. The μCSi layer needs to be 1.0–1.5 μm thick due to the lower absorption of μCSi compared to α-Si. An increase in μCSi growth rates was listed as one of the critical goals in the DOE Thin Silicon Roadmap. Currently, all production processes use SiH_4 diluted in H_2 at higher pressure and/or higher-frequency PECVD. This project was targeted at determining how additives to the process of record (POR) could increase the deposition rate to allow higher process throughput and lower the overall manufacturing cost of ownership (COO). The cost associated with use of an additive must be balanced with the reduction in COO associated with higher process throughput.

As this project progressed from July 2009 through April 2012, Air Products had many discussions with original equipment manufacturers (OEMs) and device manufacturers. From these discussions, it became clear that the benefits of increased throughput would be optimized at levels of 30–50% over current production rates. Higher throughput enhancement would result in bottlenecks at other manufacturing steps. This information helped to set the criteria for commercial success, provided technical success could be achieved. The barriers to technical success included not only an enhanced deposition rate for both μCSi and αSi-H films, but also equivalent or better performance of these films in solar cells.

Influenced by these guidelines, Air Products set out to investigate the impact of additives on the deposition rate of both μCSi and αSi-H films. One criterion for additives was that they could be used in conventional PECVD processing, which would require sufficient vapor pressure to deliver material to the process chamber at the required flow rates. The flow rate required would depend on the size of the substrate onto which silicon films were being deposited, potentially ranging from 200 mm diameter wafers, as were used in Air Products' PECVD chamber, to the 5.7 m^2 glass substrates used in GEN 8.5 flat-panel display tools. In choosing higher-order silanes, both disilane and trisilane had sufficient vapor pressure (33.1 psig and 4.4 psia @ 20^oC, respectively) to withdraw gas at the required flow rates of up to 120 sccm.

This report presents results obtained from testing at Air Products' electronic technology laboratories, located in Allentown, PA, which focused on developing processes on a commercial IC reactor (Applied Materials Precision 50000 PECVD reactor) using silane and mixtures of silane plus additives. These processes were deployed to compare deposition rates and film properties

with and without additives, with a goal of maximizing the deposition rate while maintaining or improving film properties.

This report also contains results from Air Products' subcontractors, the University of Delaware's Institute of Energy Conversion (IEC) and the University of Toledo. IEC focused on characterizing plasma parameters based on optical emission spectroscopy (OES) and Langmuir probe measurements, along with making devices using the additives at enhanced growth rates. The University of Toledo focused on characterizing the microstructural evolution of silicon films being deposited with and without additives using *in-situ* spectroscopic ellipsometry (SE).

Facility Upgrades at Air Products to Support this Program

During this study, Air Products invested over $500,000 to provide the capability to deposit and characterize silane-based μCSi films on the P5000 process tool. These upgrades included installation of the following: a new process chamber on the tool; gas and chemical handling equipment to safely deliver silane, disilane and trisilane; and a thermal-wet abatement system to remediate emissions from the process chamber. Metrology equipment was also purchased, including a Raman spectrometer and a wide-range spectroscopic ellipsometer.

Facility Upgrades at IEC to support this program

During this study, the University of Delaware's IEC invested over $150,000 of internal funds to enable the work reported here. Some of this was cost share, and some was additional investment. Third-party vendors installed three new hazardous gas cabinets and upgraded the hazardous gas plumbing for several other cabinets. This enabled the use of Si_2H_6, Si_3H_8, SiH_3Cl and a higher-volume H_2 cylinder (higher H_2 flow is required for nanocrystalline growth). The mass flow controllers were replaced to allow higher H_2 and lower B_2H_6 flow. Additional toxic gas monitoring capability was added. Installation of a dry pump donated by Air Products required the addition of a LN_2 dewar and supply line. Installation of a new higher-power (1200W) RF power supply required water cooling and new high-power-compatible feedthrough in order to excite high-power plasma for nanocrystalline deposition. All of these new devices required a complete upgrade of the SCADA, which controls the multichamber PECVD and gas supply. IEC also purchased a Raman spectroscopy unit (Nicolet) to characterize crystalline fractions in the nc-Si films. Toward the end of this project, IEC purchased a Langmuir probe to characterize the plasma and add insight to the OES and film data.

PART 2: PLASMA CHEMISTRY AND DEPOSITION RATE SCREENING

Film Metrology

Thin film metrology was a critical component used to characterize film thickness and composition during this study. Three well-accepted techniques were used for primary characterization: Fourier transform infrared spectroscopy (FTIR), Raman spectroscopy and spectroscopic ellipsometry (SE)

FTIR was deployed to determine the bonding nature of αSi-H films. The microstructure fraction, R^*, is defined as the ratio of $Si-H_2$ to Si-H moieties in the αSi-H films. Figure 2-1 shows IR absorption bands for both types of bonded hydrogen. These absorption bands were deconvolved and integrated using commercially-available software to yield R* for each αSi-H film deposited. Figure 2-2 shows FTIR spectra for a typical αSi-H film where the addition of an additive to silane has caused the microstructure fraction to increase. This metrology was a critical component in estimating how changes in process parameters would impact film performance.

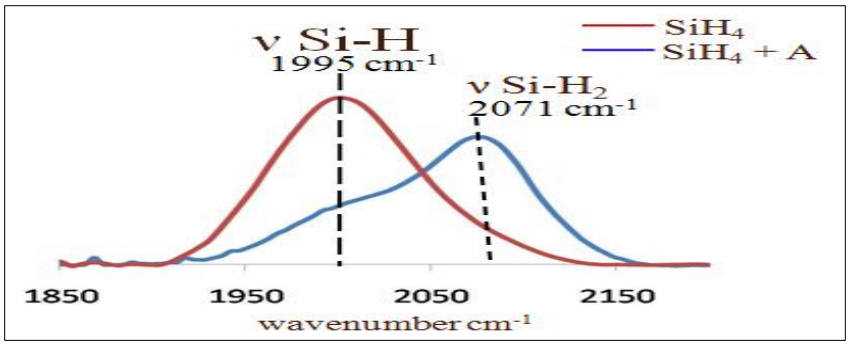

Figure 2-1: FTIR spectra showing absorbance of Si-H and $Si-H_2$ bonded moieties in PECVD-based αSi-H films.

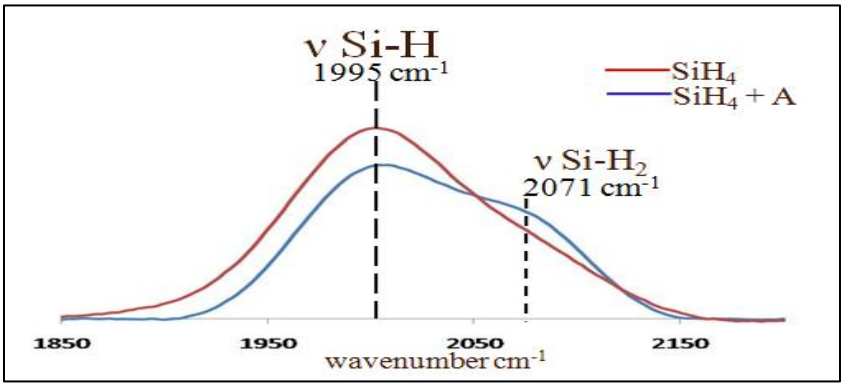

Figure 2-2: FTIR spectra showing the impact of additive A on the microstructure fraction (R*) as a result of increased $Si-H_2$ bonding in the deposited film.

Raman Spectroscopy

Raman spectroscopy was used to differentiate amorphous silicon from silicon containing both amorphous and microcrystalline phases. The films were deposited on PV glass slides and measured using a Thermofisher Scientific DXR Raman microscope consisting of a 532nm laser in the 2 milliwatt range. The samples were exposed to the laser using a 50x lens and 50 micron aperture so the spot size was ~0.7 microns. The resulting spectra were analyzed using a curve fitting program in Gaussian mode to determine if the deposited films were amorphous or contained microcrystalline structures. The peak occurred in the 400 to 550 wave number region. If most of the peak was in the 480 region, the film was predominantly amorphous. The microcrystalline fraction was determined by the ratio of the area under the peak centered between 510-520 versus the area of the entire peak. If the microcrystalline fraction was below 0.25, the film was considered amorphous. Figure 2-3 shows absorption profiles for amorphous and microcrystalline silicon films. During the microcrystalline portion of this study, typical microcrystalline fractions were 50–70%.

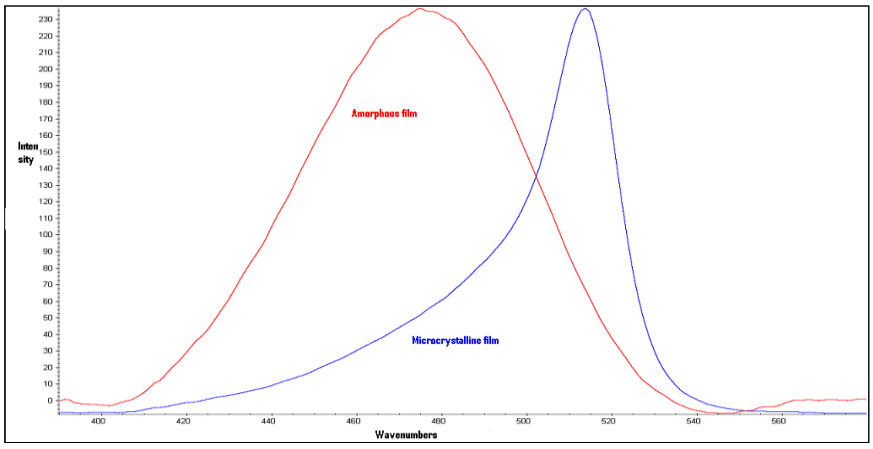

Figure 2-3: Raman spectra showing broad amorphous silicon absorption centered at 470 cm^{-1} and crystalline absorption centered at 517 cm^{-1}.

Spectroscopic Ellipsometry

Hydrogenated silicon (Si:H) thin films have been deposited onto native oxide-covered crystal silicon (c-Si) substrates by plasma-enhanced chemical vapor deposition (PECVD) and studied using *ex situ* spectroscopic ellipsometry to characterize the film structure in the form of thickness, surface roughness, and degree of crystallinity (amorphous versus nanocrystalline). Ambient ellipsometric spectra (in Δ, ψ) were collected *ex situ* at multiple angles of incidence from $\Theta_i = 50^o$ and 80^o, using a variable-angle multichannel spectroscopic ellipsometer based on the rotating-compensator principal[1,2,3] over a spectral range of 0.75–5.0 eV. Spectra collected below 1.2 eV were not analyzed due to the presence of reflections from the back surface of the c-Si wafers used. The complex dielectric function spectra ($\varepsilon = \varepsilon_1 + i\varepsilon_2$) and microstructural parameters (bulk layer thickness d_b, surface roughness thickness d_s) for the Si:H layers were extracted using a least-squares regression analysis and an unweighted error function,[4] σ, to fit the experimental ellipsometric spectra to an optical model consisting of a semi-infinite c-Si substrate

/20-30 Å of native oxide /bulk Si:H film/surface roughness/air ambient structure. Free parameters correspond to the bulk and surface roughness thicknesses of the Si:H film and a parameterization of ε for Si:H. ε for amorphous Si:H (a-Si:H) is represented by a Tauc-Lorentz[5,6] oscillator:

$$\varepsilon_2 = \begin{cases} \dfrac{AE_0\Gamma}{\left(E^2 - E_0^2\right)^2 + \Gamma^2 E^2} \dfrac{\left(E - E_g\right)^2}{E} & E > E_g \\ 0 & E \le E_g \end{cases},$$

Equation 1

and

$$\varepsilon_1 = \frac{2}{\pi} P \int_{E_g}^{\infty} \frac{\xi \varepsilon_2(\xi)}{\xi^2 - E^2} d\xi,$$

where A is the amplitude, Γ is the broadening, E_0 is the resonance energy, and E_g represents an absorption onset determined from a parabolic band, constant momentum matrix element. A constant additive term to ε_1, represented by ε_∞, is also included. Nanocrystalline Si:H (nc-Si:H), denoted by ε, is represented by a model using a parametric critical point structure based on the joint density of states.[7]

The optical properties of the components of the surface roughness layer are represented by a Bruggeman effective medium approximations[8] (EMA) consisting of variable fractions of bulk Si:H material and void. Reference spectra in ε for c-Si and native oxide were obtained from literature.[9]

The surface roughness itself is modeled as a single layer consisting of 0.5 bulk Si:H and 0.5 void for most a-Si:H and some nc-Si:H samples. For those samples exhibiting structural gradients either due to density variations or grain growth, the structure becomes more complicated. In this scenario, up to four EMA layers with variable bulk material and void fractions are used to represent surface roughness. In the case of nc-Si:H, the surface roughness is much larger that of a-Si:H and continues to increase with film thickness.[10] As the surface features increase in size, one EMA layer acting as a heterogeneous mixture is not sufficient to model the optical response of surface roughness, therefore this layer is divided into smaller sections as illustrated in Figure 2-4. The results of this process allow for determining the thickness of the Si:H material and respective values of ε. Based on the results of the optical modeling, the shape of ε varies with structure[10] and can be used to determine if the film is amorphous or nanocrystalline, as shown in Figure 2-5.

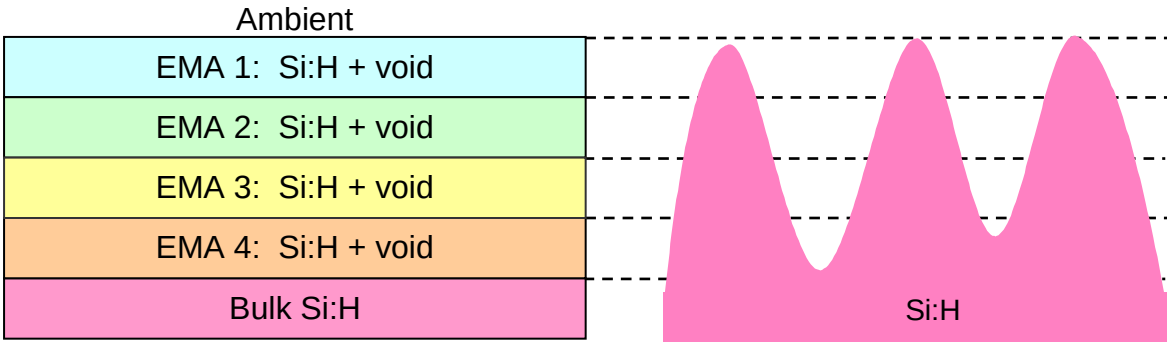

Figure 2-4: Schematics of the sample structure for hydrogenated Si layers exhibiting large surface roughness or other density gradients. The surface region is represented multiple Bruggeman effective medium approximation (EMA) layers consisting of Si:H and void. An illustration of the actual layer structure showing surface roughness is shown to the right, where the dashed lines demarcate the representations of the EMA layers.

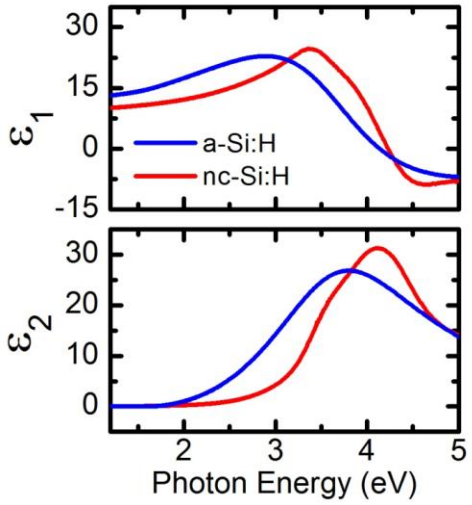

Figure 2-5: Comparison of complex dielectric function spectra ($\varepsilon = \varepsilon_1 + i\varepsilon_2$) for amorphous and nanocrystalline Si:H determined by *ex situ* spectroscopic ellipsometry analysis.

Other Critical QA/QC Issues

The screening process conducted on a 200 mm IC platform required the use of relatively low flows of silicon precursor gases. Experiments required a flow of as little as 1 sccm of additive gases such as disilane or trisilane. An important quality concern of data acquired under these conditions was to ensure that the mass flow controllers (MFCs) used were delivering accurate and linear flows of gas over the intended range.

An experiment was designed to measure the concentration of process gases in process effluent over a range of gas flows set at the process tool. Extractive FTIR was utilized, as per a U.S. EPA protocol developed by Air Products and the EPA for measuring emissions from semiconductor processes,[11] to determine the linearity of MFC response to SiH_4 and Si_2H_6 over the range of MFC flows. This was necessary to ensure that conditions where 10% disilane were called for actually delivered 10% relative to the total silicon precursor flow.

Calibrations of gas flow response relative MFC flow settings on the process tool were conducted by flowing gas through the process chamber tool and associated pump, with RF power turned off. The concentration of each species was determined for each flow setting. The process pump was purged with nitrogen to help carry process effluents from the pump and into the exhaust plenum. Typical nitrogen pump purges for the chamber used in this study were ~60–70 slm. Figure 2-6 shows the results obtained for silane, which was flowed over a range of 1–25 sccm. Table 2-1 contains the averaged silane concentrations determined for each flow. These data indicate a linear response from a setting of 25 sccm down to 3 sccm. At 1 sccm, the MFC was not linear and thus could not be used reliably at this flow setting for quantitative-based experiments.

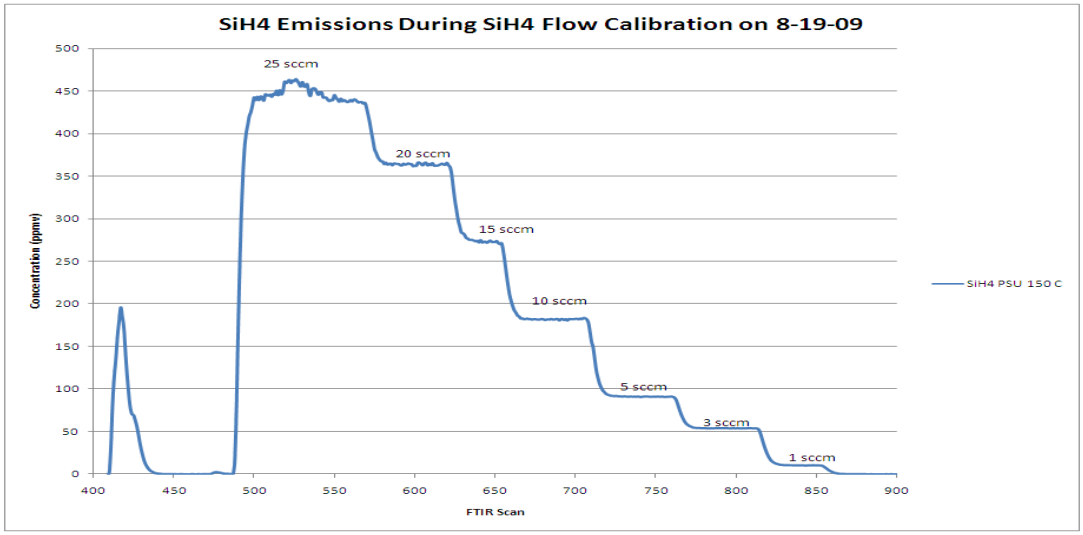

Figure 2-6: Emission profile of SiH_4 determined in the process pump effluent while SiH_4 flows were varied on the tool. These data indicated a linear response down to a setting of 3 sccm.

Table 2-1: Average SiH_4 concentration determined at each MFC flow setting.

MFC Setting (sccm)	SiH_4 Concentration (ppmv)
25	447
20	364
15	274
10	182
5	91
3	54
1	11

The same process was repeated for the MFCs used to deliver disilane. Two MFCs were required to cover the flow ranges necessary to conduct testing at the desired mixing ratios. Figure 2-7 shows the results obtained for the higher flow unit, which was found to be linear from 20 sccm down to 3 sccm (disilane concentrations and flows are shown in Table 2-2). A second, smaller MFC was used to deliver flows of <5 sccm, as shown in Figure 2-8. Carefully calibrating these MFCs at very low flows provided assurance that small differences in process parameters related to flow settings would actually be realized in the process chamber during testing.

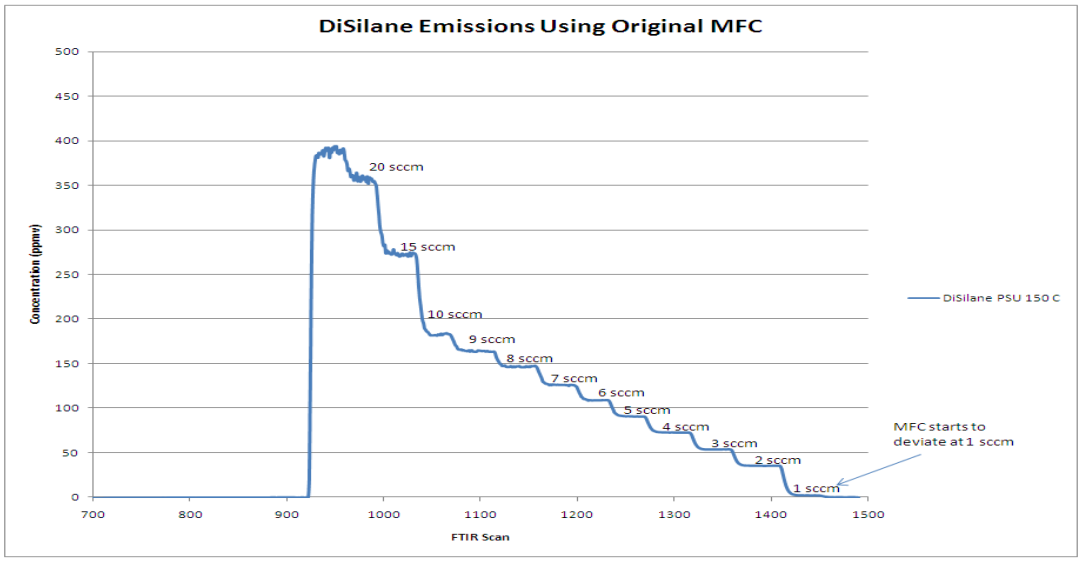

Figure 2-7: Emission profile of Si_2H_6 determined in the process pump effluent while Si_2H_6 flows were varied on the tool. These data indicate a linear response down to a setting of 3 sccm.

Table 2-2: Average Si_2H_6 concentration determined at each MFC flow setting for the larger MFC used to deliver additive.

MFC Setting (sccm)	Si_2H_6 Concentration (ppmv)
20	358
15	273
10	183
9	164
8	147
7	127
6	109
5	91
4	73
3	54
2	36
1	3

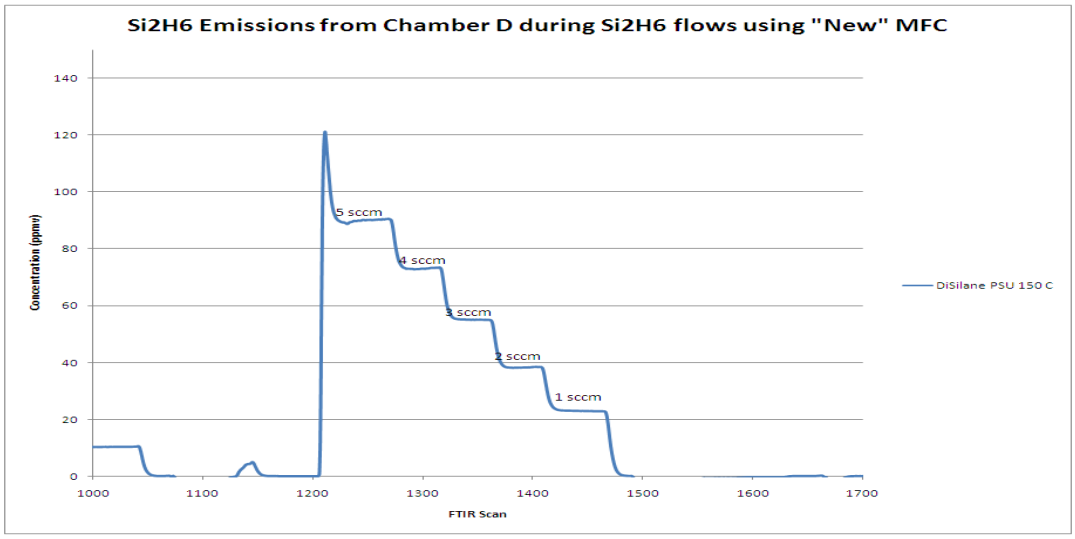

Figure 2-8: Emission profile of Si_2H_6 determined in the process pump effluent while Si_2H_6 flows were varied on the tool. These data were obtained on a 10 sccm maximum flow MFC and indicated a linear response down to a setting of 2 sccm. The concentration determined at 1 sccm was ca. 33% over the expected value of 18 ppmv suggesting that flow settings of 1 sccm could actually be 1.33 sccm relative to other MFC settings.

Silane Plasma Chemistry

The 13.56 MHz RF discharge used in this study yielded plasma chemistry initiated by electron collisions with silane, disilane and hydrogen. Excitation to electronically excited states and subsequent dissociation products have been studied previously[12,13] and are represented by the series of reactions for silane and disilane shown below. The deposition of amorphous silicon films reportedly arises from silicon fragments containing odd numbers of hydrogen, such as the sillyl radical (SiH_3), while fragments containing even numbers, such as silene radical (SiH_2), contribute to formation of higher-order silanes[14] as shown in R5-R7 below. The growth rate of highly photoconductive αSi-H films will ultimately be controlled by the flux of sillyl and other odd-numbered radical species[15] to the surface of the growing film.

The branching ratio for silane dissociation has been reported to vary from predominantly R2 (≈ 1)[16] to a 43:36:17 ratio for R2:R3:R1. This ratio could be significant in determining the film quality as indicated by the microstructure fraction R^* of the deposited film. Higher partial pressures of SiH_2 will lead to higher flux of high order silane (HOS) and higher R^*. The branching ratio can be controlled by the plasma frequency, as higher frequencies will yield collisionally-induced electronic excited states with lower internal energy that can be stabilized by ejection of a single hydrogen to yield SiH_3 radicals. The electron density can be controlled by the plasma power density, with higher powers yielding higher electron density resulting in greater dissociation of silicon precursors. In the case of disilane, avoidance of SiH_2 is not as easy given the reported branching ratio of 0.91:0.09 for reactions R10 and R8 occurring during the electron-induced dissociation of Si_2H_6. Dissociation of each Si_2H_6 molecule will yield a

potential HOS initiating SiH_2 radical. Thus, deposition of highly photoconductive αSi-H films using disilane requires different processing conditions.

SiH_4 Formation:

$SiH_4 + e$	$\rightarrow$	$SiH_3 + H$	**R3**
	$\rightarrow$	$SiH_2 + 2H$	**R2**
	$\rightarrow$	$SiH + H + {}_2$	**R1**
$H + SiH_4$	$\rightarrow$	$SiH_3 + H_2$	**R4**

Higher-Order Silane Formation:

$SiH_2 + SiH_4$	$\xrightarrow{M}$	Si_2H_6	**R5**
$SiH_2 + SiH_4$	$\xrightarrow{M}$	$H_3SiSiH + H_2$	**R6**
$H_3SiSiH + SiH_4$	$\rightarrow$	Si_3H_8	**R7**

Si_2H_6 Formation:

$e + Si_2H_6$	$\rightarrow$	$Si_2H_5 + H$	**R8**
	$\rightarrow$	$SiH_3SiH + 2H$	**R9**
	$\rightarrow$	$SiH_3 + SiH_2 + H$	**R10**
	$\rightarrow$	$Si_2H_3 + H_2 + H$	**R11**

αSi-H Deposition Rate Enhancement & Film Properties

Investigation of the impact on growth rate and microstructure fraction (R*) when adding higher order silanes was carried out using disilane and trisilane. Films were deposited at various RF powers and flow compositions and were characterized using spectroscopic ellipsometry (SE) and FTIR to determine film thickness and R*.

The platform used was the AMAT P5000 that was operated at a process pressure of 5 torr with the electrodes spaced at 5 mil. The wafer temperature was held at 220°C. For all experiments, the total hydrogen flow was kept at 10 times the total flow of Si precursor to ensure growth of αSi-H films (R=10), avoiding conversion to the nanocrystaline phase.

The impact on deposition rate of silane-based films was investigated by varying power and total process flow while keeping the Si/H_2 at 10. Figure 2-9 shows the impact of these parameters on the deposition rate for silane-based films. These results served as the baseline for comparison when substituting di- and trisilane.

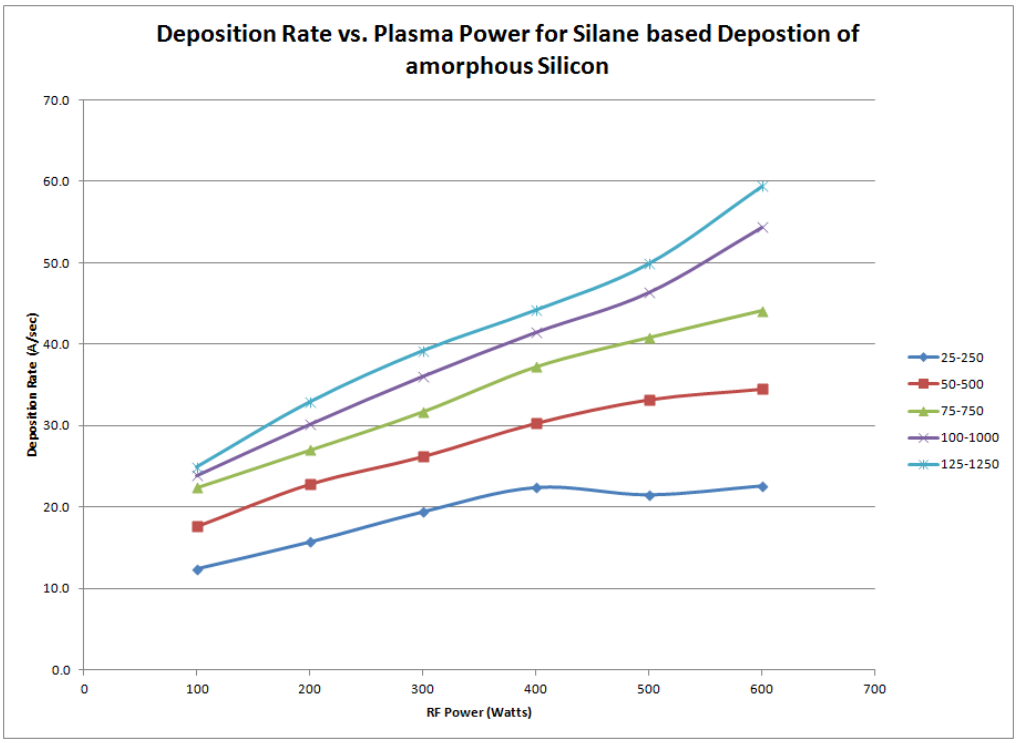

Figure 2-9: Impact of total flow and plasma power on silane based deposition of αSi-H films. The legend shows the silane-hydrogen flows.

The deposition rate trends for the lower flows (25-250 & 50-500) show a flattening of the curves, indicating that the deposition rate is maximized as the reactive radical flux reaches a maximum based on the number density of precursor and does not increase with increasing plasma power. Under these conditions, the silane dissociation efficiency is maximized. At higher total flows, higher power densities are required to reach these conditions. The data for the higher flows suggest that the same conditions were not met at 500-600W and that continued increases in power would lead to higher deposition rates. These power densities (1.18 watts/cm^2 @ 600W) may not be practical for large-area electrodes such as those used in the TF PV industry.

Typical industry standard deposition rates of 5-7 Å/sec for αSi-H were readily exceeded on the P5000 platform. Table 2-3 shows the relative increase in deposition rate for each flow when comparing to the lowest power density of 0.197 watts/cm^2 (100W). The data in Table 2-3 demonstrate a wide range of potential deposition rates for silane based on applied power and total flow through the reactor.

Table 2-3: Relative deposition rates at varying flow rates and RF power for silane-based films. The deposition rate achieved under the lowest flow (25-250 sccm) and power (100W) was 12.4 Å/sec. This could be increased by increasing power and total flow by ~4.8X at the highest conditions for power and flow reported here.

Power (Watts)	Sih4-H2 Flow 25-250 sccm	Sih4-H2 Flow 50-500 sccm	Sih4-H2 Flow 75-750 sccm	Sih4-H2 Flow 25-250 sccm	Sih4-H2 Flow 25-250 sccm
100	1.00	1.42	1.81	1.93	2.01
200	1.27	1.84	2.18	2.44	2.65
300	1.56	2.11	2.56	2.91	3.16
400	1.81	2.44	3.00	3.35	3.56
500	1.73	2.68	3.29	3.74	4.02
600	1.82	2.78	3.56	4.39	4.79

The first additive screened was disilane, Si_2H_6, which is a liquefied gas with a relatively high vapor pressure of 33.2 psig @ 20^{o}C. Disilane could readily be delivered to the tool at any flow rate required during testing. The same deposition conditions were used as for silane, except 10% or 20% of the silane flow was replaced with disilane. The gases were delivered from separate gas lines to the chamber through individual mass flow controllers (MFCs) and mixed in the common delivery line feeding the process chamber.

The deposition rates at various power densities and total flows were determined for 10% and 20% substituted volumes of disilane. The deposition rates plotted vs. RF power are shown in Figure 2-10. The deposition rate increased for all flows with increasing power, with the largest increases being observed at the highest total flows. At the lowest flow of 25 Si+Si_2-250 H_2, deposition approached a maximum value at 100W RF power. At all other flows, the deposition rate increased as the RF power was increased to 600W.

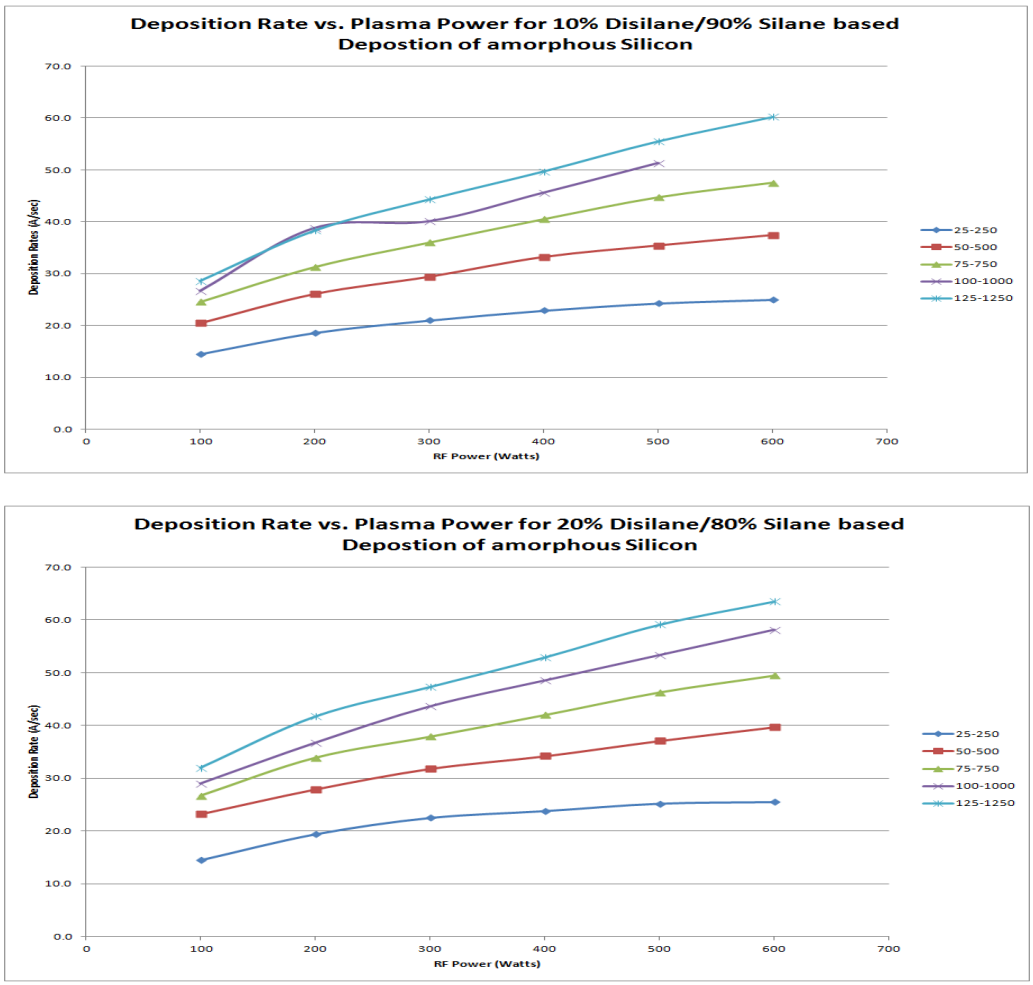

Figure 2-10: Impact of total flow and plasma power on silane-dislane mixtures based on deposition of αSi-H films. The top profile shows impact of 10% disilane substituted for silane; the bottom shows 20% substitution. The legend shows the silane-hydrogen flows.

An important distinction is the comparison of silane-disilane mixtures with silane-only depositions to determine the impact on film growth rate. Figure 2-11 shows the comparison for 10% and 20% disliane vs. neat silane at various flows and powers. The largest benefits were observed at lower power densities, where presumably a higher relative dissociation of disilane would be expected given the lower Si-Si bond energies. As the power density increases, it appears the advantages of disilane diminish and become closer to stoichiometric, defined as gaining a 10% increase in deposition rate for a 10% substitution of disilane given the increase Si atoms per molecule. In these data, it appears the optimum power density for enhancing the growth rate of the mixtures would be 0.39 wcm^{-2} or 200W on the P5000 platform.

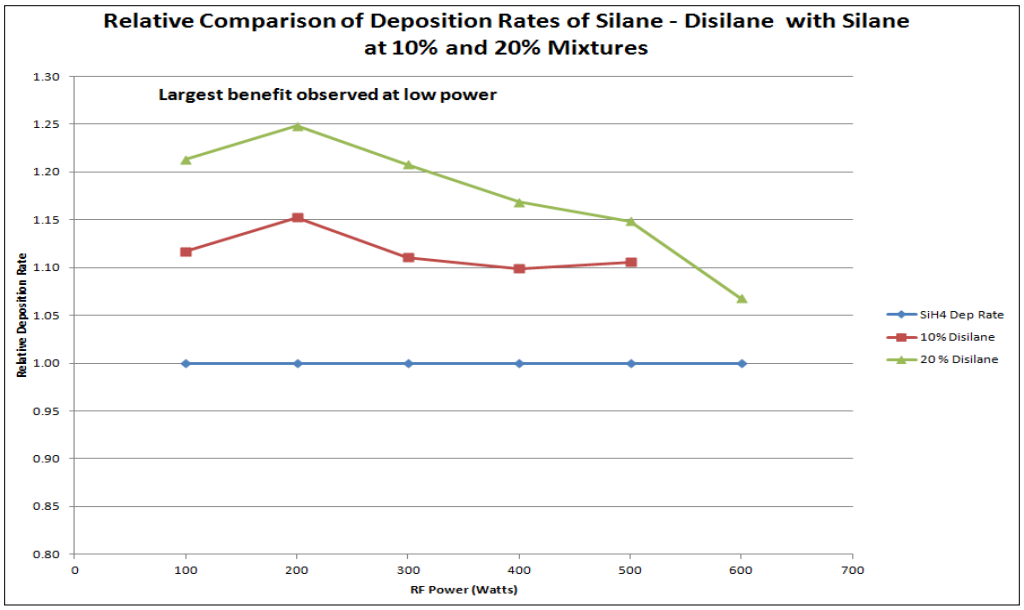

Figure 2-11: Comparison of relative deposition rates of αSi-H films from silane-disilane mixtures with films deposited using neat silane. Mixtures containing 10% disilane appear to reach a maximum benefit at 200W of applied power and quickly become stoichiometric. Mixtures containing 20% become less than stoichiometric above 300W.

The next additive screened was trisilane, Si_3H_8, which is a liquid at room temperature with a vapor pressure of ~5 psia @ 20°C. Total flow was limited to 0.016 slm based on the MFC used in this study. The same deposition conditions were used as for silane, except 10% or 16-20% of the silane flow was replaced with trisilane, which was delivered via vapor-phase withdrawal from the headspace of a heated cylinder.

The deposition rates at various power densities and total flows were determined for 10% and 16-20% substituted volumes of trisilane. The deposition rates plotted vs. RF power are shown in Figure 2-12. The deposition rate continued to increase with RF power at the higher flows, but leveled off at the lower flows. The trends were similar to those for both silane and silane-disilane mixtures.

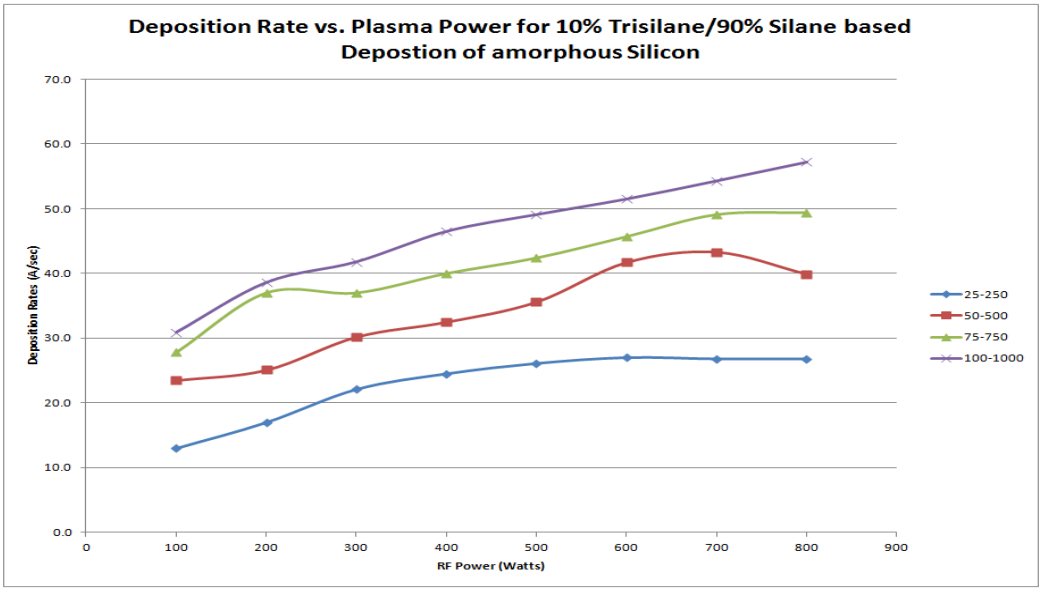

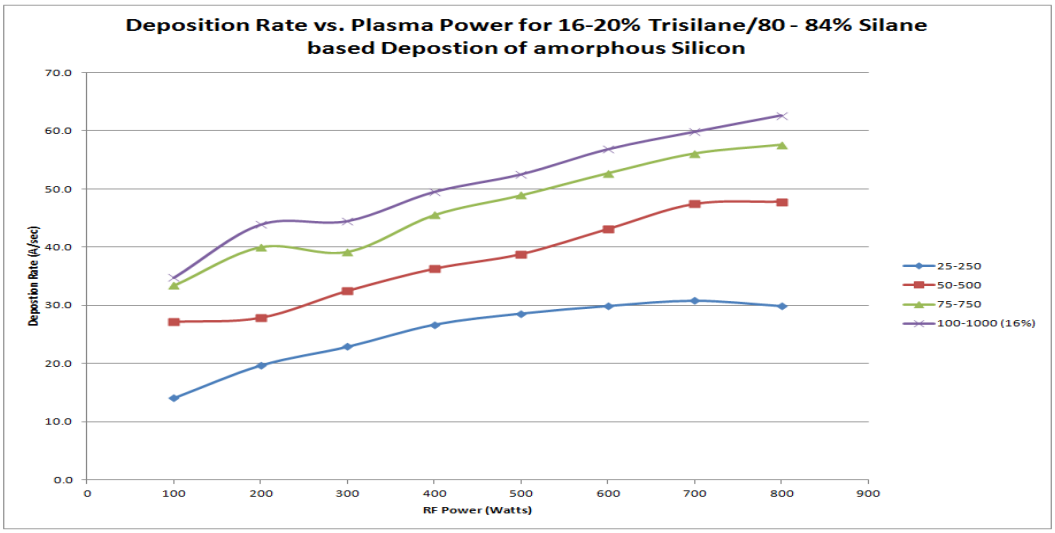

Figure 2-12: Impact of total flow and plasma power on silane-trisilane mixture-based deposition of αSi-H films. The top profile shows impact of 10% trisilane substituted for silane; the bottom shows a 16-20% substitution. The legend shows the silane-hydrogen flows. (The 100-1000 total flow runs used 16% trisilane)

A comparison of silane-trisilane mixtures with the silane-based process is shown in Figure 2-13. The maximum relative gain in deposition rate was observed at low power densities of ~0.39Wcm^{-2} or less. Higher RF powers yielded deposition rate increases not equivalent to the Si added to the process.

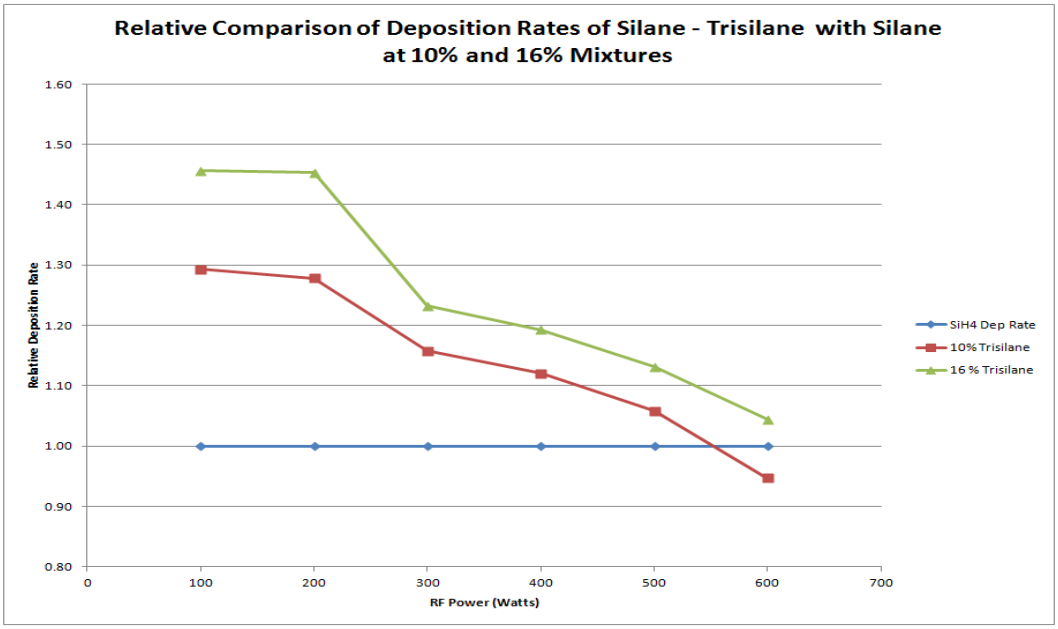

Figure 2-13: Deposition rates of silane-trisilane mixtures relative to the silane-based process. At low power densities, the increase in deposition rate is non-stoicheometric. As the power density increases from 200–300W, the difference becomes sub-stoicheometric.

Achieving higher deposition rates using higher-order silanes as additives under certain processing conditions is only part of the solution. The photoconductive film quality is critical if such processes are to be implemented in high-volume manufacturing (HVM). To examine the potential film quality, deposited films were analyzed by FTIR to determine the microstructure fraction, as discussed above, for each set of conditions.

The R* values for silane-based films at differing powers and total flows are shown in Figure 2-14. The R* values reach a minimum at RF power densities of 0.40–0.80 w/cm^2 (200-400W) and then increase with power. The reason for this observed increase could be related to the deposition rate increase at higher power, which leads to greater micro-void formation. The optimized conditions for lowest R* appear to be flow-dependent on the P5000, with increasing total flows achieving minimums at increasing power.

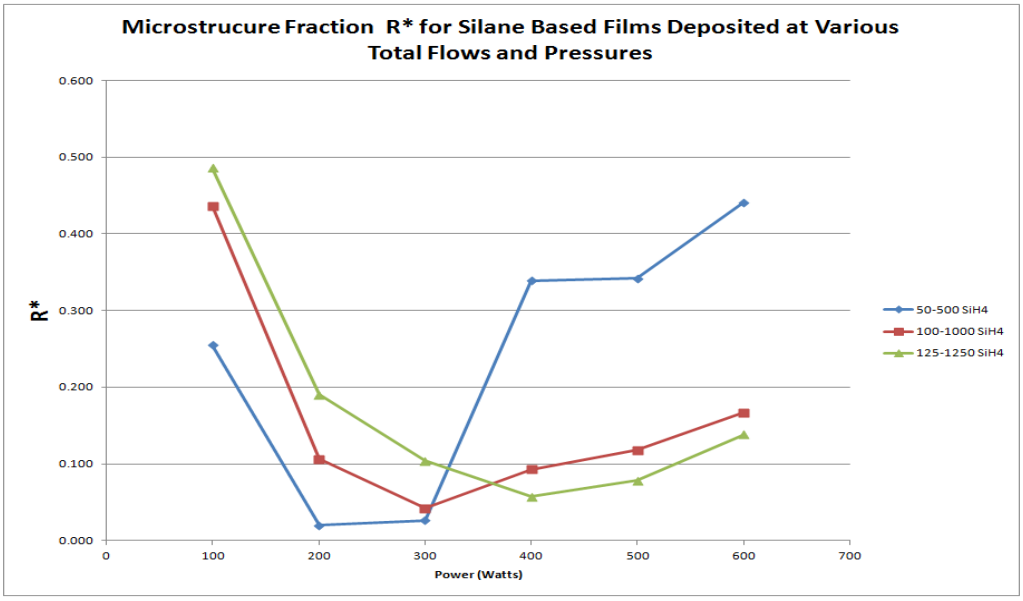

Figure 2-14: Microstructure fractions (R*) obtained for various flows and RF powers for silane- based films.

The R* values obtained for the silane–disilane mixture-based films at differing powers and flows are shown in Figure 2-15. These data show a shift of minimum R* to higher power for the higher-flow processes. Comparing these results to those obtained for the silane-based process suggests that, when used as an additive, disilane provides the opportunity to use higher flows and RF power to deposit αSi-H films at higher rates while maintaining low R*. The deposition rate for the 125 sccm–20% disilane–1250 sccm H_2 @ 500W process was 59 Å/sec (~10 times the current industry standard) and yielded an R* of 0.037.

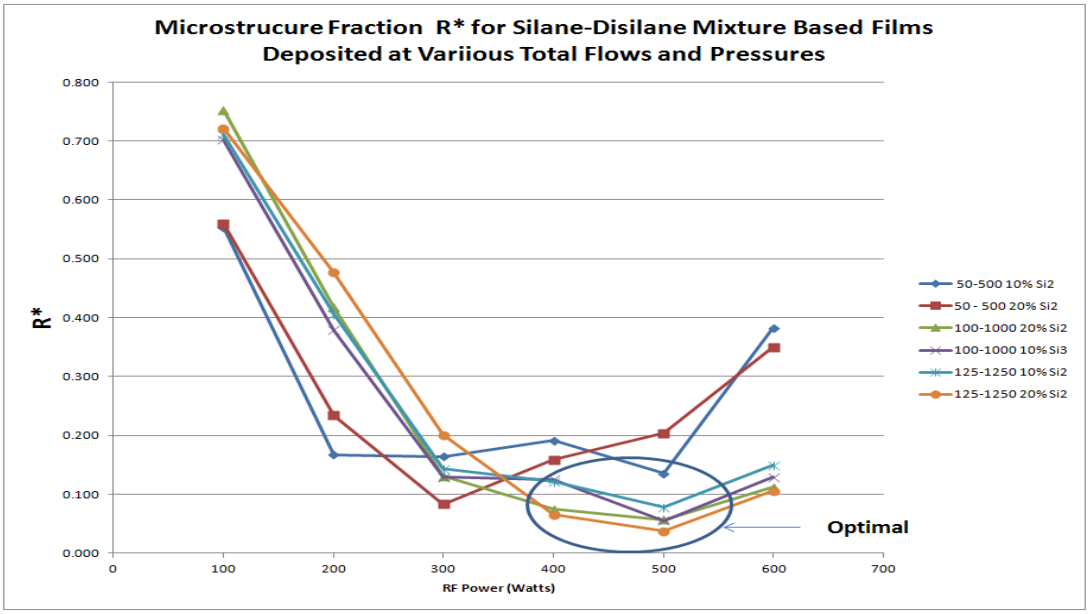

Figure 2-15: Microstructure fraction (R*) obtained for various flows and RF powers for silane-disilane mixture based films.

The R* values obtained for the silane–trisilane mixture based films at differing powers and flows are shown in Figure 2-16. These results were similar to those for silane, where minimum R* values were achieved at applied powers of 200-400W, with R* increasing with power. A minimum R* of 0.047 and deposition rate of 50 Å/sec were obtained for the process at 100 sccm 16% trisilane–1000 sccm H_2 @ 400W.

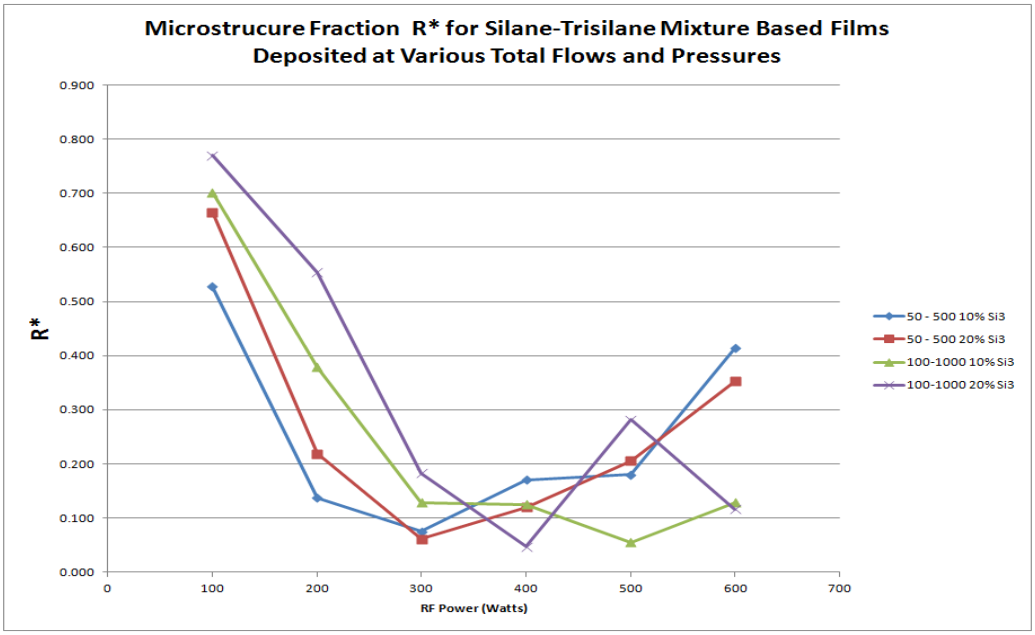

Figure 2-16: Microstructure fraction (R*) obtained for various flows and RF powers for silane-trisilane mixture based films.

In consideration of all the data obtained during screening of disilane and trisilane additives for αSi-H deposition, it became apparent that both additives provided the largest increase relative to neat silane in deposition rate at low power densities of 0.20-0.40 W/cm^2. However, these conditions also yielded R* values higher than those obtained from silane processes, suggesting relatively poor film performance due to greater light-induced degradation. The surprise finding was the ability of the additives, particularly disilane, to allow an increase in applied RF power to 1 w/cm^2 yielding a substantial increase in deposition rate while maintaining R* values of <0.10. These results suggest that higher deposition rates can be deployed to deposit αSi-H films with chemical bonding environments indicative of films yielding lower LID effects.

µCSi Deposition Rate Enhancement

Nanocrystalline or microcrystalline silicon deposition, referred to µCSi hereafter, is a film that typically requires long process times to achieve deposition of film thicknesses necessary to match the current generation of the amorphous layer in the tandem cell design. Typical HVM deposition rates of 4–5 Å/sec are used on large scale substrates. An important portion of this project was to determine what impact higher order silanes could have on enhancing these deposition rates.

One of the challenges in optimizing this process is to use conditions that yield the highest deposition rate while maintaining sufficient hydrogen dilution to deposit a film with a relatively high µCSi fraction (50–70%), with interstitial αSi-H to passivate the grain boundries. The first step in process development consisted of characterizing the performance of Air Products' 200mm PECVD platform for depositing µCSi. This was conducted using silane as the silicon source. The process chamber was evaluated by varying power, pressure, total Si flow, and the ratio of total hydrogen to silane flow (R). These process parameters would serve as a baseline for evaluating the impact on deposition rate and for comparison to deposition rates obtained by using of higher-order silanes, including disilane and trisilane.

The impact of hydrogen dilution on obtaining µCSi was investigated at constant power and pressure. The power was kept at 400W and the pressure at 5 torr. The silane flow was varied from 10 – 40 sccm, with a concomitant increase in hydrogen, except for the condition of 40 sccm silane at R=100, which could not be achieved due to the 3000 sccm limit of the H_2 mass flow controller used for the process. Table 2-4 shows the deposition rates obtained for the various dilutions. The microcrystalline fractions were verified by both Raman spectroscopy and spectroscopic ellipsometry. Process conditions where the total silane flow did not exceed 20 sccm yielded µCSi for all dilution factors. Higher flows (30 sccm) yielded µCSi at higher R values. The deposition rates increased with increased Si loading and decreasing dilution as shown in Figure 2-17. These data show that increasing the silane flow by 3X at sufficiently high R values to allow µCSi growth, yields a potential 50 - 60% increase in deposition rate relative to lower silane flows processed at lower dilution.

Table 2-4: Deposition rates determined for several silane flows at differing hydrogen dilutions. Conditions not yielding µCSi films are designated as α. The hydrogen flow was limited to 3000 sccm, therefore not allowing the 40 sccm @ R=100 condition to be tested.

SiH_4 Flow (sccm)	R=100 Dep Rate (Å/sec)	R=70 Dep Rate (Å/sec)	R=50 Dep Rate (Å/sec)	R= 40 Dep Rate (Å/sec)
10	**9.1**	**9.8**	**10.4**	**11.2**
20	**12.8**	**14.3**	**14.8**	**15.0**
30	**14.7**	**16.6**	**α**	**α**
40	**NA**	**α**	**α**	**α**

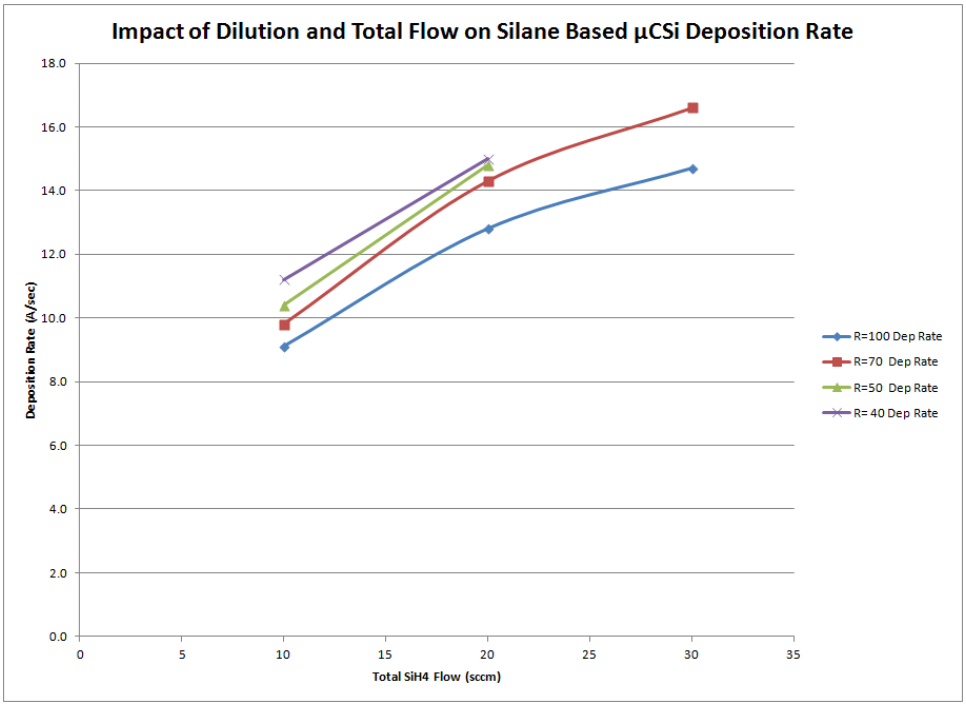

Figure 2-17: Deposition rates determined for SiH_4 at varying flows and hydrogen dilutions. µCSi could not be deposited at higher SiH_4 flows (30 sccm) when R values were <70.

The impact of pressure was investigated on the deposition rate of µCSi. Figure 2-18 shows deposition rates for silane-based films at varying silicon flow rates and pressures of 2 and 5 torr. The process power was kept constant at 800W. These data indicate that the increase in deposition rate was ~30–40% for all flows excluding 5 sccm, which had an 80% increase in deposition rate, when increasing process pressure from 2 to 5 torr. These data also indicate that deposition rate increases begin to level off as the silane flow exceeds 30 sccm, suggesting that the process becomes reaction-rate-limited at higher flows and that further increases in silane flow will not yield higher deposition rates. Figure 2-19 shows the relative ratio of deposition rates at 5 torr to 2 torr for differing RF powers and silane flows. These data also show a leveling of the pressure benefit to deposition rate at higher silane flows. It appears that lower power densities may benefit to a slightly greater extent at higher pressures. The greatest impact is observed at very low silane flows, such as 5 sccm. In this case, the increase in deposition rate was ~80% compared to the 30-40% observed at higher flows.

.

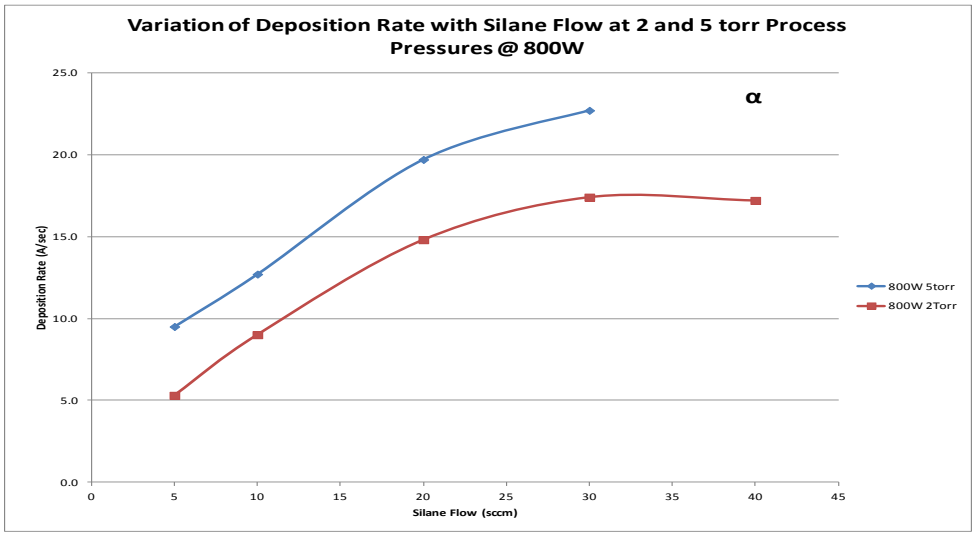

Figure 2-18: Variation of deposition rate with silane flow at 2 torr and 5 torr process pressures with 800W applied power. The 5 torr–40 sccm silane flow condition yielded αSi-H.

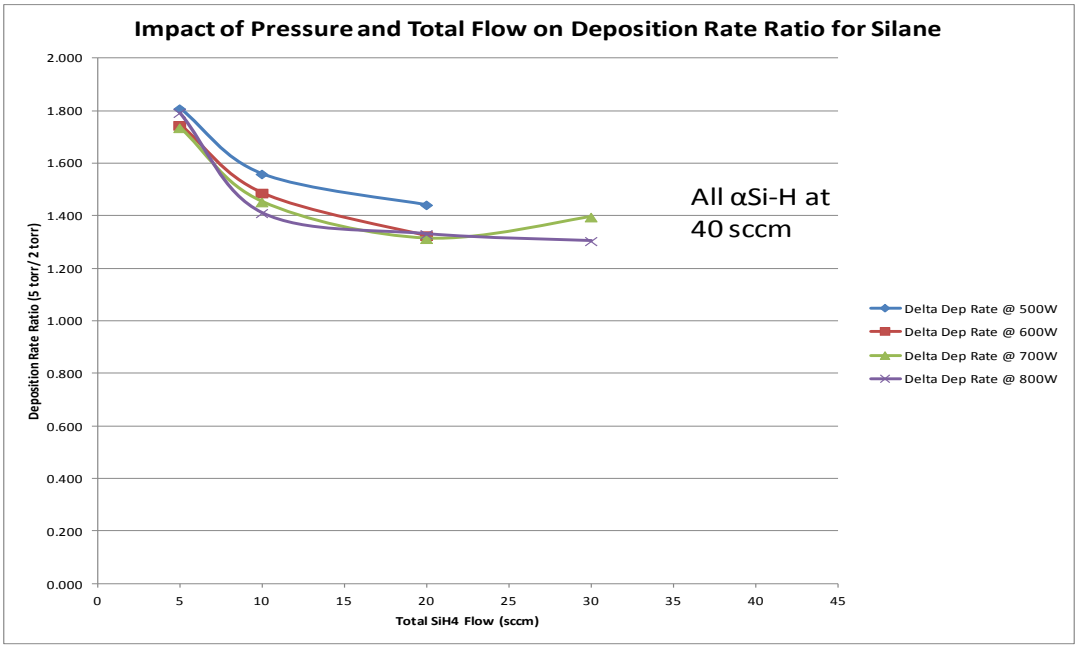

Figure 2-19: Deposition rate of µCSi at 5 torr relative to 2 torr process pressure over an RF power range of 500 – 800 W.

The impact of applied RF power on deposition rate was investigated by varying the power from 400 to 800W at two different process pressures. The dilution was maintained at R=40, and the total silane flow was maintained at 20 sccm. These were conditions that were known to yield µcSi films over the range tested. The data in Figure 2-20 show the increases in deposition rate observed at each pressure. The relative deposition rate increase was consistently higher at the lower pressure of 2 torr, with an increase of ~53%, compared to a 25% increase at 5 torr with applied power of 800W.

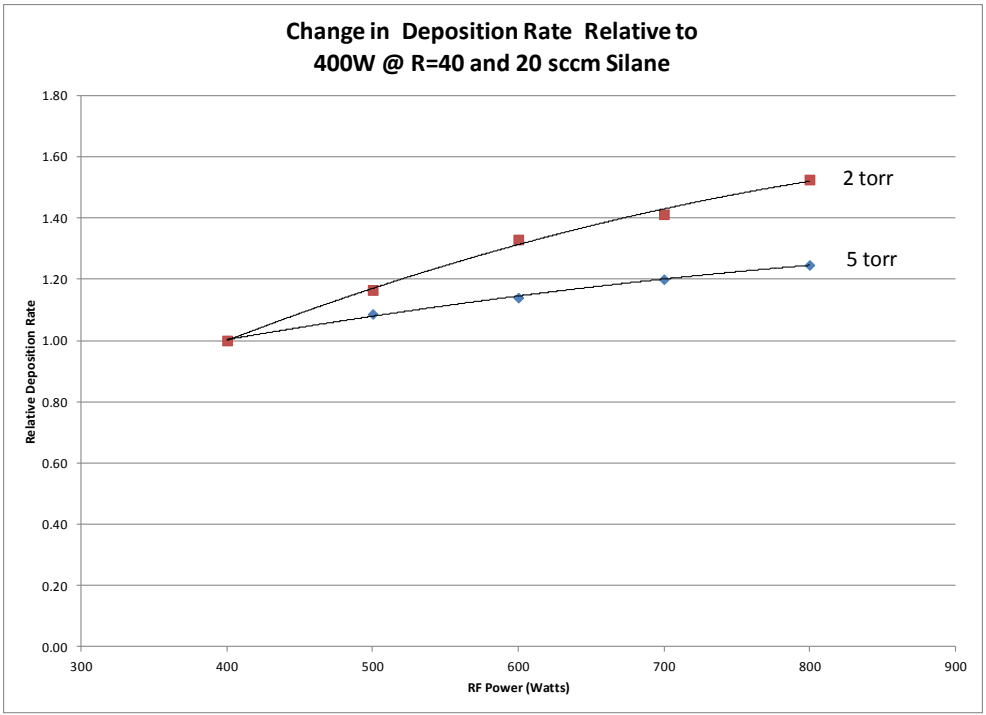

Figure 2-20: Relative change in deposition rate as a function of applied RF power. The baseline condition was 400W.

A comparison of these data to those shown in Figure 2-18 above, where the power was maintained at 800W and the silane flow was increased, indicates that the advantage of higher power density would be lost at higher flows either through the inability to nucleate µCSi growth (5 torr) or a leveling of the growth rate curve (2 torr) as the growth process becomes surface reaction rate-limited.

Once the process chamber was characterized for conditions allowing for deposition of µcSi and deposition rate using silane and hydrogen, screening tests were conducted on additives to determine the impact on growth rate. Disilane and trisilane are the two additives that were screened. Both of these molecules have physical properties that make them amenable to gas-phase delivery in sufficient volume to be used on the PECVD platform.

The first additive screened was disilane. The same sampling parameters used in silane-based depositions were deployed with a substitution of 10% or 20% dislane by volume. Figure 2-21 shows a comparison of deposition rates for silane, 10% dislane and 20% disilane at 20 sccm total silicon flow and dilution set at R=70. These data show a consistent increase in deposition rate at varying power with the additives. The increase in deposition rates relative to silane is shown in Table 2-5.

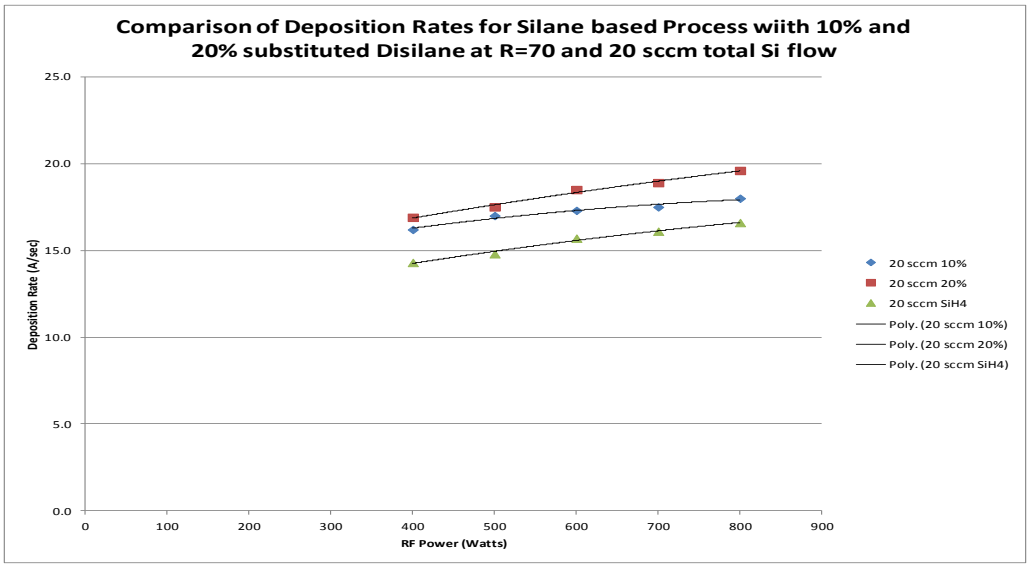

Figure 2-21: Relative comparison of deposition rates for µcSi at varying RF power under conditions of neat silane, 10% and 20% substituted disilane by volume. Dilution was maintained at R=70 or 1400 sccm H_2 flow.

Table 2-5: Increase in deposition rates compared to silane.

Power (W)	10% Disilane 20 sccm Total Si Flow	20% Disilane 20 sccm Total Si Flow
400	1.13	1.18
500	1.15	1.18
600	1.10	1.18
700	1.09	1.17
800	1.08	1.18

These results indicate that the increase in deposition rate was approximately equivalent to the increase in silicon loading from the substitution of 10% or 20% disilane for silane. Under these conditions of R=70 dilution, 5 torr pressure and RF power varied from 400–800W, disilane yielded only modest increases in deposition rates relative to neat silane.

These findings were also duplicated at lower dilution values. Figure 2-22 shows a similar experiment conducted at R=40, where the relative deposition rates are plotted vs. RF power at both 10 and 20 sccm Si flows. The bracketed data show deposition rate enhancements of 8–24% for all conditions.

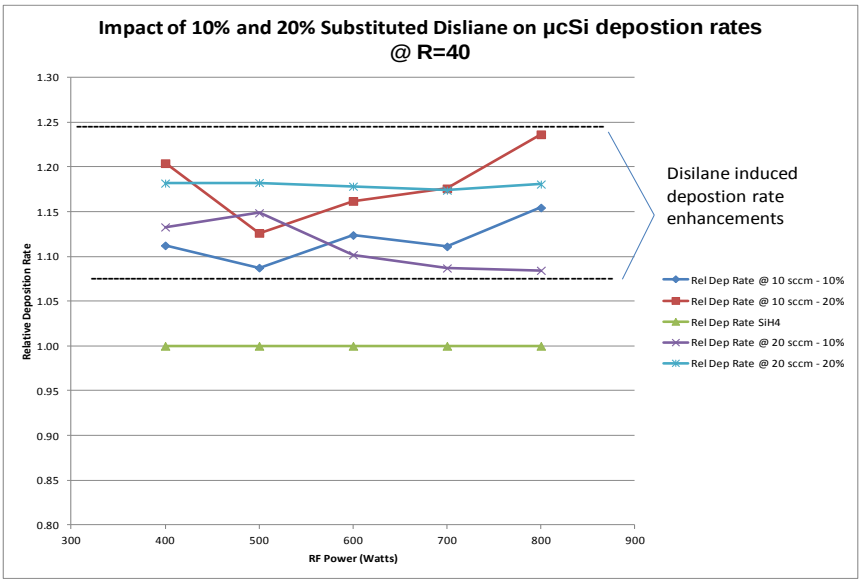

Figure 2-22: Relative comparison of deposition rates for µcSi at varying RF power under conditions of neat silane, 10% and 20% substituted disilane by volume. Total Si flow was varied from 10 to 20 sccm. Hydrogen dilution was maintained at R=40 (400 or 800 sccm).

The condition which yielded a non-stoichiometric increase in deposition rate was when the dilution was increased to R=100. Figure 2-23 shows the relative deposition rates for silane, 10% and 20% substituted disilane for total Si flows of 10, 20 and 30 sccm. These data indicate deposition rate increases of ~20% for 10% disilane and 30% for 20% disilane. The power was kept at 400W during all depositions. Use of the higher dilution allowed for growth of µCSi films during all 30 sccm total flow conditions.

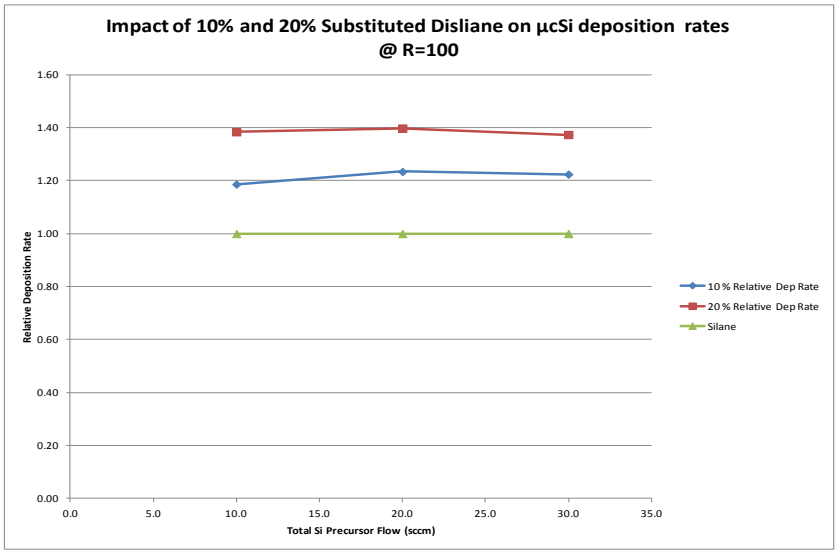

Figure 2-23: Relative deposition rates for 10% and 20% substituted disilane relative to neat silane at three total Si flows. The hydrogen dilution was kept at R=100 and power was kept at 400W.

Data generated for disilane-substituted depositions have indicated that there are certain process conditions, such as a high hydrogen dilution ratio, which will allow for a greater-than-

stoichiometric increase in the deposition rate of µCSi films. Possible mechanisms attributing to increased deposition rates have been probed through the work conducted by Air Products' subcontractors, the University of Delaware and the University of Toledo, during this study. These results will be presented in subsequent sections.

Trisilane was investigated as an additive to silane to determine the impact on deposition rate. The same experimental conditions were used for trisilane as for disilane. The results for trisilane were very similar to those obtained for disilane. A comparison of deposition rates for 10% and 20% substituted trisilane and disilane are shown in Table 2-6. These data were obtained at a dilution ratio of R= 100 and RF power of 400W. There is no significant difference in deposition rates of µCSi between the two additives. The extra silicon in trisilane does not appear to be utilized in enhancing the deposition rate. Both additives provided a greater than stoichiometric rate enhancement compared to neat silane at R=100. Figure 2-24 shows the relative rate increase observed for the conditions of R=100.

Table 2-6: Deposition rates for 10% and 20% disilane and trisilane substitutions.

Total Si Flow (sccm)	10% Disilane @ 400W	10% Trisilane @ 400W	20% Disilane @ 400W	20% Trisilane @ 400W
10.0	10.8	10.8	12.6	12.6
20.0	15.8	15.0	17.9	17.9
30.0	18.0	18.1	20.2	α

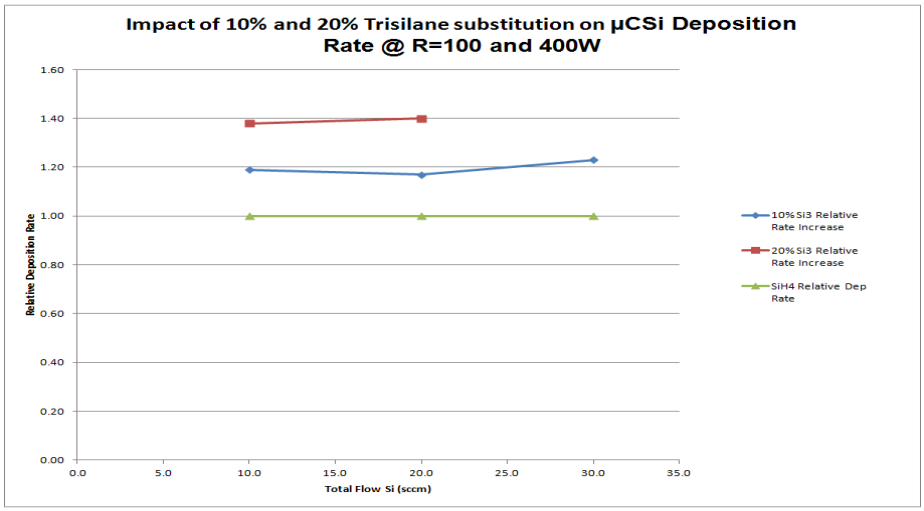

Figure 2-24: Relative deposition rates for 10% and 20% substituted trisilane relative to neat silane at three total Si flows. The hydrogen dilution was kept at R=100 and power was kept at 400W.

The performance of trisilane was very similar to disilane in increasing the deposition rate of µCSi films. It therefore was determined that, given its significantly higher price, lower volatility and lower supply chain capacity, it was not investigated in device manufacturing efforts at the University of Delaware.

PART 3: PLASMA CHARACTERIZATION USING OPTICAL EMISSION SPECTROSCOPY (OES)

OES detects the emitted species which undergo a radiative transition from an excited state to a lower energy state. The information about the species could be determined by the optical emission from their specific wavelength. The emission density is proportional to the species concentration which is determined by the electron density, electron energy distribution and gas mixture.

Figure 3-1 shows a typical OES spectrum of SiH_4/H_2 plasma with a Si_2H_6 additive (a-Si condition). The emission lines of interest include Si* (288nm), SiH* (414nm), H_α (656nm) and H_β (486nm). The emission species result from the impact between electron and molecules. This mechanism for Si* and SiH* is described as follows:

$$SiH_4 + e \rightarrow SiH_4^* \begin{cases} SiH_4^* \rightarrow Si^* + 2H_2 + e; & Si^* \rightarrow Si + hv\ (288nm) \\ SiH_4^* \rightarrow SiH^* + H_2 + H + e; & SiH^* \rightarrow SiH + hv\ (414nm) \end{cases}$$

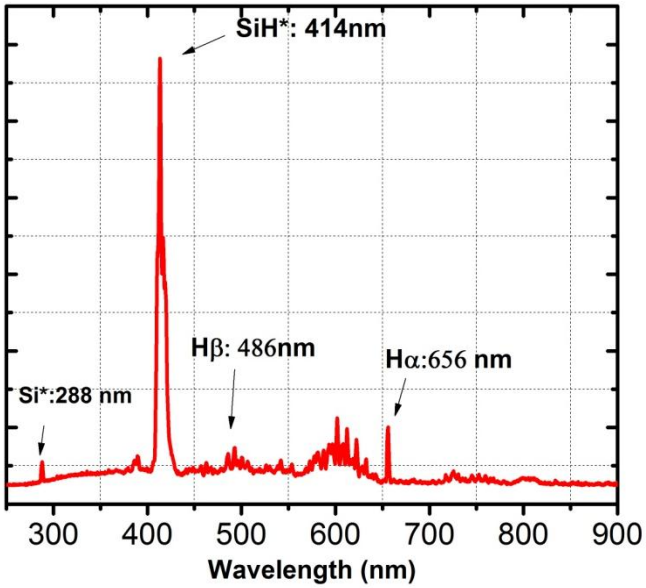

Figure 3-1: OES of SiH_4/ Si_2H_6/H_2 plasma for a typical a-Si deposition condition.

The threshold electron energy to form SiH* is 10.5eV compared with Si* at 11.5eV [J. Perrin and J. F. M. Aarts, Chemical Physics, 80 (1983) 351-365]. These species are very small part (<0.1%) of the total species in SiH_4 plasma compared with the main deposition precursors SiH_3 and SiH_2 (nonradiative). Moreover, as is well known, H dilution of SiH_4/ Si_2H_6 plasma will affect the film properties such as Rmf and H content of a-Si film and crystalline volume fraction of nc-Si. The ratio Hα/SiH* of plasma is also studied to understand the relationship between plasma and material properties.

a-Si: Material Properties

Air Products investigated a-Si film properties deposited with SiH_4+Si_2H_6 additive with and without H_2 dilution, as well as their plasma properties. Figure 3-2a shows the relationship between growth rate and power with and without 10% Si_2H_6 additive with no H_2 dilution. Whether with or without Si_2H_6 additive, the growth rate increased almost linearly with RF power. It was observed that the growth rate increase from adding 10% Si_2H_6 is less than 15%. The highest growth rate with 10% Si_2H_6 is ~5.4 Å/sec, compared with the baseline growth rate 1.8 Å/sec at IEC. The plasma becomes unstable when RF power is larger than 80W. There is no significant growth rate change for the deposition at higher total SiH_4+ Si_2H_6 flow (30sccm) at 30W and 80W.

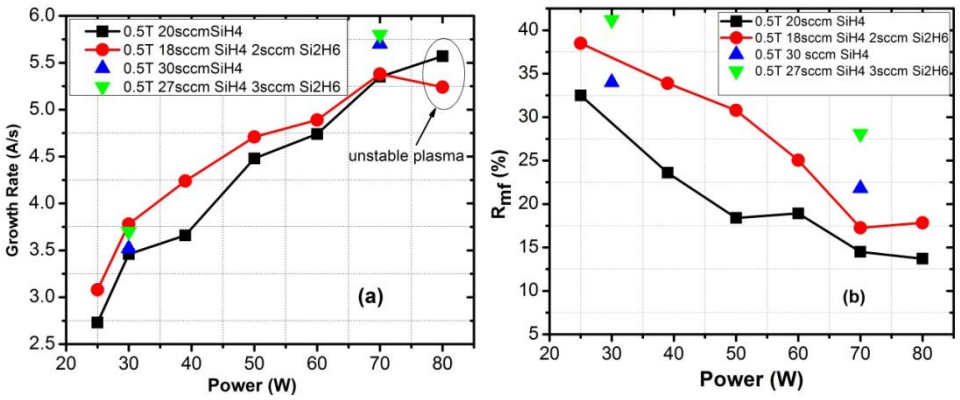

Figure 3-2: (a) Growth rate as a function of power without H_2 dilution; (b) microstructure factor.

It was found that R_{mf} decreases with increasing of RF power despite an increase in growth rate. At 20sccm without Si_2H_6 additive, R_{mf} decreased from 32% at 25W (2.7Å/sec) to 15% at 70W (5.2Å/sec). By adding 10% Si_2H_6, the Rmf slightly increased to 37% at 30W and to17% at 70W. Increasing the total flow of SiH_4/Si_2H_6 also increased the Rmf. The p-i-n solar cells with these i layers without H_2 dilution have relatively larger light-soaking degradation (>30%). Thus, to achieve both high growth rate and stability, deposition conditions are optimized by H_2 dilution, different pressure and Si_2H_6 additive.

Figure 3-3 presents the variation of deposition rate by increasing RF power at 1.25 Torr and 2.5 Torr. For the series without any Si_2H_6 (SiH_4/ Si_2H_6/H_2=10/0/50) at 1.25 Torr, the growth rate increases from 1.8Å/sec at 30W to 2.7Å/sec at 50W and saturates ~2.8 Å/sec with higher power, unlike the trend shown for the deposition rate without H_2 dilution. By adding 10% Si_2H_6 in the gas mixture, 1.7% of the total gas flow (10% more Si atoms into the chamber) at SiH_4/ Si_2H_6/H_2=9/1/50, the growth rate increased by ~30% at a power of 50W. At 2.5 Torr, the power and growth rate have a trend similar to that for 1.25 Torr. However, the growth rate increased by ~60% at 50W RF power by adding a small amount of Si_2H_6. The absolute value of growth rate enhancement is 1.6 Å/sec , which is almost 2.5 times that of the low-pressure (1.25 Torr) case. It was also found that adding another 1sccm SiH_4 (SiH_4/ Si_2H_6/H_2=11/0/50), which also leads to a

10% increase of Si atom concentration, results in less than 0.2 Å/sec growth rate enhancement at either 1.25 Torr or 2.5 Torr.

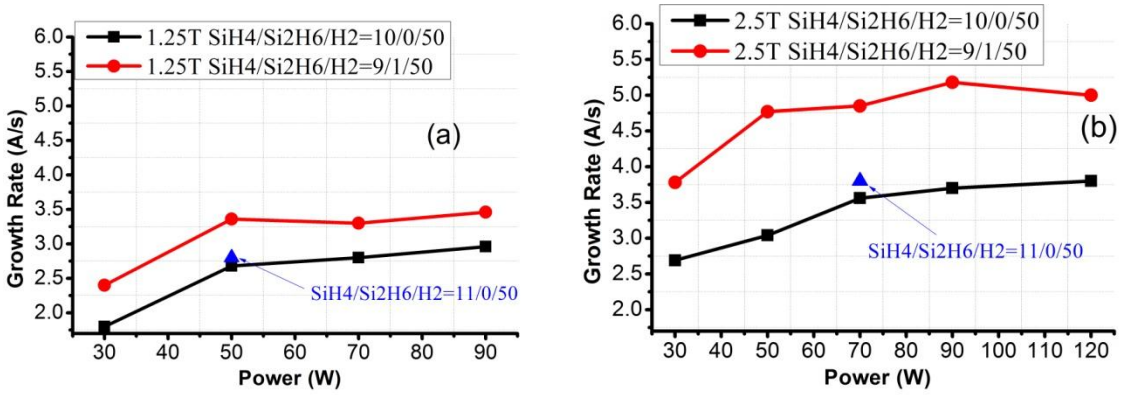

Figure 3-3: Variation of growth rate as a function of RF power at 200 ^{o}C with deposition pressure of (a) 1.25 Torr and (b) 2.5 Torr

Figure 3-4a shows the relationship between R_{mf} and power at 1.25 Torr and 2.5 Torr with and without Si_2H_6 additive with H_2 dilution (R=H2/SiH_4) of five. The R_{mf} decreases with an increase of power, a similar trend observed for the films deposited without H_2 dilution. Addition of 10% Si_2H_6 in the gas mixture slightly increases R_{mf}. However, by optimizing power, R_{mf} can be achieved <5% at 1.25 Torr and <10% at 2.5 Torr with 10% Si_2H_6 additive. Figure 3-4b presents the total hydrogen content of these films. The film H content at 1.25 Torr is lower compared with 2.5 Torr, and it decreases with increase of RF power. Addition of 10% Si_2H_6 does not increase H content in the film. The variable solar cell Voc obtained at different pressure (results shown in solar cell part) may result from the band gap change effected by the H content. (Normally higher H content increases the band gap).

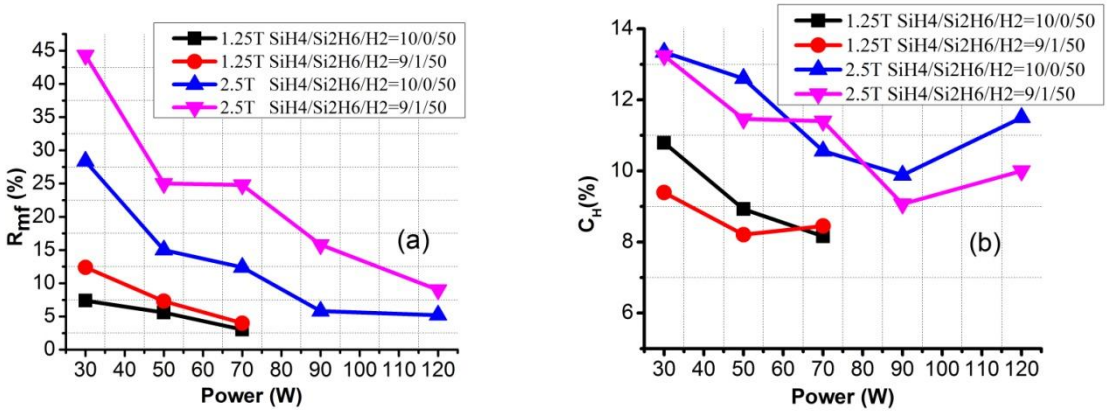

Figure 3-4: FTIR results (a) microstructure factor R_{mf}, (b) H content C_H for a-Si:H films on c-Si.

To summarize the deposition with and without H_2 dilution: the growth rate enhancement by adding 10% Si_2H_6 is much more significant in H_2 dilution compared with the one without H_2 dilution. The growth rate without H_2 is almost linear with RF power. However, the growth rate with H_2 dilution saturates at high power but could be largely enhanced by Si_2H_6 additive in gas mixture. R_{mf} is reduced by H_2 dilution which leads to the better stability for the solar cells.

a-Si: Plasma Properties

OES data of SiH_4/ Si_2H_6/H_2 discharge is studied to understand the relationship between plasma properties and the material properties. Air Products has studied OES intensities corresponding to the SiH* (414nm) and Hα (656nm) emission under different plasma conditions. Figure 3-5 presents the relationship between normalized SiH* intensity vs a-Si film growth rate with and without Si_2H_6 additive. It was found that, for a unit SiH* intensity, the gas phase with Si_2H_6 additive results in a higher growth rate. Moreover, for the gas mixture without H_2 dilution, the growth rate increase almost linear with SiH* intensity. However, for the case of H_2 dilution, further increasing SiH* by RF power doesn't lead to a higher growth rate which suggest that the growth rate is not solely dependent on Si species density for H_2 diluted plasma. The role of H is also important for both growth rate and film properties.

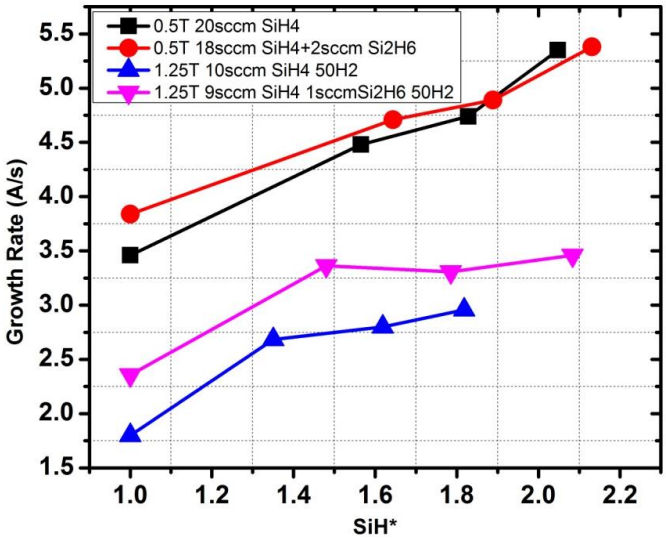

Figure 3-5: Growth rate vs normalized OES SiH* intensity

Figure 3-6 shows the Hα and SiH* intensity at 1.25 Torr discharge as a function of RF power. Both Hα and SiH* intensity increase at higher RF power. However, Hα intensity increases more rapidly than does SiH* intensity. Moreover, the SiH* signal continues to increase with higher power, suggesting that the saturation of the growth rate at higher power (shown in Figure 3-3) is not due to the SiH_4 depletion condition.

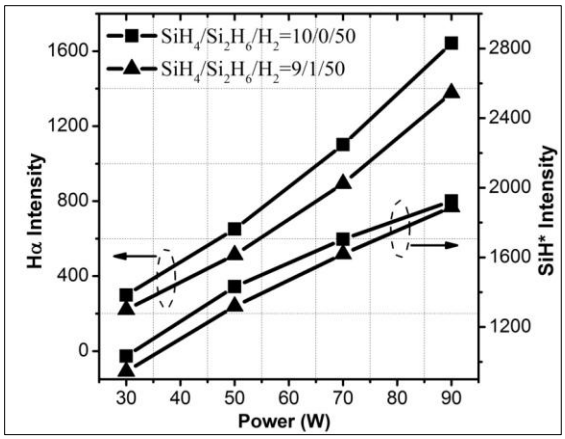

Figure 3-6: OES Hα and SiH* as a function of RF power.

Figure 3-7 shows Hα/SiH* intensity of SiH_4/ Si_2H_6 discharge with and without H_2 dilution as a function of RF power. Both with and without H_2 dilution conditions, Hα/SiH* increases at higher RF power. Hα/SiH* ratio increases much faster in SiH_4/ Si_2H_6/H_2 discharge compared with SiH_4/ Si_2H_6 discharge. In Figure 3-6, SiH* increases at high power, but H intensity increases even faster. Thus, H concentration at the growth surface is larger at higher power. Large amounts of H at the film growth surface is expected to reduce the growth rate. This might be the reason for growth rate saturation at high power with H_2 dilution. It is believed that atomic hydrogen also decreases R_{mf} by structural relaxation. Thus, reduction of R_{mf} with increasing power (Figures 3-2 & 3-4) could be explained by the higher Hα/SiH* ratio observed in OES. By adding 10% Si_2H_6, the Hα/SiH* ratio decreases (Figure 3-7) which can lead to the higher R_{mf} of the film deposited with SiH_4/ Si_2H_6/H_2 discharge compared to the film deposited without Si_2H_6.

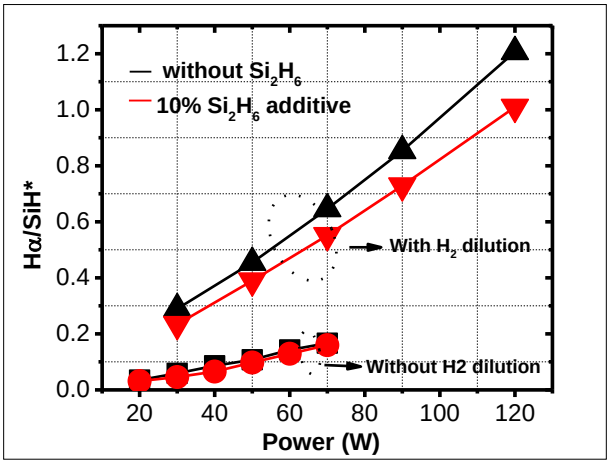

Figure 3-7: Ratio of Hα/SiH* as a function of RF power with and without H_2 dilution.

Figure 3-8 shows OES of SiH* intensity measured at different power levels with different fractions of Si_2H_6 additive. For a fixed gas mixture, SiH* intensity increases with higher power. For a fixed power, SiH* intensity decreases as the Si_2H_6 fraction increases. As mentioned before, radiative species SiH* is formed by the impact between electron (>10.5 eV) and SiH_4 molecule. The reduction in SiH* intensity by adding Si_2H_6 may indicate the reduction of high-energy electron impact, or probably lower electron temperature.

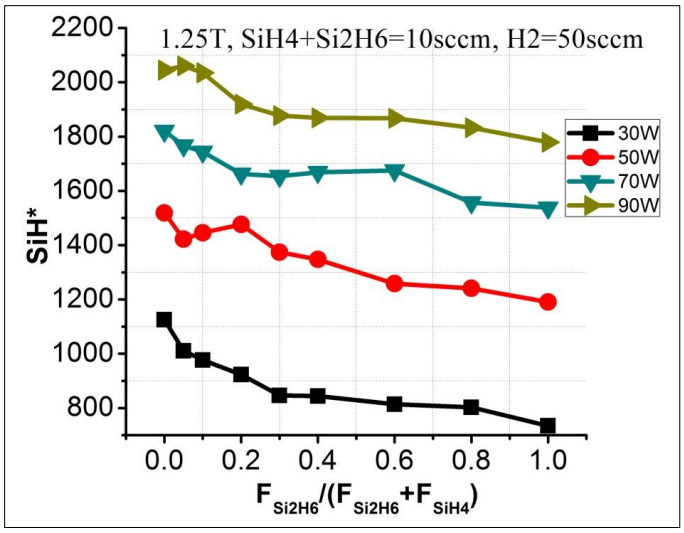

Figure 3-8: SiH* emission intensity at 414 nm as a function of Si_2H_6 fraction and RF power.

nc-Si: Material Properties

Table 3-1 lists the growth rate and Raman crystallinity (X_c) of nc-Si films with different SiH_4 / Si_2H_6 flow rates. Other parameters include RF power of 300W, deposition pressure of 3 Torr and substrate temperature of 200 C were kept constant.

Table 3-1: nc-Si growth rate, X_c with different H_2/SiH_4 ratio.

Sample ID	SiH_4 (sccm)	Si_2H_6 (sccm)	Ratio (H_2/SiH_4)	Growth Rate (Å/s)	X_c (%)
MC0684	7	0	71.4	**1.73**	67.9
MC0685	8	0	62.5	**2.02**	62.8
MC0687	9	0	55.6	**2.23**	62.3
MC0690	10	0	50.0	**2.31**	58
MC0688	11	0	45.5	**2.71**	52.2
MC0693	12	0	41.7	**2.73**	42.6
MC0692	13	0	38.5	**2.78**	38.6
MC0689	14	0	35.7	**3.19**	0
MC0704	8	2		**2.84**	56

IEC also optimized the cable connection both inside and outside of the chamber to improve the power delivery and avoid overheating at high-power conditions. Table 3-2 lists the growth rate (Xc) of nc-Si with different gas mixtures with different RF power at 3 Torr. At 500W with SiH_4/ Si_2H_6/H_2=12/1/450, the highest growth rate of 7.8 Å/sec was achieved.

Table 3-2: nc-Si growth rate, X_c with different gas mixtures and RF powers.

Sample	SiH_4 (sccm)	Si_2H_6 (sccm)	Power (w)	Rd (Å/s)	X_c (%)
MC1017	**13**	**0**	**400**	**4.5**	**66**
MC1007	**11**	**1**	**400**	**4.4**	**57**
MC1016	**12**	**1**	**400**	**5.3**	**52**
MC1018	**12**	**1**	**500**	**7.8**	**65**
MC0997	**12**	**1**	**200**	**4.9**	**10**

Effect of Substrate on nc-Si Structure: (Glass vs ZnO-Coated TEC8 versus Texture-Etched ZnO:Al)

A nc-Si thin film was deposited (8 Torr; SiH_4/H_2=8.5/300;515W) on glass, ZnO-coated TEC8 (Z-Tec8) and textured, Al-doped ZnO (AZO). Figures 3-9a and b show the surface morphology of Z-Tec8 and AZO substrate as measured by AFM. Figure 3-9c shows the XRD spectra of the nc-Si films deposited on these three substrates. Both the grain size and orientation exhibit a strong substrate dependency. The film on polished glass has the dominant (220) orientation. The film on ZnO-coated TEC8 ("V" shape texture) has slightly higher (111) and lower (220) peaks. The film on texture AZO ("U" shape texture) has a higher (220) peak compared with Z-Tec8. The film deposited on the textured substrate has smaller grain size, which may result from the boundary collision during the growth. Moreover, film on the U-shaped AZO has larger grain size compared with the V-shaped TEC8.

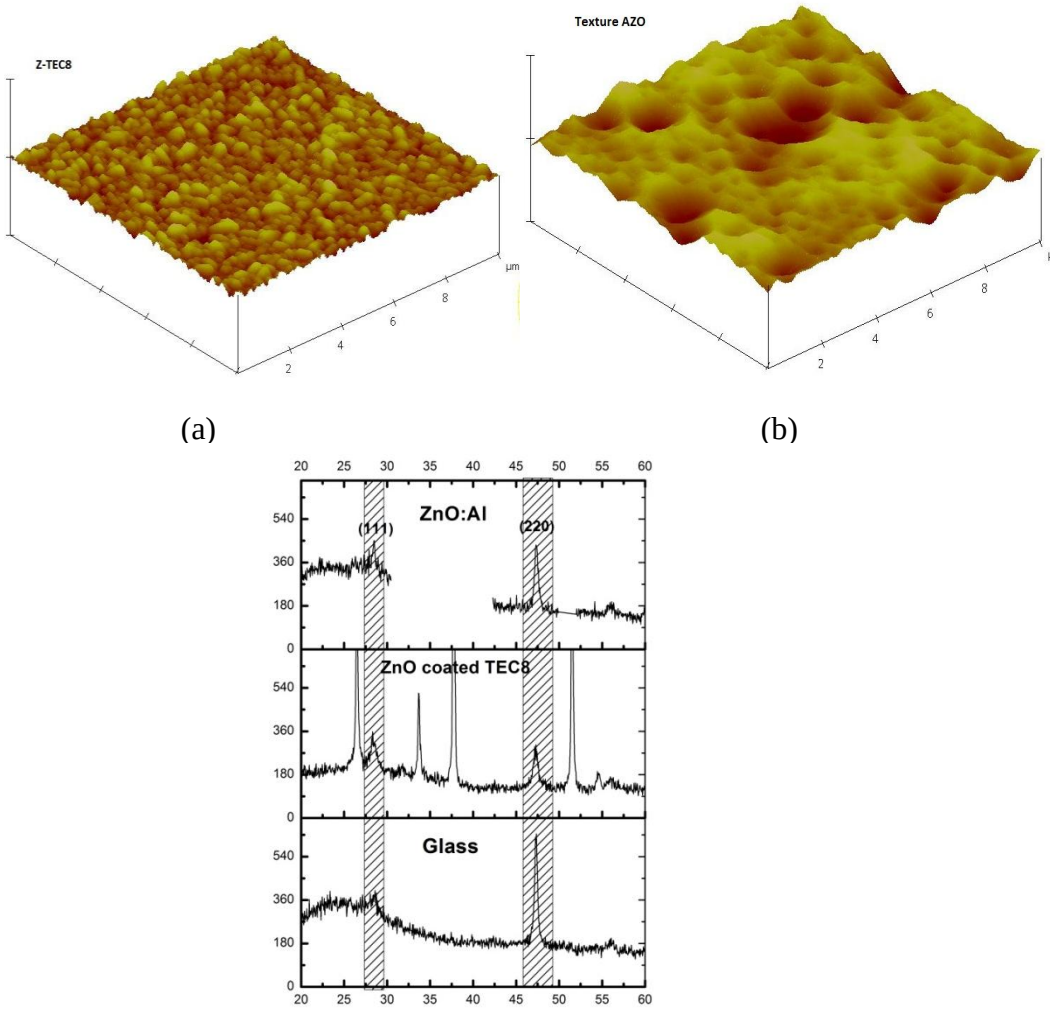

Figure 3-9: (a) AFM image of ZnO-coated TEC8, (b) AFM image of textured ZnO:Al, (c) XRD of nc-Si on glass,ZnO coated TEC8 and Textured ZnO:Al

nc-Si: Plasma Properties

OES is also used to characterize the plasma in nc-Si deposition regime. nc-Si is normally deposited with high power and high H_2 dilution (SiH_4 depletion). Figure 3-10 shows the OES spectrum of the plasma at 3 Torr with and without Si_2H_6 additive. Compared with Figure 3-1, which relates to a-Si deposition regime, the main emitted species inside plasma is H instead of SiH*. With 10% Si_2H_6 additive, Si* and SiH* intensity (from high energy impact) decreases, which is similar to what was observed in the a-Si regime. At high power and high H_2 dilution, the Si_2H_6 additive could also play a role in reducing the high-energy impact between electrons and SiH_4 molecules.

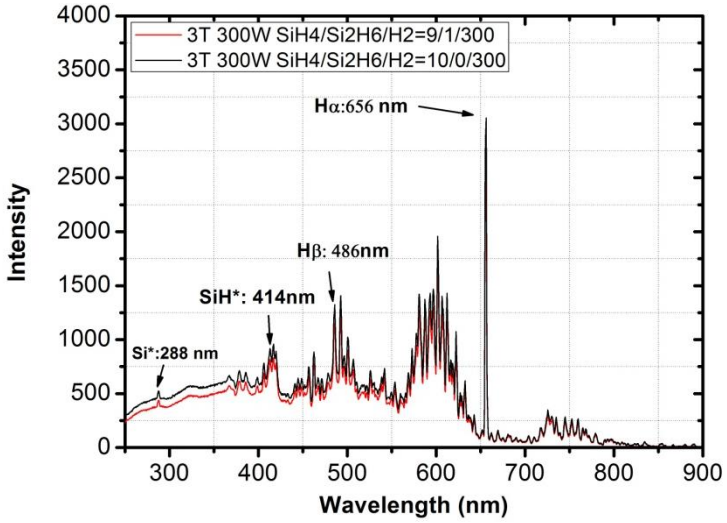

Figure 3-10: OES of SiH_4/ Si_2H_6/H_2 plasma at the nc-Si deposition condition.

Figures 3-11 and Figure 3-12 show OES data at 3 Torr; H2=500sccm; power 300W~500W. Figure 3-11 presents the intensity of SiH* and Hα with different SiH_4 flows (different H_2/SiH_4). Figure 3-12 presents the ratio of Hα/SiH* under different conditions. As shown in Figure 3-11, by increasing SiH_4 flow (lower H_2/SiH_4), SiH* intensity increases while Hα intensity remains constant. In Figure 3-12, the ratio of Hα/SiH* decreases when H_2/SiH_4 decreases, while Raman X_c also decreases. It may result from the reduction of the atomic H flux to growing surface by the H annihilation reaction in gas phase $H+SiH_4 \rightarrow H_2+SiH_3$. By increasing RF power, Hα/SiH* increases. H increased faster than SiH* inside plasma thus results in the higher Xc.

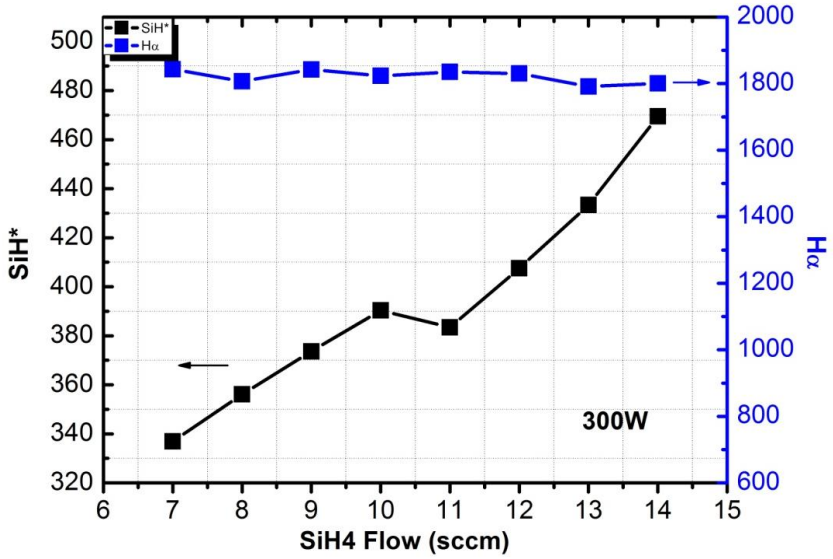

Figure 3-11: OES SiH* and Hα as a function of SiH_4 flow.

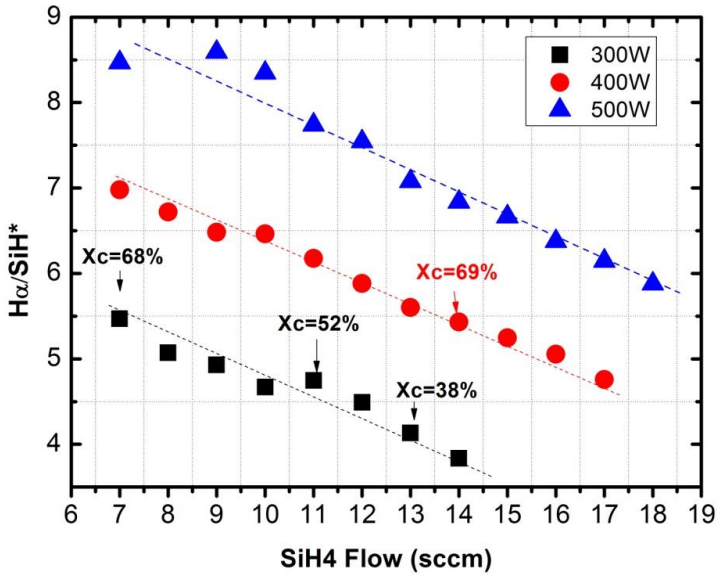

Figure 3-12: OES Hα/SiH* as a function of SiH_4 flow at different RF powers.

Figure 3-13 presents the OES data of SiH* and Hα intensity with and without Si_2H_6 as a function of pressure. The intensities of both SiH* and Hα decrease at higher pressure. By adding 10% Si_2H_6, SiH* intensity decreases, a similar effect observed in the a-Si regime.

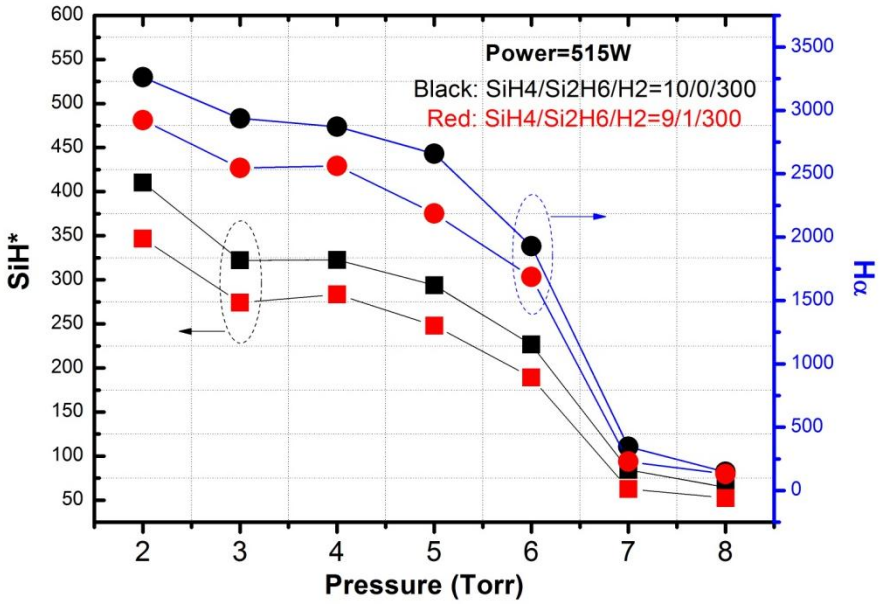

Figure 3-13: OES SiH* and Hα intensity as a function of pressure.

PART 4: PLASMA CHARACTERIZATION USING A LANGMUIR PROBE

A Langmuir probe is a metal probe inserted into a discharge and biased with positive or negative voltage to draw the electron or ion current. Plasma parameters such as electron density, electron temperature, plasma potential and electron energy distribution function (EEDF) could be calculated by analyzing the current and biased voltage. The probe tip is inserted into the plasma and a bias voltage is added to the tip, so the I-V curve can be measured. By analyzing the I-V data, various plasma properties can be obtained such as electron density, electron temperature, plasma potential and electron energy distribution.

In the basic equation of the I-V: $I = \frac{1}{4} A * e * N_e * \exp\frac{-e(V_p - V)}{kT_e} * \sqrt{\frac{8kT_e}{\pi m_e}}$. A is the tip area, V is the bias voltage, Vp is the plasma potential, Ne is the electron density, and Te is the electron temperature. Vp is determined by the voltage where $\frac{dI}{dV}$ is maximum. Te and Ne is determined by the curve fit of lnI vs V. EEDF is calculated through second differential of I-V by *Druyvesteyn Method.*

Figure 4-1 presents the ion current corrected I-V for SiH_4/ Si_2H_6/H_2 discharge at 1.25T 90W. (electron I-V). As seen in the I-V curve, the current with 10% Si_2H_6 additive is higher than the one without additive, which suggests adding Si_2H_6 increases the electron density inside plasma.

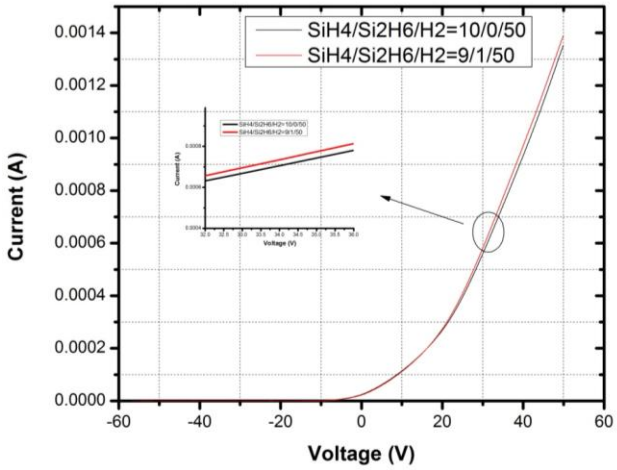

Figure 4-1: Langmuir Probe electron current as a function of bias voltage.

Figure 4-2 presents the comparison of $\frac{dI}{dV}$ with low power plasma with different fraction of Si_2H_6. Adding Si_2H_6 into the gas mixture shifts the plasma potential to lower values, which might be related to lower electron temperature. After fitting the lnI vs V curve, the average electron temperature is 5.4eV for SiH_4/Si_2H_6/H_2=10/0/50 and 5.0eV for SiH_4/ Si_2H_6/H_2=9/1/50.

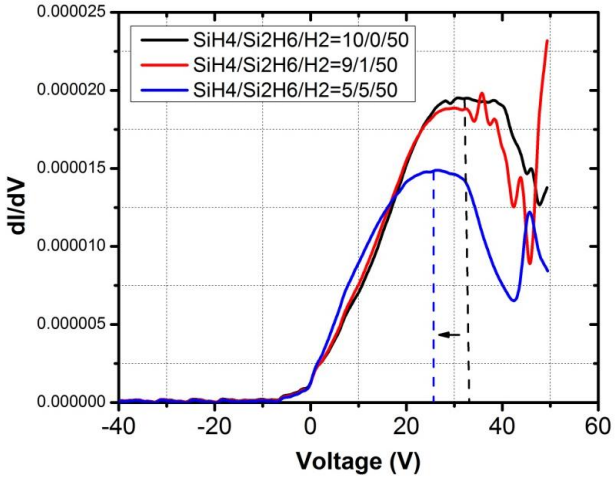

Figure 4-2: Langmuir probe $\frac{dI}{dV}$ with different fractions of the Si_2H_6 additive.

Figure 4-3 (a) and (b) presents EEDF of the plasma (nc-Si regime) at 2.5 Torr 200W and 400W. Table 4-1 shows the electron density and plasma potential estimated from the Langmuir probe IV measurements. Increasing RF power leads to higher electron density. At 200W, with 10% Si_2H_6 additive, the electron density is increased by about 10%. The corresponding EEDF curve in Figure 4-3(a) shows that the density of electrons with low energy (<15 eV) increases with the addition of Si_2H_6. However, at 400W, the effect of Si_2H_6 to increase electron density is much weaker than the effect at 200W, but the increase of low-energy (<8 eV) electron density is still noticeable in the EEDF (Figure 4-3(b)). The plasma potential decreases with Si_2H_6 additive at both 200W and 400W.

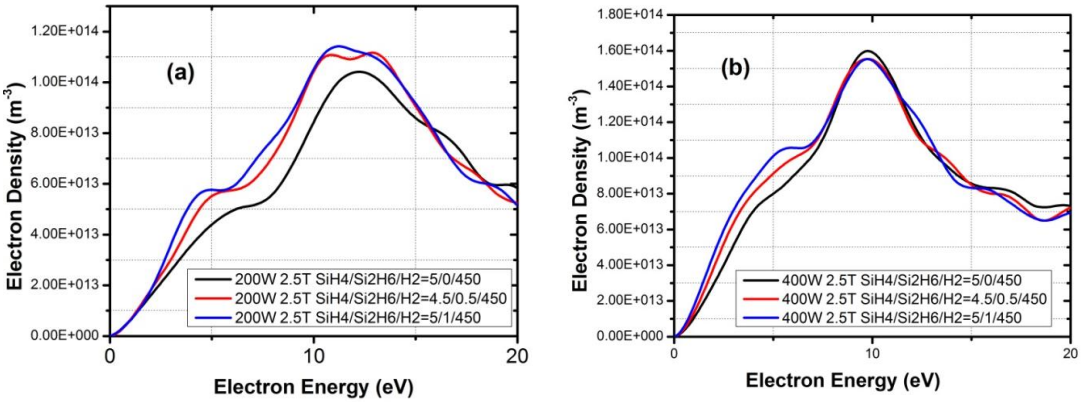

Figure 4-3: EEDF of SiH_4/ Si_2H_6/H_2 plasma at RF power 200W and 400W.

Table 4-1: Electron density and plasma potential of SiH_4/ Si_2H_6/H_2 plasma at RF power 200W and 400W.

Power (W)	SiH_4/ Si_2H_6/H_2	Electron Density (m^{-3})	Plasma Potential (V)
200	5/0/450	1.22E15	48.9
200	4.5/0.5/450	1.35E15	48.2
200	5/1/450	1.39E15	47.5
400	5/0/450	1.76E15	43.5
400	4.5/0.5/450	1.81E15	42.9
400	5/1/450	1.83E15	42.1

Therefore, the electrical characterization of plasma using a Langmuir probe suggests that the addition of Si_2H_6 leads to an increase in low-energy electron density, and the enhancement of electron density is less pronounced at higher RF power. This also explains why the intensity of SiH* (threshold energy 10.5 eV) and Si* (threshold energy 11.5 eV) diminishes with the addition of Si_2H_6 (Figure 3-8). Such a shift of EEDF to lower energy levels also increases electron impact dissociation of SiH_4 molecules (with low threshold energy of 8.75 eV to 9.47 eV) into films forming SiH_3 radicals. Meanwhile, the dissociation of single Si_2H_6 molecules also provides two SiH_3 species. The combination of these two effects, namely more Si atoms and enhanced electron density, leads to a higher growth rate with an Si_2H_6 additive.

PART 5: MICROSTRUCTURAL EVOLUTION STUDIES – IN-SITU MEASUREMENTS TO DIFFERENTIATE SILANE AND SILANE+ADDITIVE

The microstructure of hydrogenated silicon-based (Si:H) thin films of interest for photovoltaic (PV) applications may vary with deposition parameters or thickness.[10] Si:H prepared by plasma-enhanced chemical vapor deposition (PECVD) may exhibit different growth regimes – amorphous (a-Si:H), nanocrystalline (nc-Si:H), and mixed-phase (amorphous+nanocrystalline, a+nc-Si:H) – often within the same film as a function of thickness. Several structural transitions may occur during the growth evolution of Si:H. Initially, the film may nucleate as clusters of amorphous- or nanocrystalline-phase material on the substrate surface. These clusters continue to grow in size and the surface roughness increases until contact is made with neighboring clusters, at which point the surface roughness begins to decrease. In a-Si:H, a competition between atomic-scale roughening and capillary-driven diffusion of precursors across the sample surface dictates the evolution of roughness.[17,18] These same effects play a role in the growth of nc-Si:H, but competitive growth of neighboring crystalline grains also impacts the roughness evolution.

After nucleation and coalescence of a-Si:H clusters on the surface, the material's surface roughness will decrease with increasing thickness until reaching a minimum or stable-surface regime. The duration of this regime is controlled by the diffusion length of precursors across the surface, interactions with atomic hydrogen in the plasma, and the nature of the precursors. If the diffusion length of precursors across the surface is sufficiently large and the film remains amorphous, then the film will remain smooth with a consistent surface roughness value. When the surface diffusion length of precursors is smaller than the in-plane feature size of the surface roughness, the surface roughness value will increase from the minimum stable-surface regime while the material remains in the amorphous phase. This structural transition is denoted as the amorphous-to-amorphous roughening [a→a] transition.

Alternately, material may initially evolve as amorphous but nucleate crystallites at a thickness determined by processing conditions. In this case, nanocrystallites form at the film surface and grow preferentially over the surrounding amorphous material. This preferential growth causes a drastic increase in surface roughness as the crystallites protrude and continue to grow larger. The initial appearance of crystallites from the amorphous phase is denoted as the amorphous-to-mixed-phase (amorphous+nanocrystalline) [a→(a+nc)] transition. As the crystallite growth continues to dominate over the amorphous phase, the crystallite protrusions will increase in size such that they occupy the majority of the film surface – at which point the crystallites coalesce to form a single-phase nanocrystalline film. This transition is denoted as the mixed-phase-to-single-phase-nanocrystalline [(a+nc)→nc] transition, and is accompanied by the observation of a maximum in surface roughness followed by a decrease.

These types of structural transitions and growth evolutions have been observed for Si:H prepared under a variety of deposition conditions[1] and its alloys with germanium[19] ($Si_{1-x}Ge_x$:H) and carbon[20] ($Si_{1-x}C_x$:H). The comparison of the behavior of these transitions as a function of single deposition parameters has been used to produce so-called deposition phase diagrams or growth evolution diagrams, which have guided the development of optimization principles in Si:H-based PV.[10,21-25] For example, the structural evolution can be controlled by diluting reactive silicon carrying gases with H_2 during the deposition process. Films prepared at a low H_2 dilution remain amorphous throughout their total thickness, while those prepared at higher dilutions nucleate crystallites. The [a→a] transition has been observed to increase proportionally with H_2 dilution for films that remain amorphous, and the optimum a-Si:H-based PV devices incorporate layers prepared under conditions where the highest H_2-dilution is used without nucleating crystallites within the thickness desired for the amorphous layer.[10,21,23] Interestingly, optimum nc-Si:H PV devices often incorporate layers prepared at the lowest H_2 dilution where crystallite growth can occur.[22,24,25] The nc-Si:H layers are often fabricated using H_2-grading approaches in order to manipulate the evolution and degree of crystallinity with the layer.

This work studies the effects of adding disilane (Si_2H_6) to the standard silane (SiH_4) precursor on the growth evolution of Si:H, assessed through *in situ*, real-time spectroscopic ellipsometry (RTSE) during film growth. RTSE is a non-invasive, non-destructive, non-contacting optical measurement technique and, when applied during film deposition, allows for the extraction of time dependence of the structural (bulk layer thickness, surface roughness) and optical properties of a film. The results of these RTSE studies indicate the potential impact of these additives on the evolution of crystallinity, material deposition rate, and electronic quality of the material.

Experimental Details

The Si:H films for phase diagram development were deposited on native-oxide, coated-crystal silicon (c-Si) wafers in a load-locked rf (13.56 MHz) PECVD chamber. Measurements were taken in real time using a rotating-compensator, multichannel ellipsometer.[1,2] Native oxide-covered c-Si wafers were chosen to maintain the highest sensitivity to the evolution of surface roughness and bulk layer thickness with time. Fixed deposition parameters included a low substrate temperature of $T_s = 200^oC$, a low total pressure of $p = 0.8$ Torr, and a low plasma power density of $P = 0.04$ W/cm^2. Variable parameters include the hydrogen-to-reactive-gas ratio, $R = [H_2] / \{[SiH_4] + [Si_2H_6]\}$, to control the microstructure and the silane-to-disilane gas ratio, $S = [Si_2H_6] / \{[SiH_4] + [Si_2H_6]\}$, to impact the growth rate and film structure. Several different series of films were prepared: three at fixed S values (0, 0.2, and 1) as a function of R, and two with a fixed R and variable S.

Results and Discussion

S = 0, Variable R: Si:H Growth Evolution Baseline

Figure 5-1a shows the change in surface roughness thickness, d_s, as a function of bulk layer thickness, d_b, for films prepared at $S = 0$ and low values of R such that the films remain amorphous throughout growth. Figure 5-1b shows d_s as a function of d_b for material prepared at

S = 0 and higher values of R so that crystallites nucleate from the amorphous matrix. The a→a transition for the a-Si:H films in Figure 5-1a is observed as the small increase in d_s after smoothening of the initial amorphous clusters. Figure 5-1b shows the a→(a+nc) and (a+nc)→nc transitions in the Si:H films as the sharp increase in d_s from the smooth stable a-Si:H surface regime and the subsequent maximum in d_s, respectively. The results are summarized in the deposition phase diagram (Figure 5-2a) showing amorphous, mixed-phase, and nanocrystalline growth regimes, as well as the a→a, a→(a+nc), and (a+nc)→nc transitions. The highest H_2 dilution prior to crystallite nucleation occurs at R = 15 for a ~1000 Å thick layer, which also has the longest stable-surface regime among this series. This behavior indicates that optimum a-Si:H material with no Si_2H_6 may be produced at R = 15, and that optimum nc-Si:H may be produced at slightly higher R. Unfortunately, as is common for Si:H materials, the deposition rate decreases with increasing R, as shown in Figure 5-2b. The increased amount of atomic hydrogen present in the plasma expected from the increase in H_2 dilution may etch weakly-bonded material at the film surface. This etching leads to the removal of potentially defect-rich material, but slows the deposition rate.

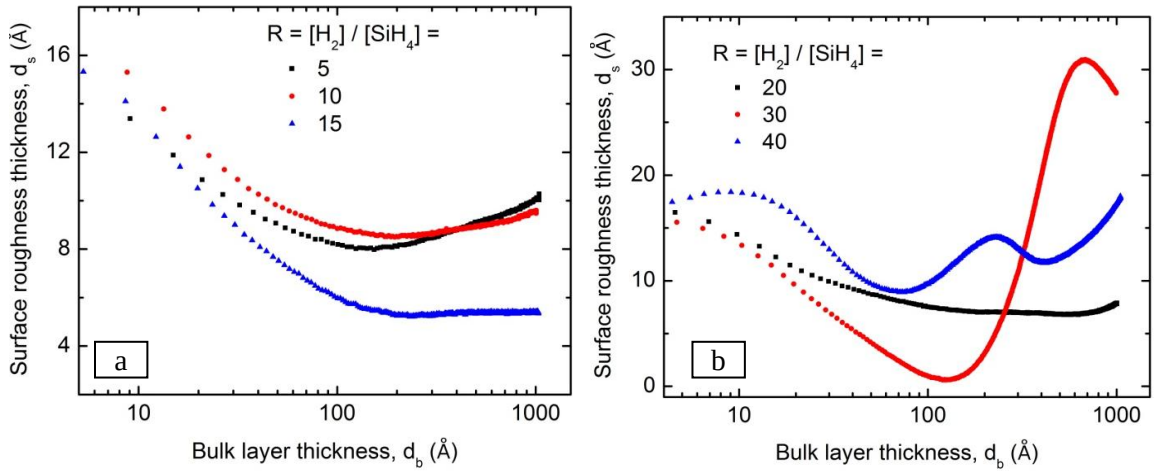

Figure 5-1. Growth evolution of hydrogenated silicon (Si:H) in the form of the surface roughness layer thickness, d_s, as a function of bulk layer thickness, d_b, for films prepared at fixed silane-to-disilane ratio, $S = [Si_2H_6] / \{[SiH_4] + [Si_2H_6]\} = 0$, and variable H_2-dilution, $R = [H_2] / \{[SiH_4] + [Si_2H_6]\}$ that (a) remain amorphous throughout growth or (b) nucleate crystallites which subsequently evolve with thickness.

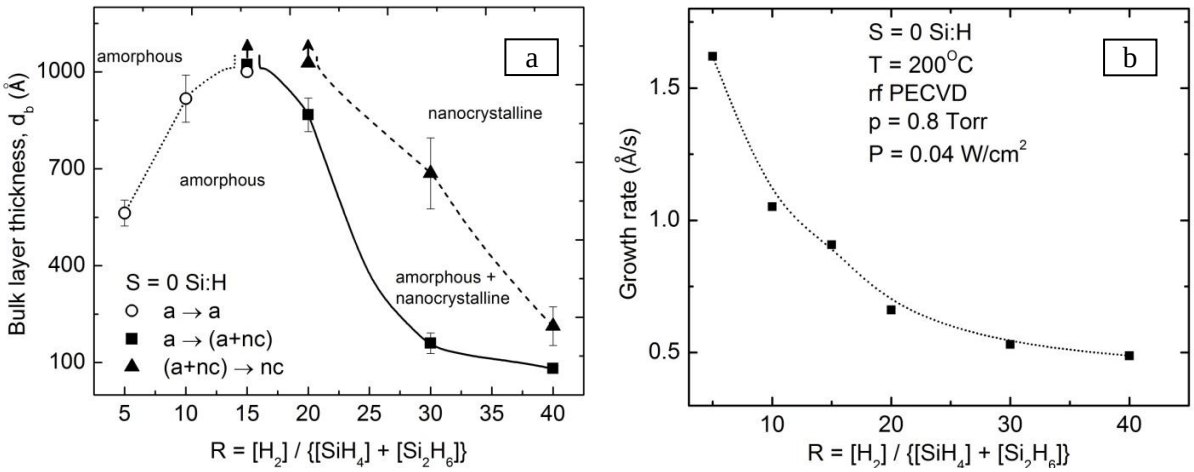

Figure 5-2: (a) Deposition phase diagram for Si:H prepared at S = 0 and variable R depicting the amorphous-to-amorphous roughening [a→a], aorphous-to-mixed-phase (amorphous+nanocrystalline) [a→(a+nc)], and mixed-phase-to-single-phase nanocrystalline [(a+nc)→nc] structural transitions. Arrows pointing upward indicate the respective transition occurs beyond the maximum thickness measured. (b) Film growth rate for Si:H prepared at S = 0 and variable R.

R = 15, Variable S: a-Si:H Growth Evolution

Beginning from *R* = 15 a-Si:H prepared at *S* = 0, *S* was increased to study its impact on material prepared near an optimum condition. Figure 5-3a shows the growth evolution for *R* = 15 a-Si:H prepared as a function of *S*. The films all remain amorphous throughout growth, but the a→a transition decreases with increasing *S* (Figure 5-3b). Growth rate increases with *S* (Figure 5-4), as expected from the increased amount of silicon present due to replacement of some SiH_4 with Si_2H_6 in the plasma. The decrease in the a→a transition accompanying this increased film growth rate indicates that the films may be of lower electronic quality, as the surface diffusion length of precursors limits the ability to form a more stable surface. Overall, increasing *S* for a fixed *R* in the amorphous growth regime results in higher deposition rates but likely degrades material quality.

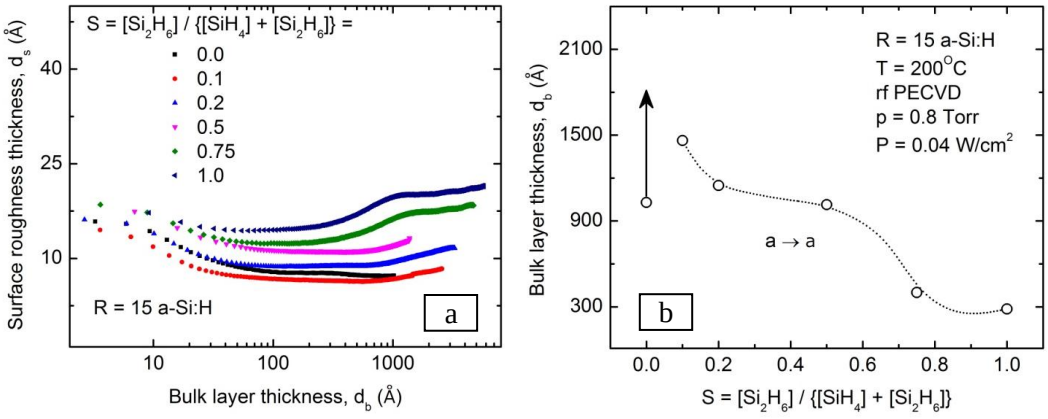

Figure 5-3: (a) Growth evolution of Si:H in the form of ds as a function of db, for films prepared at fixed R = 15 and variable S. (b) a→a transition thickness for a-Si:H at fixed R = 15 and variable S. Arrows pointing upward indicate the respective transition occurs beyond the maximum thickness measured.

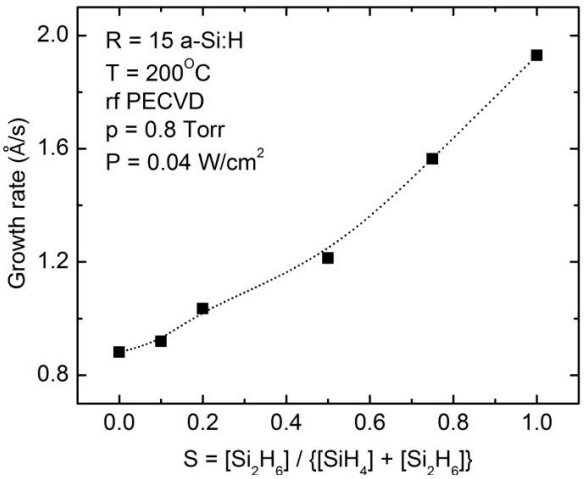

Figure 5-4: Film growth rate for a-Si:H prepared at R = 15 and variable S.

R = 30, Variable S: a→nc-Si:H Growth Evolution

An additional series for *R* = 30 Si:H prepared as a function of *S* was evaluated to detect how the addition of Si_2H_6 may alter crystallite evolution. Figure 5-5a shows the growth evolution for *R* = 30 Si:H prepared as a function of *S*. The films prepared at $S \leq 0.2$ nucleate crystallites at a given thickness, while those at $S \geq 0.5$ remain in the amorphous regime. Figures 5-5b and 5-6 show the structural transitions and growth rate, respectively, as a function of *S* for these films. At high *S*, crystallite nucleation is suppressed and the a→a transition decreases with increasing *S*, similar to the behavior of the *R* = 15 series. The deposition rate for the a-Si:H at high *S* increases at a slower rate with *S* compared to the *R* = 15 series. This behavior may be due to increased etching by atomic hydrogen in the plasma. The films nucleate crystallites at approximately the same bulk layer thickness, but crystallite coalescence and the (a+nc)→nc transitions vary drastically. There is a decrease in the thickness at which crystallites coalesce from *S* = 0 to 0.1, indicating that the material prepared at *S* = 0.1 may have a higher initial nucleation density of crystallites or a wider cone angle, assuming that the crystallites evolve using a cone growth model as has been observed for other Si:H based materials.[10,26] Crystallite nucleation and coalescence is delayed for the *S* = 0.2 deposition compared to lower *S*, as would be expected based on the suppression of crystallinity for high-*S* films. The deposition rate increases sharply from *S* = 0.1 to 0.2, which may be related to the change from promoting crystallinity (by higher nucleation density or wider cone angles) for *S* = 0.1 to suppressing crystallinity at $S \geq 0.2$. Overall, the comparison between *S* = 0 and 0.1 indicates that varying *S* may serve as another parameter in manipulating and optimizing nc-Si:H growth, in this case promoting crystallinity while improving the film growth rate.

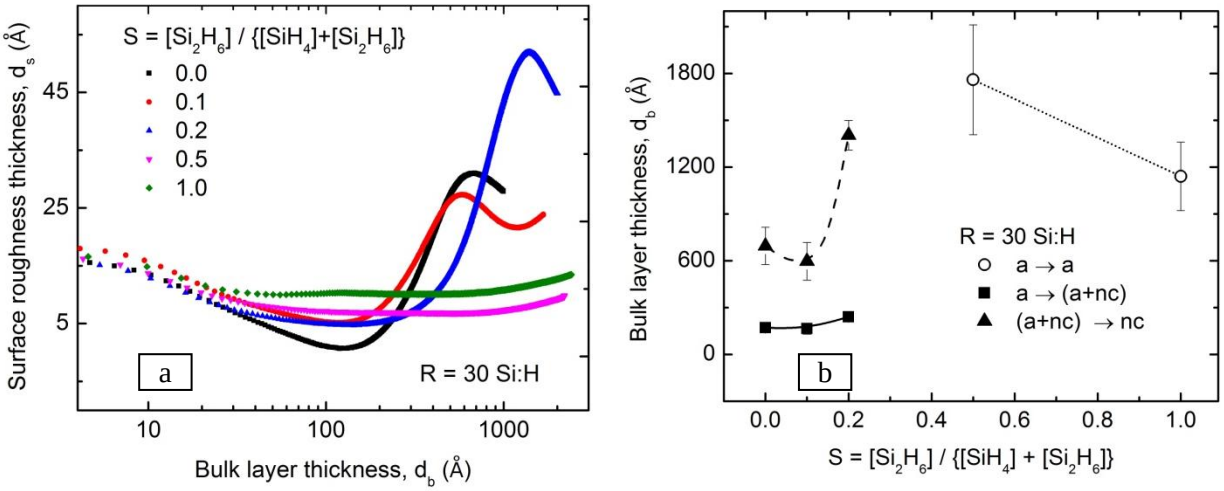

Figure 5-5: For films prepared at fixed R = 30 and variable S: (a) the growth evolution of Si:H in the form of ds as a function of db, and (b) a→a, a→(a+nc), and (a+nc)→nc transition thickness of Si:H.

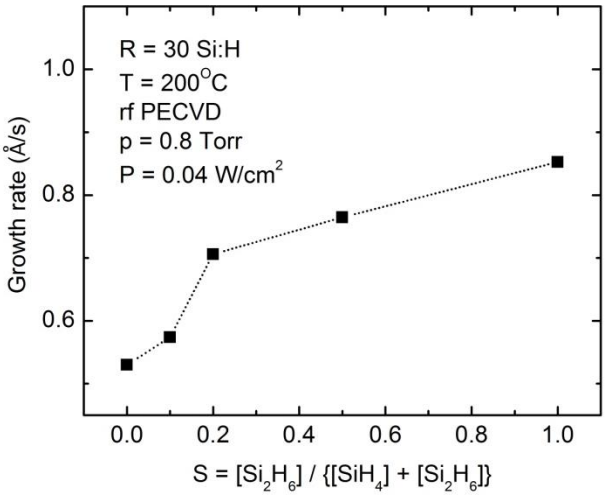

Figure 5-6: Film growth rate for Si:H prepared at R = 30 and variable S.

Si:H Deposition Phase Diagrams

Like the baseline *S* = 0 deposition phase diagram prepared as a function of *R* (Figure 5-2a), phase diagrams have been developed for films prepared at *S* = 1 and 0.2 as functions of *R* (Figure 5-7). *S* = 1 was chosen as the extreme. *S* = 0.2, chosen as the result of the *R* = 30 variable *S* series testing, showed an inflection point in the growth rate and strong delay in crystallite coalescence, but not the overall suppression of crystallinity. For the *S* = 0.2 and 1 series, the highest H_2 dilutions prior to crystallite nucleation for a ~1000 Å thick layer occur at *R* = 20 and 30, respectively. Crystallite nucleation for the *S* = 0.2 series appears to be more abrupt when *R* is greater than the a-Si:H optimum, supporting that moderate *S* can be used to promote crystallinity as inferred from the *R* = 30, variable *S* series. The a→a transition thickness appears to reach higher values when *R* is lower than the optimum for *S* = 0.2 and 1 compared to *S* = 0, potentially widening the process parameters over which improved (but not fully-optimized) a-Si:H may be deposited. Figure 5-8 shows the growth rate as a function of *R* for *S* = 0, 0.2, and 1, all of which show a decrease with increasing *R* and an increase with *S* for any fixed *R*.

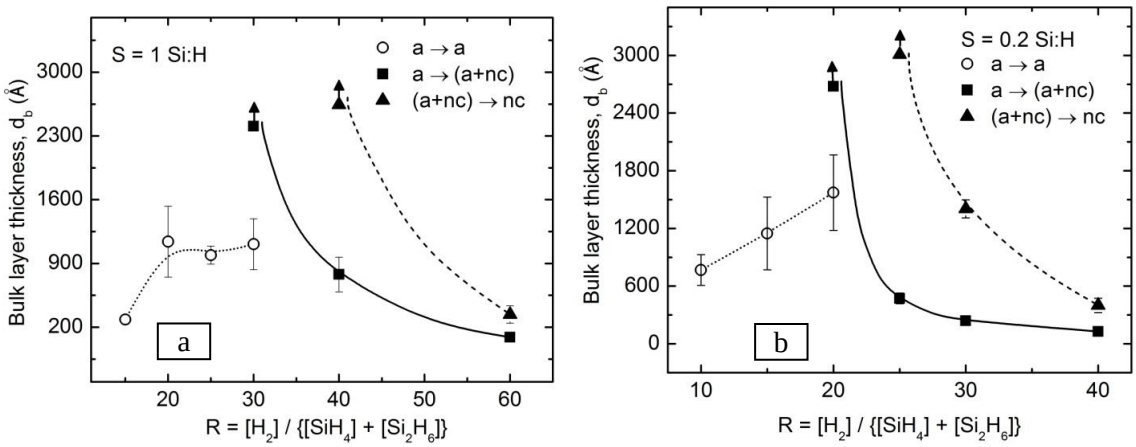

Figure 5-7: Deposition phase diagrams for Si:H prepared at (a) S = 1 and (b) 0.2 and variable R depicting the a→a, a→(a+nc), and (a+nc)→nc structural transitions. Arrows pointing upward indicate the respective transition occurs beyond the maximum thickness measured.

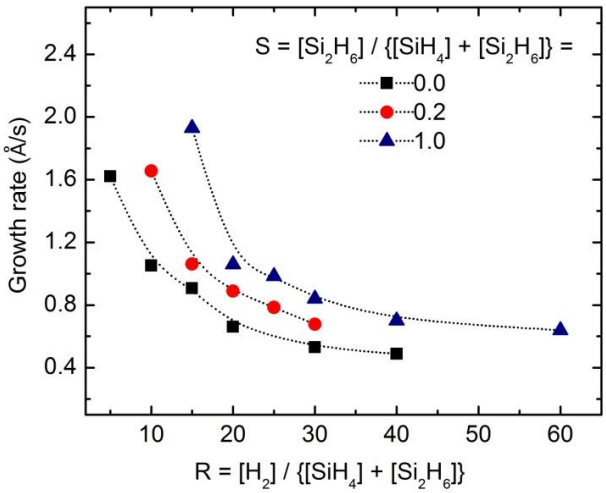

Figure 5-8: Film growth rate for Si:H prepared at S = 0, 0.2, and 1 as functions of R.

Optimized a-Si:H at R = 15 for S = 0, R = 20 for S = 0.2, and R = 30 for S = 1 all have similar deposition rates. This behavior indicates that similar etching by atomic hydrogen may be occurring regardless of the precursor gas, but unfortunately shows that only minimal gains in rate may be possible by adding Si_2H_6 under these deposition conditions. On the other hand, nc-Si:H deposition rates show improvement when comparing films among the different series. Comparing the R = 60, S = 1 and the R = 40, S = 0 samples shows that the samples have similar structural evolutions, but the R = 60, S = 1 sample has a slightly higher deposition rate. The sample with the lowest H_2 dilution at which crystallites nucleate for the S = 0 series, R = 20 has the same or lower growth rate as the corresponding samples in the S = 0.2 and 1 series at R = 25-30 and 40-60, respectively. This increase in growth rate with S observed for (a+nc)-Si:H materials is coupled with comparable or more rapid nucleation of crystallites.

Summary and Conclusions

RTSE has been used to study the growth evolution of Si:H films prepared under variable H_2 dilution and silane-to-disilane ratio deposition conditions. These studies have led to the development of deposition phase diagrams for fixed values of *S* with variable *R*, as well as variable *S* at fixed *R*. Optimized a-Si:H quality degrades with increasing *S*, but *R* can be increased to maintain film quality. The film growth rate of optimized a-Si:H material appears to stabilize regardless of *S*, but a wider process parameter range for improved, but not fully-optimized, material is available at lower *R* with higher rates. *S* has been determined to suppress crystallinity at high values and low *R*, while promoting growth at low values near $S = 0.1\text{-}0.2$ by potentially increasing the initial nucleation density or cone angle of crystallites. nc-Si:H films prepared at higher *R* and *S* can be deposited at higher rates and with a greater degree of crystallinity. This behavior indicates that the addition of Si_2H_6 to PECVD of Si:H can be used to potentially decrease the fabrication time and improve the material quality in nc-Si:H layers.

PART 6: DEVICE DATA WORK COMPARING SILANE AND SILANE+ADDITIVE

Institute of Energy Conversion (IEC), University of Delaware

Amorphous Si Solar Cell Device Results

IEC has a baseline process for deposition of single-junction a-Si p-i-n cells on textured SnO_2 using the IEC's multichamber PECVD system. The device structure was glass/textured SnO_2/a-SiC p-layer (10 nm)/a-SiC buffer i-layer (8 nm)/a-Si i-layer (240 nm)/a-Si n-layer (30 nm)/Al (500 nm). The SnO_2 was either Pilkington Tec 8 or Asahi Type U. Conditions for the a-Si i-layer are given in Table 6-1.

Table 6-1. Baseline a-Si i-layer plasma process conditions.

SiH_4 (sccm)	H_2 (sccm)	Pressure (Torr)	RF power (Watts)	Temperature (°C)	Time (minutes)
20	0	0.5	20	200	15

The initial performance of baseline devices is given in Table 6-2, which shows the average values of 32 cells from run MC0910, deposited around the same time frame as many of the device runs described here. They had an initial efficiency of 7.7±0.3%. This demonstrates the spatial uniformity within the deposition zone and the repeatability of cleaning and contacting, both of which can negatively impact performance and yield. Device conditions had not been optimized for stabilized efficiency since the primary tasks involved supporting industry in comparing different TCOs. Replacing the Al contact with a ZnO/Al back reflector increased Jsc by about~1 mA/cm^2 but for simplicity was typically not used in the work described here.

Table 6-2. Average and standard deviation of 32 cells from baseline a-Si p-i-n cell run MC0910.

MC0910	Voc (V)	Jsc (mÅ/cm^2)	FF (%)	Eff (%)
Average	0.872	12.4	72.0	7.75
Std Dev	0.006	0.26	1.6	0.25

After completing a series of i-layer depositions with varying percentage of Si2H6 as a gas phase additive described in previous sections, a p-i-n cell with 10% Si_2H_6 was deposited. Figure 6-1 shows the JV and QE data compared to a similar baseline cell without Si_2H_6. The growth rate increased from 1.8 to 5.4 Å/sec in part due to the higher power. Table 6-3 shows the JV performance for each. Clearly, the addition of 10% Si_2H_6 has no negative or positive influence on performance while tripling the growth rate. In fact, several depositions of devices were made under varying power levels with 10% Si_2H_6 having efficiency in the 7.5-8.0% range. The best was MC0651 with RF=40 W having cells with 7.8-8.3% efficiency.

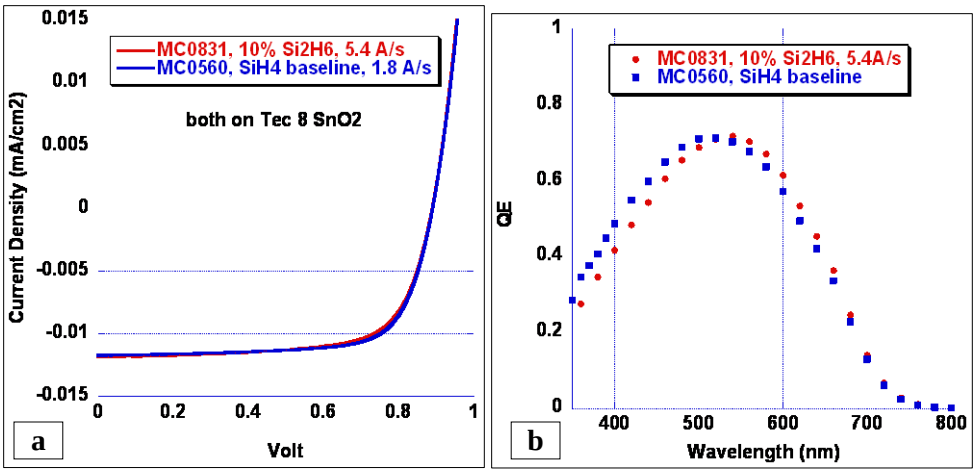

Figure 6-1. Curves for light JV (a) and QE (b) for devices with 0% and 10% Si_2H_6.

Table 6-4. Comparison of performance of devices with 0% and 10% Si_2H_6.

	SiH_4 (sccm)	Si_2H_6 (sccm)	Power (W)	Thick (Å)	GR (Å/s)	Voc (Volts)	FF	Jsc (mÅ/cm^2)	Eff (%)
MC0560 (baseline)	20	0	20	2180	1.8	0.89	72	11.7	7.5
MC0831	18	2	70	2000	5.4	0.89	70	11.8	7.3

However, upon performing extended light soaking (under metal halide lamp illumination, 100 mW/cm2, 50°C) it was determined that the baseline devices had poorer stability than expected. They typically degraded 25-30%. A series of devices was made with varying RF power, with and without Si_2H_6 and light soaked for 250 hours. Figure 6-2 shows that stability correlated more with low SiH_2 percentage in the film rather than growth rate or additive. So testing was conducted using a higher temperature (250°C) and 5:1 H_2 dilution (H_2=100 sccm, SiH_4=20 sccm), resulting in much-improved stability as expected, with 15-17% degradation instead of 25-30%. Either of these conditions reduces the SiH_2 content from 20-30% to < 10%. Table 6-5 shows the relative improvement in stability. Films deposited with H dilution require higher pressure to maintain similar growth rate as undiluted films, so pressure was increased from the baseline of 0.5 T to 1.25 or 2.5 T with H dilution.

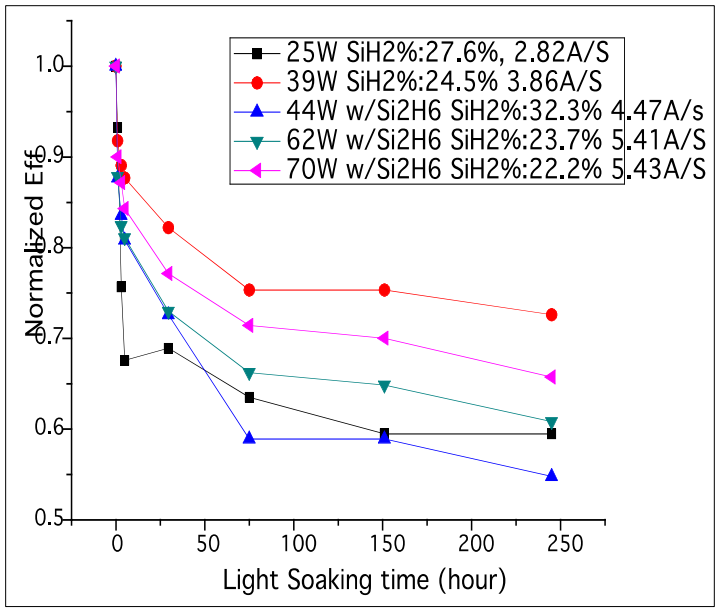

Figure 6- 2. Normalized stability from 5 runs having different RF power with or without 10% Si_2H_6. The R_{mf} in the film (from SiH_2%) and growth rate are listed for each. The two most stable have the lowest H content, and the least stable has the highest H content. None of these had H-dilution of the i-layer and all were deposited at T=200°C.

Table 6-5. Relative decrease in cell parameters with i-layer temperature or H_2 dilution compared to the baseline. Bonded H content decreased from ~ 25% to <10% with either higher T or high dilution.

Pure i-layer= 20sccm SiH_4 0.5T, 25W	H_2 dilution (R=H_2:SiH_4	Degrade% of Voc	Degrade% in Jsc	Degrade% of FF	Degrade% of Eff
200C i layer	None	5.2%	5.0%	19.1%	27%
250C i layer	None	2.3%	1.7%	12.4%	17%
200C i layer	50:10	1.0%	4.4%	10.5%	15%

Therefore, investigation was done on devices with i-layers deposited at 5:1 H_2-dilution, at 200 or 250°C, at 30 to 90W, and at 1.25 or 2.5 T. Table 6-6 lists the initial J-V results of solar cells processed with these different i-layer conditions. H concentration in the i-layer was 9-13%. The higher V_{oc} and lower J_{sc} for runs with 2.5 T is due to higher E_g i-layer. But for deposition at 250°C and 2.5 T, V_{oc} decreases and J_{sc} increases due to the reduction in i layer E_g. An initial efficiency of 7.4% is achieved for i-layer deposited with Si_2H_6 additive at a growth rate of >5A/s, which is similar to the baseline cell grown at 1.8 A/s without Si_2H_6 additive. Also shown is the degradation after 250 hours of light soaking. Figure 2 shows degradation of 30-40% for the un-optimized devices with no H dilution. Table 6-6 shows the optimized devices with H dilution degrade ~20-25% while the growth rate is still high at >5A/s. This data indicates that cells with Si_2H_6 behave same as cells without additive regarding effect of bandgap and substrate temperature. Piece MC1195 had very high microstructure RMF=0.45 which is responsible for its very high degradation.

Table 6-6. a-Si:H p-i-n cell results with different i layer conditions. Growth rate and R_{MF} also given. Cells without Si_2H_6 ($SiH_4/Si_2H_6/H_2$=10/0/50) are in **bold;** others are with $SiH_4/Si_2H_6/H_2$=9/1/50. All devices deposited at 200°C except for the last entry, which was deposited at 250°C.

#	SiH_4/ $Si2H_6/H_2$ (sccm)	Press. (Torr)	RF (W)	GR (Å/s)	R_{mf} (%)	Voc (V)	Jsc (mÅ/ cm^2)	FF (%)	Eff (%)	Eff Degade% after LS
MC1188	**10/0/50**	**1.25**	**30**	**1.8**	**7.4**	**0.882**	**11.6**	**72.5**	**7.4**	**20%**
MC1193	9/1/50	1.25	30	2.3	12.4	0.891	11.7	73.3	7.7	22%
MC1194	9/1/50	1.25	70	3.3	4	0.877	11.9	70.9	7.4	26%
MC1192	**10/0/50**	**2.5**	**90**	**3.5**	**5.8**	**0.922**	**10.7**	**71.5**	**7.0**	**23%**
MC1189	9/1/50	2.5	90	5.2	15.9	0.929	10.6	71.4	7.1	22%
MC1195	9/1/50	2.5	30	3.8	44.3	0.896	10.4	68.2	6.3	43%
MC1199 T=250°C	9/1/50	2.5	90	5.0	5.9	0.882	11.4	73.4	7.4	22%

Nanocrystalline Si Device Solar Cell Results

Unlike the case for a-Si p-i-n cells, IEC had absolutely no baseline or experience making nc-Si p-i-n cells. Deposition of nc-Si cells is much more challenging. The crystalline fraction and grain structure depends not only on the deposition conditions of the nc-Si i-layer itself, but also on: the substrate material (ZnO vs SnO_2), substrate texture, template (p-layer or TCO), p-layer thickness and crystallinity, buffer or incubation layer on top of the p-layer, and finally on the thickness of the nc-Si layer itself. It was decided that before investigating the effect of Si_2H_6 additive on nc-Si device performance, a reasonable baseline process giving around 5% efficiency was needed. The previous sections already documented that it was possible to obtain good values of Xc~50-60% for a wide range of conditions. It was decided to study the effect of the nc-Si i-lyer in devices using the simplest possible device structure: glass/SnO2/ZnO/nc-Si p-layer/nc-Si i-layer/a-Si n-layer/Al. Thus, initially there would be no back ZnO reflector and no buffer or seed layer at the p-I interface. Eventually both of these options were explored in an attempt to improve the low Jsc. This section will present results from a range of device structures and process conditions.

Influence of H dilution

As is well known, H dilution ratio R has a significant impact on increasing crystalline fraction X_c in nc-Si films. However, as the partial pressure of SiH_4 decreases, the growth rate decreases due to relatively fewer Si atoms in the plasma. Figure 6-3 shows the growth rate and X_c for a series of nc-Si films deposited at relatively low RF power (300 W) and pressure (3 T). As expected, the GR decreases almost linearly with R and X_c increases initially then saturates. At R=35, the film was amorphous. There is one pair of data deposited with SiH_4/ Si_2H_6=8/2 sccm. The GR increases significantly and the X_c decreases slightly compared to a film with no Si_2H_6.

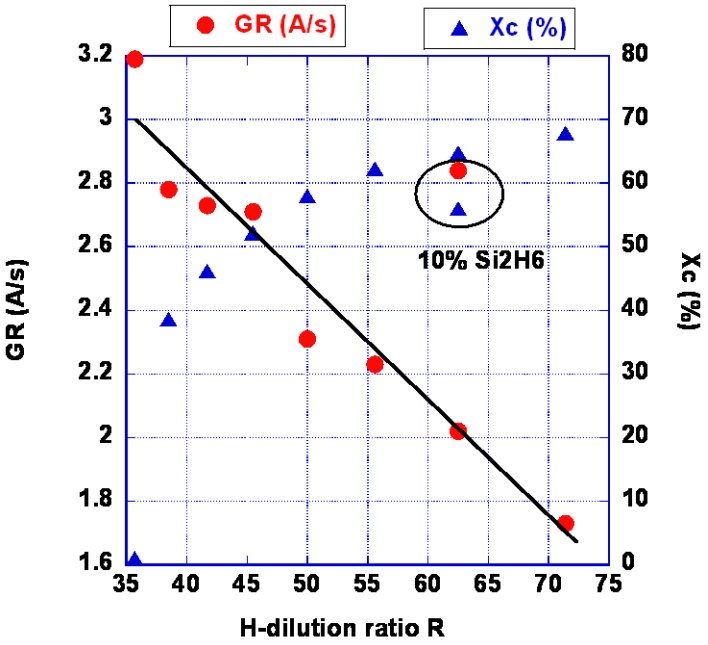

Figure 6-3. GR and X_c as a function of dilution ratio R. The RF power was 300 W, H_2=500 sccm, pressure=3 T. The two symbols in the black circle were deposited with SiH_4=8 sccm, Si_2H_6=2 sccm.

Table 6-7 lists some device results for basic nc-Si p-i-n cells as function of R deposited under similar power and pressure as those in Figure 6-3. The Voc and FF increase as R decreases, suggesting they are inversely correlated to the X_c. However the Jsc is independent of R. This is not expected. All values are relatively low, but this was the starting point.

Table 6-7. Device performance for cells with decreasing H-dilution R. RF=250 W, p=2.5 Torr. I-layer thicknesses 1.2-1.6 um.

Sample ID	H_2 dilution R=H_2/SiH_4	Voc (V)	FF (%)	Jsc (mÅ/cm$_2$)	Eff (%)
MC0817	56.3	0.281	53.5	9.1	1.4
MC0874	45.0	0.330	55.5	8.7	1.6
MC0888	37.5	0.370	60.2	8.6	1.9
MC0913	34.6	0.403	61.7	8.7	2.2

Influence of substrate on Xc for p-layer

It is well established that the nucleation of nc-Si grains, hence the volume crystallinity determined by Raman spectroscopy, depends on the substrate. Since the p-layer is the first layer grown on the substrate and it provides the seeded surface for the nc-Si i-layer, it was assumed that its X_c was critical. It was determined that the p-layer had to be deposited at very high R (100-200) in order to get good crystallinity. Figure 6-4 shows the Raman spectra for p-layers in the same run on three different substrates. Note that bare Tec 8 SnO_2 had X_c =0%' while Tec 8 coated with 20 nm ZnO =47% had Xc=44%.

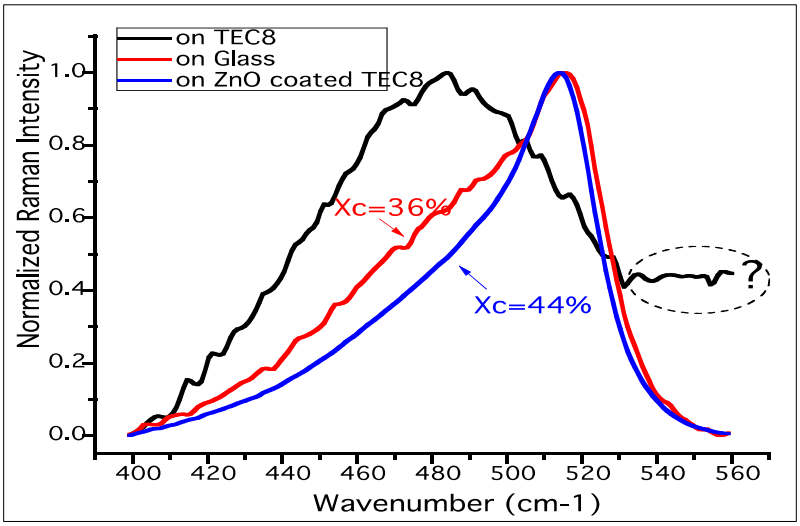

Figure 6-4. Raman spectra of 20 nm p-layer deposited with R=200 H dilution at 200°C on three different substrates.

The film on bare glass substrate had Xc=36%. Thus, amorphous glass was a better nucleation surface than crystalline SnO_2. This critical importance of the thin ZnO is consistent with the known chemical reaction of SnO_2 with highly-diluted H plasmas, leading to reduction of SnO_2 to metallic Sn. The bare SnO_2 was noticeably darker, consistent with the formation of the Sn layer. Thus, most of the results reported here are on ZnO-coated Tec 8 SnO_2, sometimes labeled as Z-Tec or Z-SnO_2.

It is also well known the X_c increases as the film thickness increases and microstructure evolves. Figure 6-5 shows that p-layers deposited for 300 sec were amorphous, while those deposited for 600 sec had X_c =39%. Figure 6-6 shows the QE for simple p-i-n devices with nc-Si i-layers on p-layers whose deposition time ranged from 7 to 20 minutes. It is speculated that the short wavelength response decreased due to decreasing p-layer transmission, while the long wavelength response increased due to increasing X_c of the i-layer caused by increased X_c of the underlying p-layer. Table 6-8 shows the solar cell performance for two series of devices with different p-layer doping gas flows each for three thicknesses. It appears that thicker p-layers with higher dopant values are better.

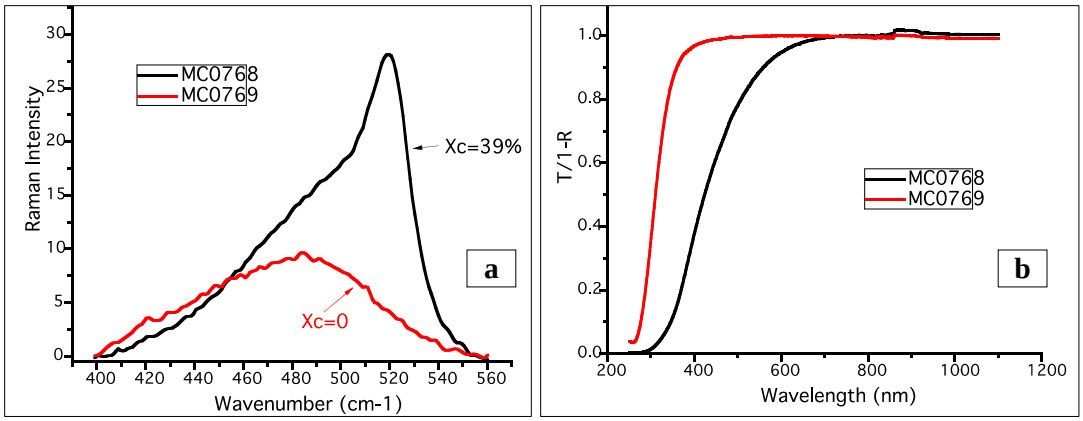

Figure 6-5. Raman spectra (a) and Transmission (b) of nc-Si p-layers deposited for different length of time; 300 sec (red curvesMC0769) and 600 sec (black curvesMC0768).

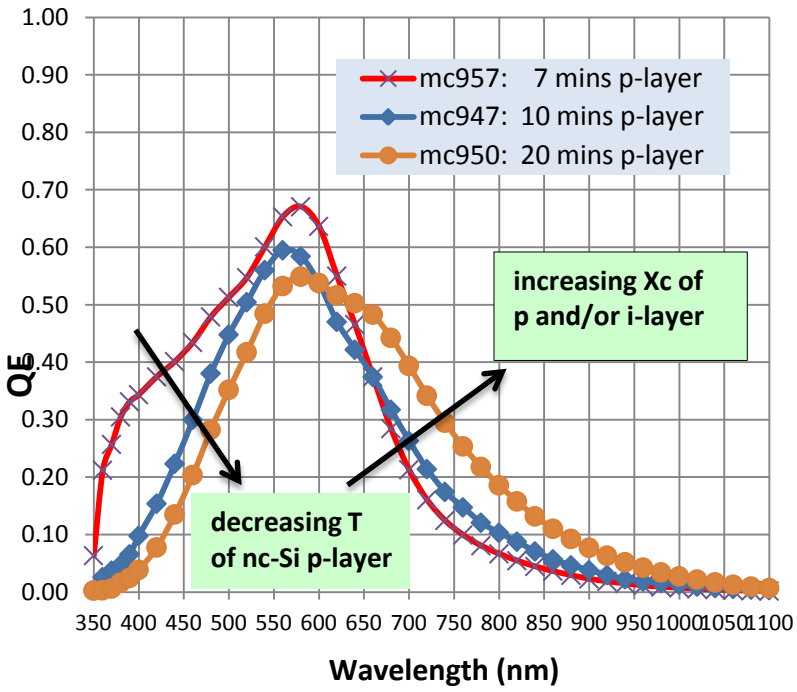

Figure 6-6. QE for simple p-i-n nc-Si devices having different p-layer deposition times.

Table 6-8. Effect of nc-Si p-layer gas flow and thickness on nc-Si device performance.

Sample ID	Voc (V)	FF (%)	Jsc (mÅ/cm^2)	Eff (%)	p-layer gas flow and time
MC963	0.133	37.9	5.8	0.4	SiH_4/B_2H_6=2/1.5, **7 min**
MC944	0.391	55.5	8.7	1.9	SiH_4/B_2H_6=2/1.5, **10 min**
MC951	0.328	53.1	8.5	1.5	SiH_4/B_2H_6=2/1.5, **20 min**
MC957	0.372	57.3	10.1	2.1	SiH_4/B_2H_6=2.5/2, **7 min**
MC947	0.363	61.7	10.2	2.3	SiH_4/B_2H_6=2.5/2, **10 min**
MC950	0.392	61.3	10.7	2.6	SiH_4/B_2H_6=2.5/2, **20 min**

Effect of graded buffer at p-I interface

It is well known in that a-Si p-i-n cells have improved performance when the transition between a-SiC p and a-Si i-layer is graded in bandgap. Decreasing the C concentration to zero over ~ 10 nm smooths the abrupt band misalignment and provides a high field region to repel majority carrier electrons from back-diffusing to the p-layer. Thus, it improves the blue response (increases Jsc) and recombination (increases Voc). In the case of nc-Si devices, it will also serve as a transitional template layer for the nc-Si bulk i-layer. The growth of the nc-Si film evolves sharply with thickness. Figures 6-7 and 6-8 show the Raman and FTIR spectra of the initial i-layer deposited in a device configuration (glass/Z-Tec8/nc-S p-layer) after 2, 4 and 6 minutes of deposition, or approximately 30, 60 and 90 nm of thickness. Clearly, the crystalline fraction is initially zero and increases over the first 100 nm. The initial phase of a-Si film growth is referred to as the 'incubation layer." The goal of good device processing is to reduce the incubation layer and to transition to nc-Si film as soon as possible.

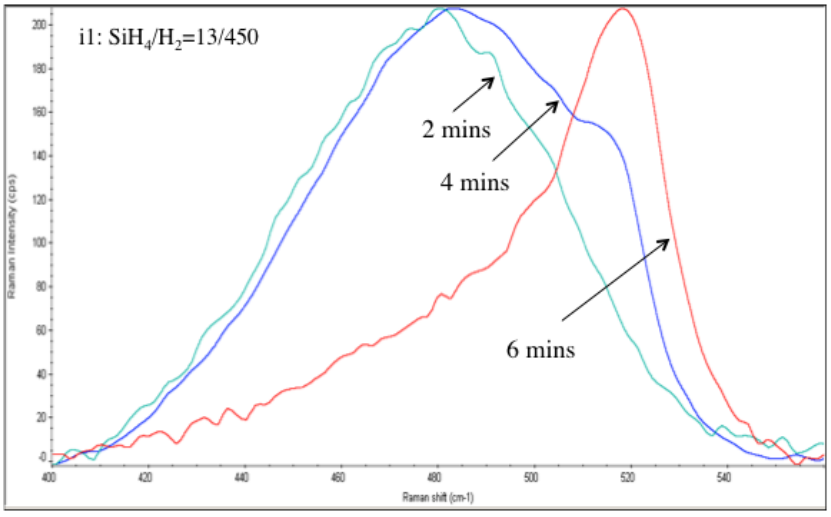

Figure 6-7. Raman spectra of device as i-layer thickness increases after 2, 4, and 6 minutes (30, 60, or 90 nm).

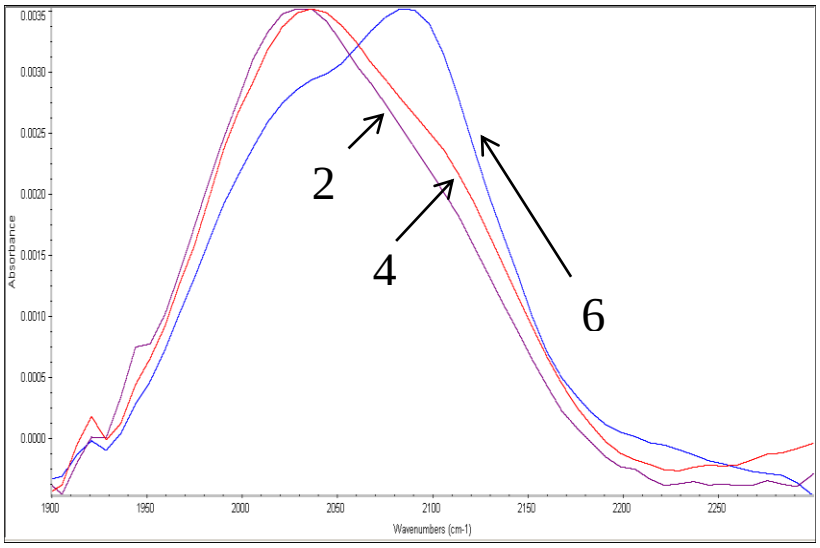

Figure 6-8. FTIR spectra of device as i-layer thickness increases after 2, 4, and 6 minutes.

Investigations were conducted of both graded and ungraded buffer layers to reduce the incubation layer where the grading occurred in the H dilution factor. Figure 6-9 shows four SiH_4 profiles for the buffer layer with a constant H_2=450 sccm. The bulk i-layer (i2) had SiH_4=13 and H_2=450 sccm, thus buffer layer 'ia' was no buffer at all since it was same conditions as i2. Buffers 'ib and ic' had graded R ,while 'id' had ungraded but higher R than 'ia.' Figure 6-9 also shows the Raman spectra for 'ia', 'ib' and 'ic.' IEC made test structures consisting of glass/textured Z-Tec8/nc-Si buffer and characterized their Raman and FTIR spectra. Table 6-9 shows the JV performance of devices with the three buffers of interest ('ia' is no buffer at all). Despite significant differences in the X_c of the p-buffer combination, there were no significant improvements over a baseline device without a buffer.

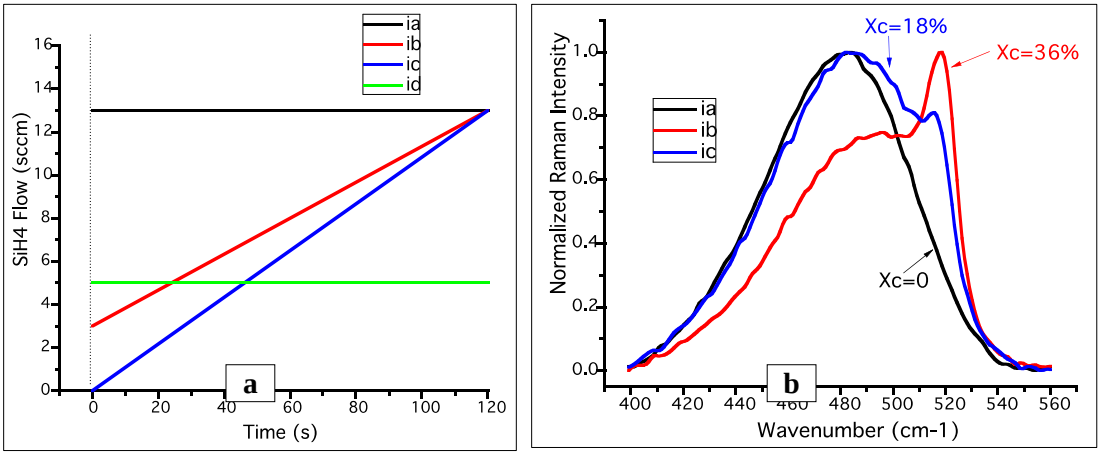

Figure 6-9. (a) SiH_4 flow during the 120 sec deposition for four different buffer layers. H_2 was constant at 450 sccm. (b) Raman spectra for three of the buffers on the nc-Si p-layer.

Table 6-9. Performance of devices with p-i grading profiles shown in Figure 6-9.

Sample ID	Voc (V)	FF (%)	Jsc (mÅ/cm^2)	Eff (%)	i_1 SiH_4 Profile
MC0913	0.403	61.7	8.7	2.2	ia : 13sccm in 120s
MC0996	0.369	59	10.9	2.4	ib : 3-13sccm in 120s
MC0999	0.362	57.5	8.7	1.8	ic : 0-13sccm in 120s
MC1002	0.364	54.7	10.6	2.1	Id : 5sccm in 200s

Comparison between Commercially-Textured SnO_2 and In-House Texture-Etched ZnO(Al) and Buffer Layer RF Power

It is widely reported that ZnO has better chemical stability in H-plasma and higher transmission than SnO_2. Further, ZnO can be textured differently, which may improve nucleation of nc-Si. IEC has previously shown that sputtering a thin ZnO layer on the textured SnO_2 improves the nc-Si device performance.

IEC developed the processing capability to make sputtered aluminum-doped ZnO(Al) or AZO. Then the specular films were textured by etching in dilute 0.5% HCl for 90 seconds. Figure 6-10 shows the Raman spectra for nc-Si devices deposited in the same run on SnO_2/ZnO bilayer and on AZO. They had similar shape, giving Xc~ 47%.

DevciesDevices were deposited in runs MC1038 and 1039 on both types of substrates. Both runs had H dilution-graded buffer layers. The RF power during the buffer was 200W on MC1038 and 300W on MC1039. Table 6-10 lists average performance for cells on two pieces for each of these two substrates. The cells on AZO had consistently higher Jsc and FF but same Voc. The buffer power seems to have had little effect. Figure 6-11 shows the QE for devices on the two substrates from MC1039. The AZO has higher blue response as expected due to its higher transmission. More importantly, there was no difference in the long wavelength response; it was very low in both cases. Thus, while AZO resulted in a slight improvement, it was not the dramatic increase IEC was looking for.

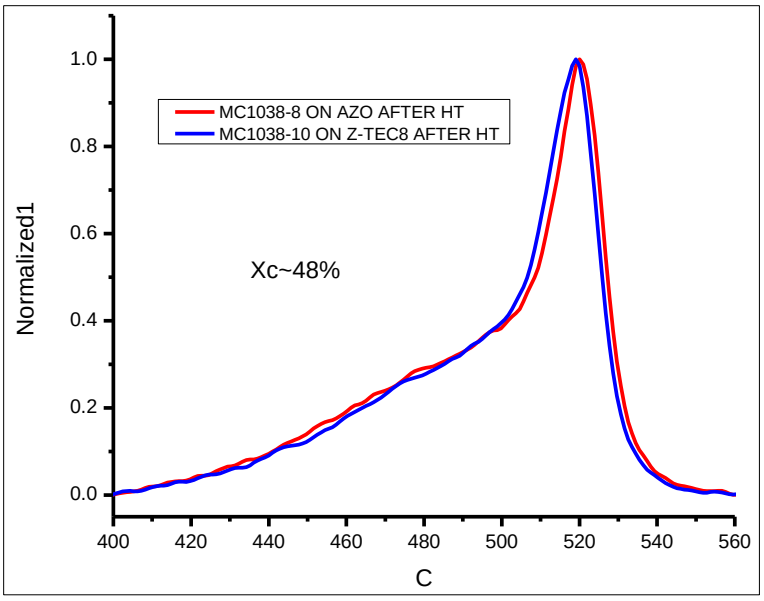

Figure 6-10. Raman spectra for nc-Si film deposited on textured-etched AZO and on ZnO-coated Tec 8 (Z-Tec8).

Table 6-10. JV performance after heat treatment for nc-Si p-i-n cells on texture-etched AZO or SnO_2/ZnO bilayer (Z-Tec8). MC1038 and MC1039 had 200W and 300W graded buffer, respectively.

Sample ID	Voc (V)	FF (%)	Jsc (mÅ/cm^2)	Eff (%)	Comment
MC1038-5	0.370	62.0	11.9	2.7	AZO, 200 W buffer
MC1038-8*	0.359	61.5	12.5	2.8	AZO, 200 W buffer
MC1038-3	0.371	58.7	10.1	2.2	Z-TEC8, 200 W buffer
MC1038-10	0.352	58.9	10.9	2.3	Z-TEC8, 200 W buffer
MC1039-5	0.361	60.9	12.2	2.7	AZO, 300 W buffer
MC1039-6	0.346	54.8	11.1	2.1	Z-Tec8, 300 W buffer

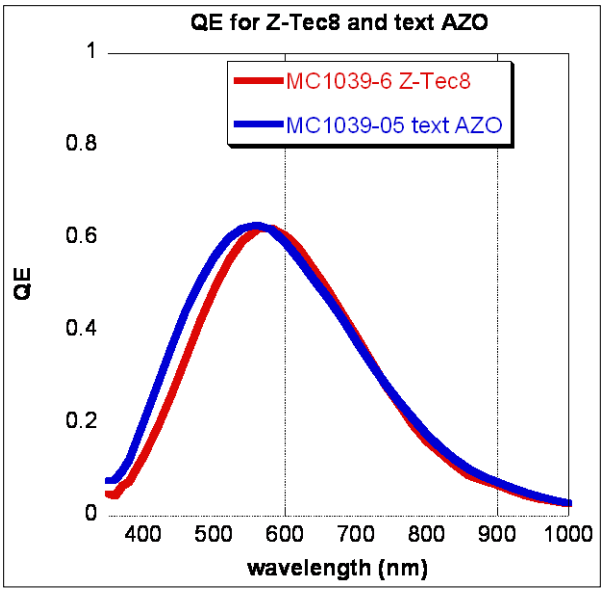

Figure 6-11. QE for two cells on different TCO as described in Table 6-10.

Deposition of Devices at Higher Power and Pressure with Larger Grain Size

As describedDespite considerable variation in nc-Si p, buffer, and i-layer deposition conditions and substrate material, IEC was unable to increase the red QE or Voc into an acceptable range for studying the effect of additives. It was concluded that X_c was insufficient to characterize our film quality so XRD was used to guide experiments. Measurements on nc-Si films made at Air Products and at IEC having X_c from 40-80% under a range of conditions all had small grain size (<5nm). IEC was barely able to resolve the (220) or (111) peaks. Reports in the literature from groups making good solar cells indicates grains >20 nm with a dominant (220) orientation are needed. Most of those groups used higher RF power and pressure than have been used here.

Significant effort was made to modify the deposition chamber at IEC to allow delivery of higher RF power without heating of the feedthrough or creating plasma along the connection between the feedthrough and the electrode. It ultimately was possible to deposit nc-Si films at 500-800W. Increasing the RF power and pressure increased the grain size from ~ nm to >15 nm. Increasing R was found to change the relative intensity of the Si (220) and (111) peaks. A series of devices was made at higher power (515W) and pressure (8 T) compared to the devices whose data was presented above. Figure 6-12 shows the XRD spectra for four films on glass having dilution of 60, 43, 40, and 35. A film with R=30 was amorphous. The (220) peak decreases with increasing H dilution, while the (111) peak increases. Table 6-11 lists the grain size, determined from analysis of the peaks, for the (220) and (111) orientation for the films deposited on glass and Z-Tec8. The values and trends are the same on both substrates. The grains are much larger than previously obtained on low power, low pressure nc-Si films. Table 6-12 lists the JV performance for R=60, 43, and 40. X_c and grain size are also shown. Despite larger grains than before, the device performance was not improved. The FF was especially low. This might be due to the use of an a-SiC p-layer instead of nc-Si, although previous results showed no significant difference between devices with nc-Si or a-SiC p-layers. As a check, two runs were done using nc-Si p-

layer. Results in Table 6-13 show that FF is indeed higher with the nc-Si and especially on IEC's AZO. Run MC1143 had the highest Voc (0.41 V) and Jsc (13.8 ma/cm2) obtained for any nc-Si device. Overall, Tables 6-12 and 6-13 show there was no significant increase in Jsc with larger grains. Figure 6-13 shows that the higher-power, higher-pressure deposition produces a higher blue QE, suggesting a better p-i interface but a decrease in the long wavelength region. QE at 800 nm remained <10%, which was even less than MC0969 that had lower Xc and much smaller grains.

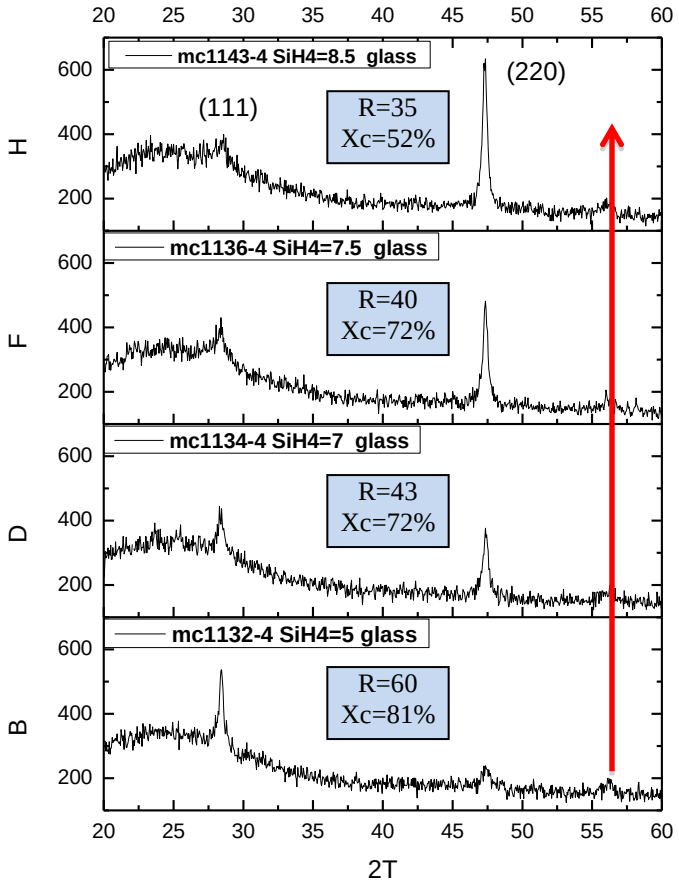

Figure 6-12. XRD spectra of films on glass deposited with 515W, 8 T, H_2=300 sccm and SiH_4 flows of 8.5, 7.5, 7, and 5 sccm. Opposing trends for the (111) and (22) peaks can be seen. Results for (111) and (220) grain size are in Table 6-11.

Table 6-11. Grain size for nc-Si films on glass and Z-Tec8 for varying H dilution. XRD spectra in Figure 6-12.

SiH_4/H_2	Xc (%)	Z-Tec8: (111) Grain Size (nm)	Z-Tec-8: (220) Grain Size (nm)	Glass: (111) Grain Size (nm)	Glass: (220) Grain Size (nm)
5/300	81	21.0	Noise	22.9	Noise
7/300	72	15.8	12.3	15.8	20.0
7.5/300	72	11.9	13.8	14.7	24.3
8.5/300	52	11.9	14.6	<10	24.4

Table 6-12. Performance of devices MC1137, 1138, 1139 at higher power and pressure (515W, 8 T) and larger grain size as function of H dilution. All samples had a-SiC p-layer instead of nc-Si p-layer. Results from MC0969 with lower power (250W), pressure (2.5 T) and dilution (R=35) also shown for reference since it also had same a-SiC p-layer. All samples had 2-step i-layer with initial i1 having higher R than bulk i2.

Run#	i layer SiH_4/H_2	Voc (Volts)	Jsc ($mÅ/cm^2$)	FF %	Eff %	Xc (%)	111,220 grain size (nm)
MC1137	5/300, R=60	0.366	8.6	41.2	1.3	81	21/~0
MC1138	7/300, R=43	0.373	12.5	41.9	2.0	~72	16/12
MC1139	7.5/300, R=40	0.362	12.3	39	1.7	72%	12/14
MC0969	13/450, R=35	0.345	13.2	48	2.2	~60%	<6 nm

Table 6-13. Performance of devices with nc-Si i-layer with R=35 deposited at 515W, 8T like those in Table 6-12 except with nc-Si p-layer instead of a-SiC p-layer. Results on Z-Tec8 and IEC made textured AZO shown for two thickness of p-layer.

Run#	Substrate	nc-Si p-layer	Voc (Volts)	Jsc ($mÅ/cm^2$)	FF %	Eff %
MC1143-2	Z-TEC8	300 sec	0.321	13.8	47.7	2.1
MC1143-5	AZO	"	0.411	10.3	62.6	2.6
MC1144-2	Z-TEC8	600 sec	0.347	11.2	55.9	2.2
MC1144-3	AZO	"	0.370	10.1	64.6	2.4

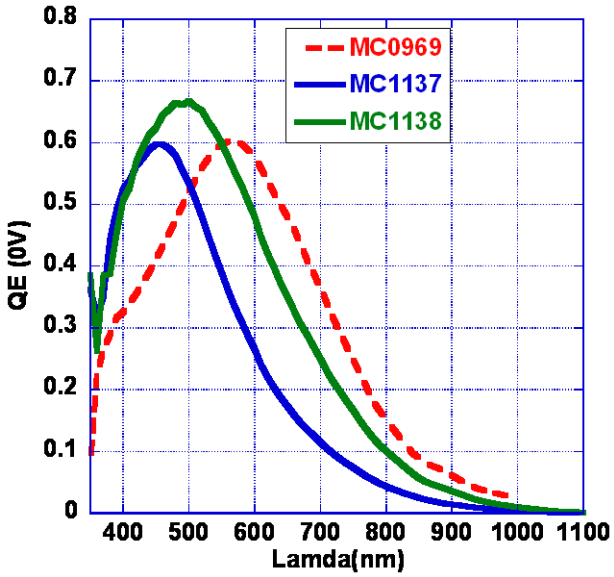

Figure 6-13. QE for devices from Table 6-12 with i2 layer deposited at higher power and pressure leading to larger grain size. MC0969 also with same a-SiC p-layer is shown, deposited with lower power, pressure, and dilution.

Effect of Si_2H_6 Additive on nc-Si Films at Higher Power and Pressure

Having established higher crystallite size at higher power and pressure, IEC investigated the effect of Si_2H_6. Depositions were made on Z-Tec8 substrates at 10% and 20% additive in SiH_4. Table 6-14 lists the flows, X_c and GR. The 10% additive increased deposition rate from 2.0 to 2.6 Å/sec with no change in Xc. The film with 20% additive was amorphous, indicating the H dilution was insufficient as the number of Si atoms increased. Figure 6-14 shows the XRD scan. The film with additive had a better ratio of (220)/(111) peaks. This data verifies that Si_2H_6 can be added to the plasma at typical nc-Si conditions without reducing the film structural quality.

Table 6-14. nc-Si film properties with 10 and 20% additive deposited at 515W, 8 T, 200°C, with H_2=300 sccm.

#	SiH_4 (sccm)	Si_2H_6 (sccm)	Raman Xc (%)	GR (Å/s)
MC1132	5	0	81%	2.0
MC1175	4.5	0.5	81%	2.6
MC1158	5	1	~0	2.7

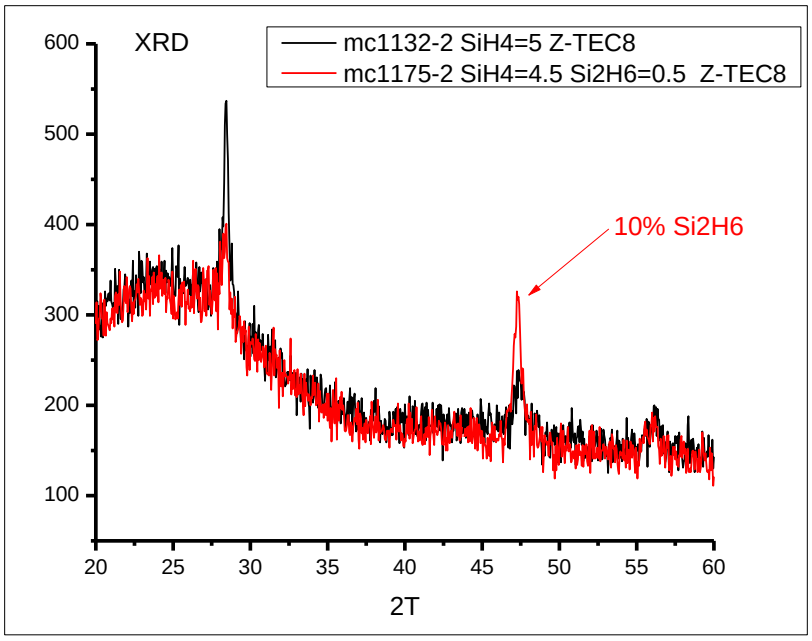

Figure 6-14. XRD scan of 2 nc-Si films from Table 6-13 with 0 and 10% additive.

Tandem a-Si/nc-Si Device Results

Although the performance of the nc-Si devices was not as good as expected, IEC integrated them into a tandem 'micromorph' device structure using a a-Si top cell. This was done for two reasons: 1) growing the nc-Si device on top of a-Si layers might decouple it from the substrate crystallinity; and 2) it would demonstrate the ability to make the ultimate device for this technology.

Calculations and literature examples suggested the required range of top and bottom cell thickness. Three depositions of tandem devices were made using IEC's standard a-Si p-i-n cell (R=5) for the top cell. Runs MC1150 and MC1155 used R=20 for the bottom nc-Si device. The top and bottom cell i-layer deposition time and thickness were varied as indicated in Table 6-15. On MC1165, the bottom cell was graded from R=50 to 35 and time was extended to account for the lower growth rate.

The tandem cell Voc is consistent with the top cell Voc~0.85V and bottom cell Voc~0.3V. The Jsc indicates poor current matching. In all 3 cases, the bottom cell was limiting the current, as indicated by the integrated QE (IQE) represents the photocurrent contribution from the top and bottom cells independently. This indicates that the bottom cell is determining the FF. It is very significant to note that the FF>65% on MC1155 and MC1160 is greater than obtained on single junction nc-Si devices. This suggests better electronic properties for the nc-Si device when it is deposited on the a-Si top cell. Figure 15 shows the QE for the top and bottom cell on MC1155 (obtained using red and blue filters on the bias light to turn off the bottom and top cell, respectively).

Table 6-15. Device performance for 3 nc-Si limited tandem cells .

Run	Top a-Si (sec)	Bot nc-Si (sec)	Voc (V)	Jsc (mÅ/cm^2)	FF (%)	Eff (%)	T/B IQE (mÅ/cm^2)
MC1150	780	3600 (R=20)	1.16	3.5	60.6	2.5	7.6/2.6
MC1155	660	5400 (R=20)	1.16	5.9	67.1	4.5	7.3/4.8
MC1165	780	6300 (R=50-35)	1.13	4.2	65.4	3.0	7.6/4.1

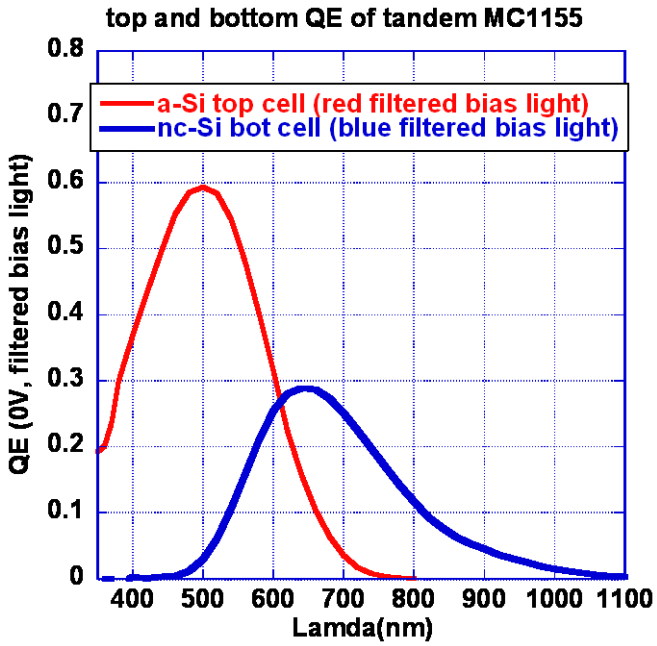

Figure 6-15. Individual cell QE from tandem configuration. Integrated QE values in Table 6-14.

Conclusions Regarding nc-Si Devices

IEC explored a wide range of substrates, p-layers, 'seed' layers, buffer layers, and nc-Si bulk i-layer deposition conditions. Most of this was without Si_2H_6 to establish a reasonable baseline first without additive. To enhance the deposition of the nc-Si material, IEC also modified the PECVD system hardware several times by adding a higher RF power (1200W) supply, a dry pump, new electrode material (stainless steel instead of Mo), and new mass flow controllers to allow higher or lower flow rates. Despite these efforts, cells could not be made with efficiency >3% and Jsc >13 mA/cm^2. The target was 5% and 16 mA/cm^2.

IEC's nc-Si material behaved as expected in terms of dependence of Xc, growth rate and grain size on the key process variables of power, pressure, and H-dilution. Throughout the program, IEC used the volume fraction crystallinity Xc from Raman as the key metric, consistent with many other groups. However, it was found that this was not sufficient to characterize the film's electronic quality because it was independent of the grain size. XRD showed that the devices made with RF power <300W had small grain size (~5-8 nm) and orientation not preferred for

good solar cells. This manifested in IEC's solar cells having very poor long wavelength response (QE<0.2 beyond 800 nm) regardless of deposition conditions, device structure or substrate. IEC suspects this is due to insufficient RF power delivered to the electrode. The original system was designed for ~200 W power supplies appropriate for deposition of a-Si. At the end of the program, higher power and pressure produced films with much larger grains but still low Jsc.

While the FF of our single junction nc-Si cells was typically 55-62%, IEC made several tandem cells having FF>66%. The Jsc of these devices were limited by the bottom nc-Si cell, meaning the FF was also largely determined by this cell. This is more surprising considering that the tandems had unoptimized interconnect 'n/p' shorting junctions, poor current matching, and no seed layer.

Nanocrystalline Si i-layer and Single-Junction Solar Cells Using 40.68 MHz VHF Plasma

40.68 MHz very high frequency (VHF) generator was installed recently in IEC to study the effect of plasma frequency on nc-Si deposition. It is well known that the benefit of VHF includes higher electron density, lower electron temperature and higher growth rate.

Properties of nc-Si Film Deposited by VHF

The films are deposited at different H_2 dilution with and without Si_2H_6 additive at 3 Torr and relatively low power 250W. Table 6-16 lists the deposition conditions, and Figure 6-16 shows the film growth rate (GR) and crystalline volume fraction determined by Raman spectroscopy (Xc) as a function of H dilution ratio (H_2/SiH_4).

Table 6-16: nc-Si growth rate, X_c with different H_2/SiH_4 ratios by VHF.

Sample ID	SiH_4 (sccm)	Si_2H_6 (sccm)	H_2 (sccm)	Ratio (H_2/SiH_4)	Growth Rate (Å/s)	X_c (%)
MC1249	8.5	0	300	35.3	**2.6**	73.4
MC1250	7.7	0.8	300	--	**3.8**	63.8
MC1253	8.5	0	200	23.5	**3.4**	76.9
MC1255	8.5	0	150	17.6	**3.7**	83.5
MC1256	8.5	0	100	11.8	**3.9**	82.2
MC1258	10	0	100	10	**4.6**	75.0
MC1267	9	1	100	--	**5.7**	71.1

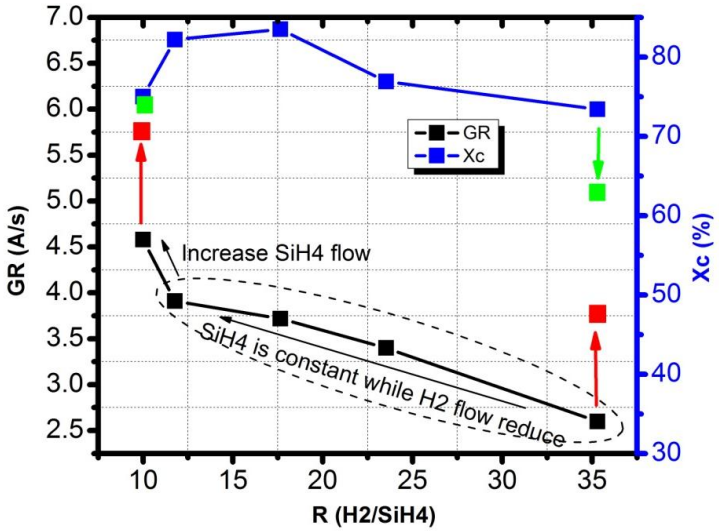

Figure 6-16: GR (rlack square = no Si_2H_6, red square = 10% Si_2H_6 additive) and Xc (blue square = no Si_2H_6, green square = 10% Si_2H_6 additive) as a function of H_2 dilution ratio R (H_2/ SiH_4).

The significant difference between RF (13.56 MHz) and VHF (40.68 MHz) is the dependence of H_2 dilution on Xc. IEC compared the film deposited by RF and VHF at same pressure (3 Torr) and similar power density and found that for RF at R=35, the film is amorphous; at R=71, Xc of the film is about 68%. For VHF, however, even when the R is reduced to as low as 10, Xc remains high (~70%). When R is reduced from 35 to 11 (constant SiH_4 flow of 8.5 sccm and H_2 flow reduce from 300 sccm to 100 sccm), the growth rate increases linearly from 2.6 Å/s to 3.9 Å/s, while Xc does not change appreciably and remains >70%. At a H_2 flow 100 sccm, the growth rate increases to 4.6 Å/s when SiH_4 flow increase to 10 sccm. The growth rate increase with lower H_2 dilution by increasing SiH_4 flow is more significant than reducing H_2 flow in this deposition regime. Also the film growth rate deposited using VHF plasma is higher than RF at similar conditions. At H_2 flow=300 sccm, with 9.5% Si_2H_6 additive, the growth rate increases from 2.6 Å/s ($SiH_4/Si_2H_6/H_2$=8.5/0/300) to 3.8 Å/s (SiH_4/ Si_2H_6/ H_2=7.7/0.8/300). The Raman

Xc decreases from 73% to 64%. At a H_2 flow of 100 sccm, similar growth rate enhancement is observed with the addition of 10% Si_2H_6 (4.6 Å/s without Si_2H_6 vs 5.7 Å/s with 10% Si_2H_6 additive, ΔGR=1.1 Å/s), while the Raman Xc slightly decreases from 75% to 71%. For the film deposited using RF plasma at similar deposition pressure and power density, the growth rate increases only by 0.5 Å/s even with 20% Si_2H_6 additive. Therefore, the effect of Si_2H_6 additive to the film growth rate seems to be more effective in VHF plasma than RF plasma. Additionally, the nc-Si film can be deposited at much lower H_2/ SiH_4 ratio in VHF plasma compared to RF, which would be beneficial for achieving higher growth rate.

Figure 6-17 shows the XRD results of nc-Si deposited on glass at different H_2 dilution by VHF at 3 Torr and 250W. Unlike the RF plasma, where crystal orientation of the films change from (111) preferential growth at high H_2 dilution to (220) preferential growth at low H_2 dilution, neither the crystal orientation nor the volume fraction change appreciably for the films deposited by VHF in a wide range of H_2 dilution and all films are strongly (220) orientated no matter how the H_2 dilution is changed (either decreasing H2 flow or increasing SiH_4 flow). The grain size, calculated from the FWHM of (220) peak, is around 28 nm for all three conditions. Considering RF, the similar grain size could only be obtained at a much higher pressure ~8 Torr and grain size reduces significantly for the film deposited at lower pressure. Ion bombardment is one of the primary reasons to suppress the grain size. The large grain size obtained by VHF at low pressure may indicate the less ion bombardment in VHF plasma compared with RF.

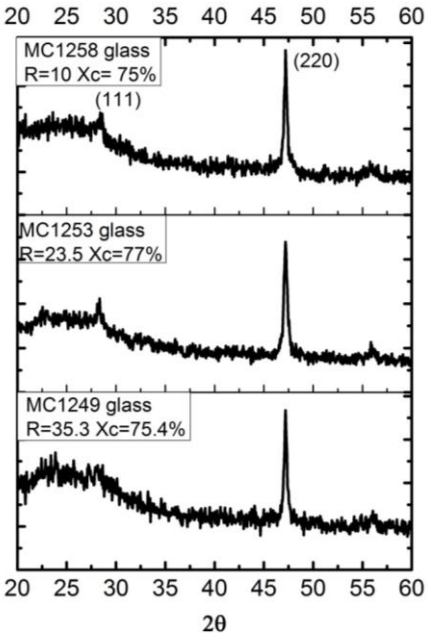

Figure 6-17: XRD spectra of nc-Si films on glass deposited by VHF at different H_2 dilutions.

Figure 6-18 shows the XRD spectra of films deposited by VHF with and without 10% Si_2H_6 additive at two different H_2 flows. With RF, adding Si_2H_6 could change the preferential growth direction from (111) to (220). However, with VHF, there is no significant change of growth orientation with Si_2H_6 additive. All four films are preferentially (220) oriented with no

discernible differences in grain size (~28 nm). Therefore, the Si_2H_6 additive in VHF plasma increase film growth rate and achieved 5.7 Å/s (as shown in Table 6-16) without any apparent differences in film structure (grain size, crystal fraction or orientation).

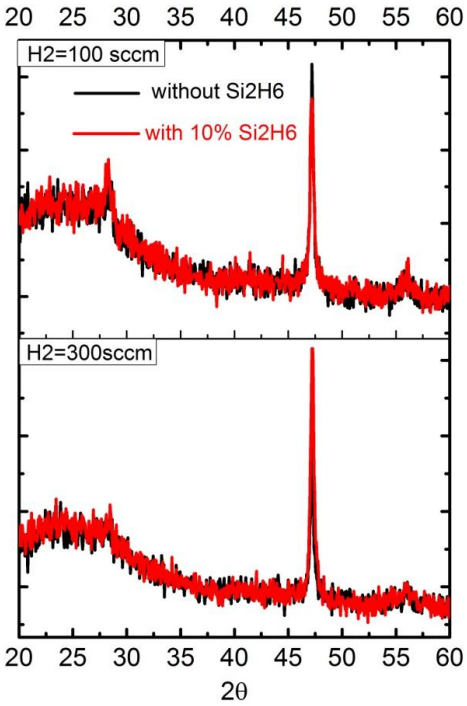

Figure 6-18: XRD spectra of nc-Si films on glass deposited by VHF with (red) and without (black) 10% Si_2H_6.

nc-Si solar Cell Performance by VHF with Si_2H_6 Additive

An nc-Si solar cell is fabricated with a standard RF nc-Si p layer and DC a-Si n layer. The bulk intrinsic layer is deposited by VHF at 3 Torr, 250W, SiH_4/ Si_2H_6/ H_2=7.7/0.8/300, 1.3μm at GR 3.8 Å/s. A seed layer is used at p/i interface. Three ZnO- coated TEC8 and a relatively smooth AZO were used as substrates. A simple 500nm Al is used as back reflector and contact.

Table 6-17 lists the JV results for the first solar cell made by VHF in IEC. The cell performance is almost identical on the three ZnO-coated TEC8 substrates, which indicates t uniform deposition by 40 MHz VHF with an ~1100cm^2 electrode. On the textured ZnO-coated TEC8 substrate, the Voc is close to 0.4 V and FF is ~61%. The Jsc is ~15mA/cm^2, the highest level obtained for a nc-Si device. On the relatively smooth AZO substrate, the Voc is 0.45 V and FF is ~69%. Both of these parameters are the highest obtained so far. The high Voc and FF also indicate the excellent electronic quality of the i layer with Si_2H_6 additive. Higher Voc and FF on the AZO substrate indicate the better i layer bulk quality on the smoother substrate compared to more textured ZnO coated TEC8. The suboptimum textured surface of TEC8 substrate may induce bulk defects inside the i layer due to possible grain growth collision. The lower Jsc with the AZO substrate is most likely affected by the poorer front surface light scattering/ trapping.

Table 6-17: MC1252 nc-Si pin solar cell performance with i layer deposited by VHF at 3 Torr, 250W, SiH_4/ Si_2H_6/ H_2=7.7/0.8/300, 1.3μm at GR 3.8 Å/s.

Sample ID	Voc (V)	Jsc (mÅ/cm^2)	FF (%)	Eff (%)	Substrate
MC1252-2	0.392	14.7	60.6	3.5	Textured Z-TEC8
MC1252-3	0.397	14.7	60.8	3.6	Textured Z-TEC8
MC1252-4	0.386	14.9	61.3	3.5	Textured Z-TEC8
MC1252-6	0.452	12.2	69.0	3.8	Smooth AZO

Figure 6-19 shows the QE of MC1252 on two substrates. Z-TEC8: the QE at 400nm is about 40% and the QE peak is around 75% at 550nm, which is much better than the RF plasma deposited i-layers. The QE at 800nm is low about 20%, which may result from the poor optical properties of Al back reflector. The Jsc could be largely increased with ZnO/Ag back reflector. The QE on AZO substrate is much lower at short wavelength, while it's almost the same at longer wavelength compared with Z-TEC8. Considering the higher Voc and FF on AZO, the main reason for the low blue QE on AZO is most likely from the optical loss due to less front surface light scattering by smoother AZO surface. Further optimization of nc-Si p layer (increase blue response), i layer (increase Voc and red response) and back reflector (increase red response) is undergoing for better cell performance.

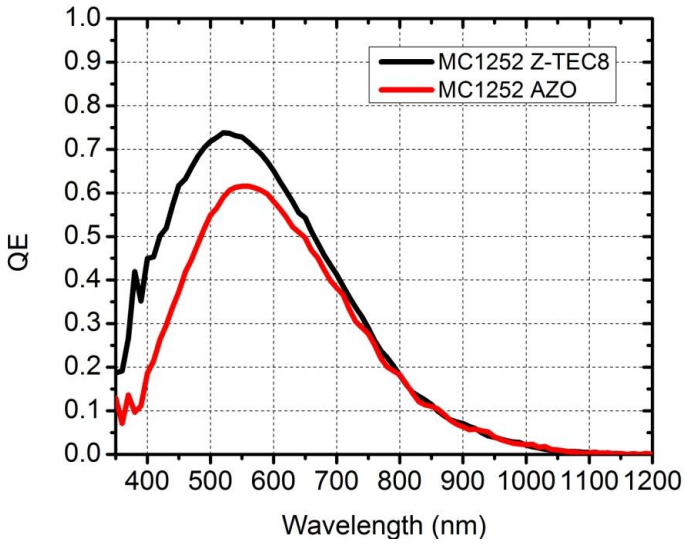

Figure 6-19: QE of MC1252 on ZnO-coated TEC8 and AZO substrates.

Summary of VHF

nc-Si could be deposited at much lower H_2 dilutions using VHF plasma compared to RF. By adding Si_2H_6, the growth rate is enhanced more with VHF compared with RF. Unlike RF, the nc-Si film deposited by VHF shows favorable (220) orientation in wide range of H_2 dilutions with large grain size.

REFERENCES

[1] J. Lee, P. I. Rovira, I. An, and R. W. Collins, "Rotating-compensator multichannel ellipsometry: applications for real time Stokes vector spectroscopy of thin film growth," *Review of Scientific Instruments* **69**, 1800-1810 (1998).

[2] B. Johs, J. A. Woollam, C. M. Herzinger, J. Hilfiker, R. Synowicki, and C. L. Bungay, "Overview of variable angle spectroscopic ellipsometry (VASE), part II: advanced applications," *SPIE Proceedings* **72**, 29-58 (1999).

[3] C. Chen, I. An, G. M. Ferreira, N. J. Podraza, J. A. Zapien, and R. W. Collins,"Multichannel Mueller matrix ellipsometer based on the dual rotating compensator principle," *Thin Solid Films* **455-456**, 14-23 (2004).

[4] Y. Cong, I. An, K. Vedam, and R. W. Collins, "Optical characterization of a four-medium thin film structure by real time spectroscopic ellipsometry: amorphous carbon on tantalum," *Applied Optics* **30**, 2692-2703 (1991).

[5] G. E. Jellison, Jr. and F. A. Modine, "Parameterization of the optical functions of amorphous materials in the interband region," *Applied Physics Letters* **69**, 371-373 (1996).

[6] G. E. Jellison, Jr. and F. A. Modine, "Erratum: 'Parameterization of the optical functions of amorphous materials in the interband region'," *Applied Physics Letters* **69**, 2137 (1996).

[7] B. Johs, C. M. Herzinger, J. H. Dinan, A. Cornfeld, and J. D. Benson, "Development of a parametric optical constant model for $Hg_{1-x}Cd_xTe$ for control of composition by spectroscopic ellipsometry during MBE growth," *Thin Solid Films* **313-314**, 137-142 (1998).

[8] H. Fujiwara, J. Koh, P. I. Rovira, and R. W. Collins, "Assessment of effective-medium theories in the analysis of nucleation and microscopic surface roughness evolution for semiconductor thin films," *Physical Review B* **61**, 10832-10844 (2000).

[9] C. M. Herzinger, B. Johs, W. A. McGahan, and J. A. Woollam, "Ellipsometric determination of optical constants for silicon and thermally grown silicon dioxide via a multi-sample, multi-wavelength, multi-angle investigation," *Journal of Applied Physics* **83**, 3323-3336 (1998).

[10] R. W. Collins, A. S. Ferlauto, G. M. Ferreira, C. Chen, J. Koh, R. J. Koval, Y. Lee, J. M. Pearce, and C. R. Wronski, "Evolution of microstructure and phase in amorphous, protocrystalline, and microcrystalline silicon studied by real time spectroscopic ellipsometry," *Solar Energy Materials and Solar Cells* **78**, 143-180 (2003).

[11] EPA 403-R-10-003. Protocol for Measuring Destruction Removal Efficiency of Fluorinated Green House Gas Abatement Equipment in Electronics Manufacturing, 2010.

[12] Doyle J. R., Doughty D. A., Gallagher A.; *Journal of Applied Physics* **68** (9) 1990.

[13] Perrin J, Leroy O., Bordage M. C.; Contrib *Plasma Physics*, **36** (1), 1996.

[14] Shiratani M., Koga K., Kaguchi N., Bando K., Watanabe Y.; *Thin Solid Films* 506-507, 2006.

[15] Takai M., Nishimoto T., Takagi T., Kondo M., Matsuda A.; *J. Non Crystalline Solids*, 266-269, 2000.

[16] Doyle J. R., Doughty D. A., Gallagher A.; *Journal of Applied Physics* **71** (10) 1992.

[17] N. J. Podraza, C. R. Wronski, and R. W. Collins, "Model for the amorphous roughening transition in amorphous semiconductor deposition," *Journal of Non-Crystalline Solids* **352**, 950-954 (2006).

[18] Y. A. Kryukov, N. J. Podraza, R. W. Collins, and J. G. Amar, "Experimental and theoretical study of the evolution of surface roughness in amorphous silicon films grown by low-temperature plasma-enhanced chemical vapor deposition," *Physical Review B* **80**, 085403 (2009).

[19] N. J. Podraza, C. R. Wronski, and R. W. Collins, "Development of phase diagrams for $Si_{1-x}Ge_x$:H from real time spectroscopic ellipsometry," *Journal of Non-Crystalline Solids* **352**, 1263-1267 (2006).

[20] Y. Lu, S. Kim, M. Gunes, Y. Lee, C. R. Wronski, and R. W. Collins, "Process-property relationships for a-Si1-xCx:H deposition: excursions in parameter space guided by real time spectroellipsometry," *Materials Research Society Symposium Proceedings* **336**, 595-600 (1994).

[21] D. V. Tsu, B. S. Chao, S. R. Ovshinsky, S. Guha, and J. Yang, "Effect of hydrogen dilution on the structure of amorphous silicon alloys," *Applied Physics Letters* **71**, 1317-1319 (1997).

[22] X. Cao, J. A. Stoke, J. Li, N. J. Podraza, W. Du, X. Yang, D. Attygalle, X. Liao, R. W. Collins, and X. Deng, "Fabrication and optimization of single-junction nc-Si:H n-i-p solar cells using Si:H phase diagram concepts developed by real time spectroscopic ellipsometry," *Journal of Non-Crystalline Solids* **354**, 2397-2402 (2008).

[23] J. A. Stoke, N. J. Podraza, J. Li, X. Cao, X. Deng, and R. W. Collins, "Advanced deposition phase diagrams for guiding Si:H-based multijunction solar cells," *Journal of Non-Crystalline Solids* **354**, 2435-2439 (2008).

[24] J. A. Stoke, L. R. Dahal, J. Li, N. J. Podraza, X. Cao, X. Deng, and R. W. Collins, "Optimization of Si:H multijunction n-i-p solar cells through the development of deposition phase diagrams," *Proceedings of the 33rd IEEE Photovoltaic Specialists Conference*, 762-767 (2008).

[25] O. Vetterl, F. Finger, R. Carius, P. Hapke, L. Houben, O. Kluth, A. Lambertz, A. Muck, B. Rech, and H. Wagner, "Intrinsic microcrystalline silicon: a new material for photovoltaics," *Solar Energy Materials and Solar Cells* **62**, 97-108 (2000).

[26] N. J. Podraza, J. Li, C. R. Wronski, E. C. Dickey, M. W. Horn, and R. W. Collins,"Analysis of $Si_{1-x}Ge_x$:H thin films with graded composition and structure by real time spectroscopic ellipsometry," *Physica Status Solidi a* **205**, 892-895 (2008).